Global and Planetary Change 189 (2020) 103174

Contents lists available at ScienceDirect

Global and Planetary Change

journal homepage: www.elsevier.com/locate/gloplacha

Research Article

A volcanic scenario for the Frasnian–Famennian major biotic crisis and other Late Devonian global changes: More answers than questions?☆

Grzegorz Racki

Institute of Earth Sciences, University of Silesia in Katowice, Będzińska 60, 41- 200 Sosnowiec, Poland

ARTICLE INFO

Keywords:
Frasnian-Famennian biotic crisis
Global events
Climate disturbation
Volcanism
Mecury anomalies

ABSTRACT

Although the prime causation of the Late Devonian Frasnian–Famennian (F–F) mass extinction remains conjectural, such destructive factors as the spread of anoxia and rapid upheavals in the runaway greenhouse climate are generally accepted in the Earth-bound multicausal scenario. In terms of prime triggers of these global changes, volcanism paroxysm coupled with the Eovariscan tectonism has been suspected for many years. However, the recent discovery of multiple anomalous mercury enrichments at the worldwide scale provides a reliable factual basis for proposing a volcanic–tectonic scenario for the stepwise F–F ecological catastrophe, specifically the Kellwasser (KW) Crisis. A focus is usually on the cataclysmic emplacement of the Viluy large igneous province (LIP) in eastern Siberia. However, the long-lasted effusive outpouring was likely episodically paired with amplified arc magmatism and hydrothermal activity, and the rapid climate oscillations and glacioustatic responses could in fact have been promoted by diverse feedbacks driven by volcanism and tectonics. The anti-greenhouse effect of expanding intertidal–estuarine and riparian woodlands during transient CO_2-greenhouse spikes was another key feedback on Late Devonian land. An updated volcanic press-pulse model is proposed with reference to the recent timing of LIPs and arc magmatism and the revised date of 371.9 Ma for the F–F boundary. The global changes were initiated by the pre-KW effusive activity of LIPs, which caused extreme stress in the global carbonate ecosystem. Nevertheless, at least two decisive pulses of sill-type intrusions and/or kimberlite/carbonatite eruptions, in addition to flood basalt extrusions on the East European Platform, are thought to have eventually led to the end-Frasnian ecological catastrophe. These stimuli have been enhanced by effective orbital modulation. An attractive option is to apply the scenario to other Late Devonian global events, as evidences in particular by the Hg spikes that coincide with the end-Famennian Hangenberg Crisis.

1. Introduction

After the latest Ordovician mass extinction, wide-ranging recovery of marine biota and revolutionary ecological changes in the sea and on land occurred during the interval of ~100 Ma inserted between two ice ages (e.g., Walliser, 1996; Algeo et al., 2001; Copper, 2011). This global ecosystem recovery is perfectly exemplified by the Phanerozoic acme in development of the Middle to Late Devonian coral–stromatoporoid reefs (Kiessling, 2008; Copper, 2011). The sudden collapse of the diverse ecosystems is a clue in explaining the severe ecological disturbance; thus, the major intra-Devonian extinction across the broadly defined Frasnian–Famennian (F–F) transition is cause for scientific concern. Even if this biocrisis was considered earlier with crude timing (e.g., Sobolev, 1928), the truly rapid and global end-Frasnian mass extinction (EFME) was first emphasized by McLaren (1959), and was conceptually grounded by McLaren (1970); the last author mentioned was inspired by this dramatic change in the F–F stratigraphic record when he proposed extra-terrestrial impact as a causal factor. On other hand, a series of well-documented Late Devonian global events, as defined in Walliser (1996), includes the significant Hangenberg (HG) Crisis in the Devonian–Carboniferous (D–C) boundary beds. Moreover, an increasing number of studies support arguments for a stepwise and exclusively Earth-bound nature of the EFME as an alternative to a cosmic catastrophe similar to the end-Cretaceous cataclysm (Racki, 1998, 2012). The term “Kellwasser (KW) Crisis” of Schindler (1993), based on classic outcrops of the Rhine Slate Mountains and Harz Mountains, is commonly accepted to describe both the Upper Frasnian Kellwasser black shale horizons (lower, LKW; upper, UKW) and the

☆ Dmitry N. Sobolev, Andrey B. Veimarn and Wolfgang Buggisch are gratefully honored for introducing heuristic concepts that eventually led me to the Late Devonian volcanic scenario

E-mail address: racki@us.edu.pl.

https://doi.org/10.1016/j.gloplacha.2020.103174
Received 12 June 2019; Received in revised form 6 March 2020; Accepted 18 March 2020
Available online 20 March 2020

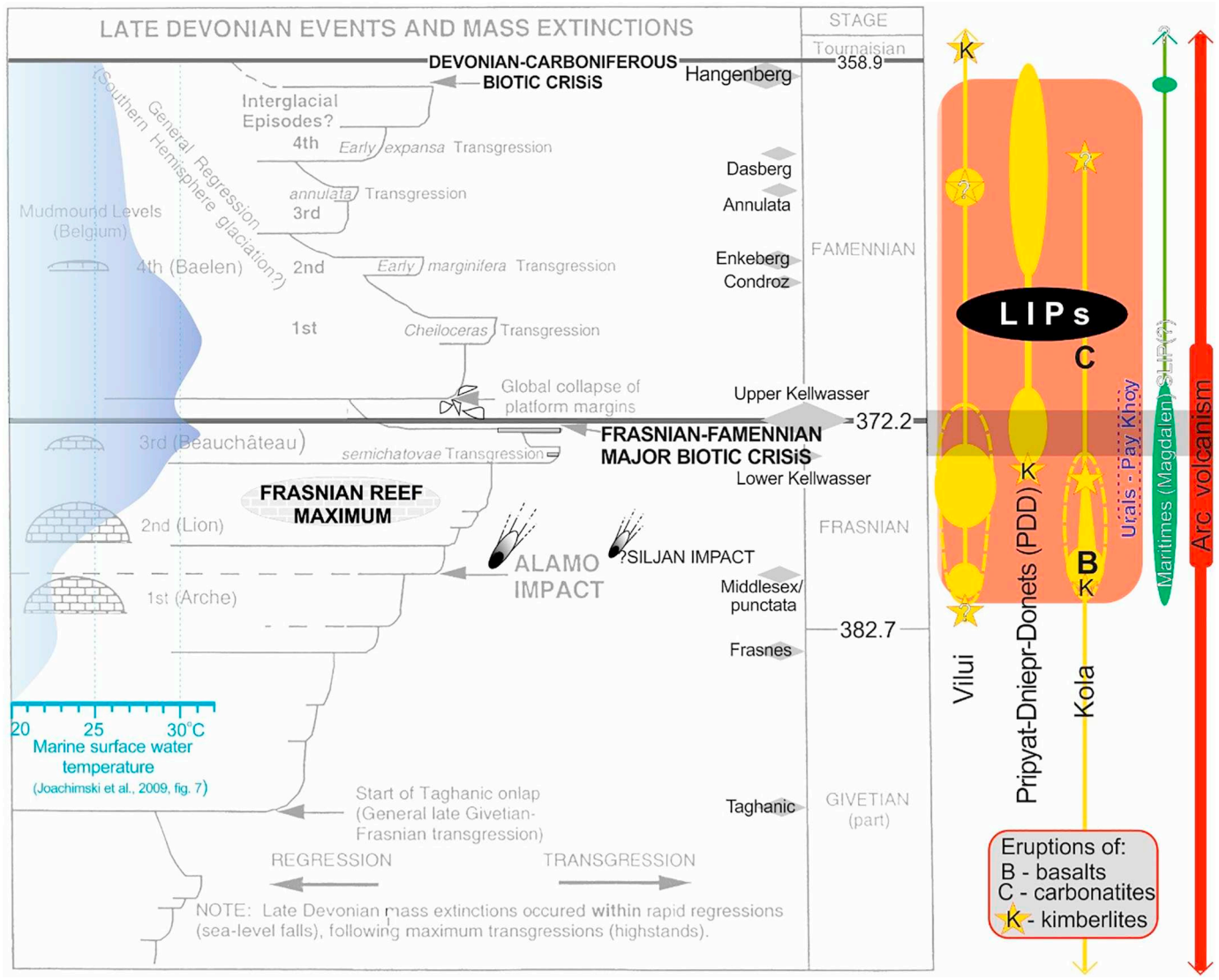

Fig. 1. Late Devonian event stratigraphy, based on sea-level eustatic cyclicity and reef succession in Ardennes (modified after Sandberg et al., 2000; for detail of the F- transition see Fig. 2), against the generalized marine temperatures (blue; Joachimski et al., 2009, fig. 7) and volcanic activity. The most important global events (grey rhombs) as ranked by Walliser (1996) and Becker et al. (2016b), Siljan crater age after Jourdan and Reimold (2012); ages (not to scale) after Becker et al. (2012). Composite timing of the Late Devonian volcanism, presented separately for large igneous provinces (LIPs; light red; overall temporal range after Ernst et al., 2020) and arc magmatism (dark red), with emphasis on eruptive pulses of flood basalts (yellow circular-elliptical varieties) and explosive outbursts (stars); compiled from Ivanov (2015) and Tomshin et al. (2018) [Viluy; see Fig. 12B], Wilson and Lyashkevich (1996), fig. 2), Aizberg et al. (2001), fig. 1) [Pripyat-Dnieper-Donets; PDD, see Fig. 13], Larionova et al. (2016), Arzamastsev et al. (2017) and Arzamastsev (2018) [Kola], Puchkov et al. (2016) [Ural – Pay Khoy], Ernst (2014) and Ernst et al. (2020) [Maritimes SLIP?], and Winter (2015), fig. 2) [amplified arc volcanism].

corresponding global anoxic events (Figs. 1, 2).

The intricate matters of the F–F mass extinction have been presented in monographs of McGhee (1996, 2013), Walliser (1996), and Hallam and Wignall (1997), as well as in several succeeding thematic volumes edited by Baliński et al. (2002), Racki et al. (2002), Over et al. (2005), and Becker et al. (2016a). The recent review articles on 'the multicausal model' include works of Ma et al. (2016), Carmichael et al. (2019) and Qie et al. (2019). This overview presents most important results of the recently ended high-budget project "Devonian deep-water marine realm as a key to elucidate global ecosystem perturbations" from the National Science Centre – Poland (to the Author). Specifically, application of mercury as a new geochemical proxy highlighted the possible significance of volcanism as the main trigger of the global changes (Racki et al., 2018b; Racki, 2020a, b). Therefore, the main goal of the contribution is comprehensive testing of the updated F–F scenario.

2. Major F–F biotic crisis: terminological and geochronological issues

Raup and Sepkoski (1982) first distinguished a particularly lengthy timespan of the Devonian biotic change to include the Givetian to Famennian ages, with first-order biotic turnover occurring near the F-F boundary (Figs. 1-2), which was finalised almost 13 Ma later by the also critical HG Crisis (Kaiser et al., 2016). In a general conceptual setting, the heterogeneity of major global events referred as five mass extinctions was emphasized by Bambach (2006, p. 148), who concluded that "only the end-Permian and end-Cretaceous mass extinctions were so severe that the nature of marine faunas changed in their aftermath" (see also McGhee et al., 2004; Roberts and Mannion, 2019). Consequently, Racki (2020a; compare Bottjer, 2016, p. 175) distinguished between two types of biosphere responses to global ecosystem perturbations: (1) *biodiversity crises*, characterized by high extinction rates and large loss of diversity in a relatively short time, and (2) *biotic (or ecological) crises,*

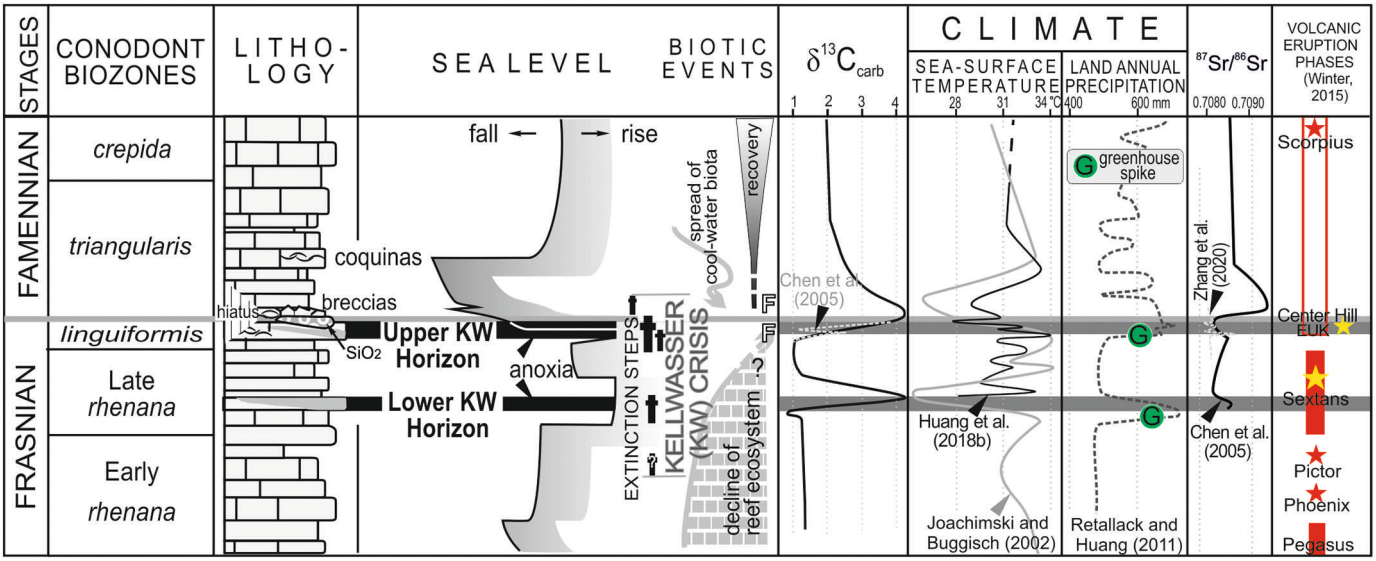

Fig. 2. Composite sedimentary and geochemical records of the Kellwasser Crisis, to show generalized eustatic, biotic and volcanic events and sea temperature variations (compiled from fig. 1 in Schindler, 1993; fig. 2 in Joachimski and Buggisch, 2002, fig. 2 in Chen et al., 2005, fig. 2 in Retallack and Huang, 2011, fig. 2 in Winter, 2015, fig. 7 in Huang et al., 2018, and fig. 4 in Zhang et al., 2020; see also Gereke and Schindler, 2012, figs. 1 and 9; Ma et al., 2016, figs. 10-11; EUK – earlier UKW eruptions). The land annual precipitation and greenhouse/CO_2 spikes interpreted from Retallack and Huang (2011) for New York basin; for updated Famennian conodont zonation see Spalletta et al. (2017).

marked by protracted and stepwise biodiversity losses, but notably combined with disproportionately large ecological consequences. For the KW Crisis, statistically refined analysis has revealed that the species losses were relatively low, at only ~40% (Stanley, 2016), mainly due to a lowered speciation rate, but not an increased extinction rate (Bambach, 2006). Therefore, the F–F mass extinction *sensu lato* should be considered as a major biotic crisis (Racki, 2020a), even although Stigall (2012) unfortunately utilized the term "biodiversity crisis" within precisely the same sense.

The isochronous marker intervals of the KW black shales (KW BS), which are time-specific facies as defined in the standard German localities (Schindler, 1993; Walliser, 1996; Gereke and Schindler, 2012), are correlated only approximately with the concomitant biogeochemical perturbations in C cycling recorded in positive $\delta^{13}C$ excursions (CIEs; Racki et al., 2019; see also Carmichael et al., 2019). For example, the LKW level in Chinese section of Wang et al. (2018), fig. 3 therein), as indicated by CIE, is extended to the *Palmatolepis linguiformis* [= *linguiformis*] Zone, and is certainly not correlated with the LKW BS.

2.1. Dating and duration

The KW Crisis refers to a lengthy stepwise Late Frasnian global perturbation with a presumed duration of 2 Ma for the principal Late *rhenana* to *linguiformis* zonal interval (Sandberg and Ziegler, 1996). Such a concept is maintained in the "Geological Time Scale 2012," which was derived from Monte Carlo analysis of U–Pb dates from selected volcanic horizons (Figs. 1 and 3; Becker et al., 2012). Conversely, orbitally driven cyclostratigraphy suggested a duration of at most half that length (e.g., Chen et al., 2005), which was finally proved by De Vleeschouwer et al. (2017). Based on eccentricity and obliquity cycles, the astronomically constrained relative timescale indicates that the crucial KW interval (= the two end-Frasnian conodont zones) lasted ~0.85 Ma (Fig. 3). In the extended definition of the KW Crisis (i.e., from late Early *rhenana* Zone to the earliest Famennian; Schindler, 1993; Gereke and Schindler, 2012; Fig. 2), this duration probably exceeded 1 Ma.

High-resolution U–Pb dating of the Steinbruch Schmidt volcanic ash horizon in Germany 2.5 m below the top of the UKW level implies 371.86 ± 0.08 Ma as the date of the F–F boundary (figs. 4–5 in Percival et al., 2018b). This numerical age, which is based on the cyclostratigraphic age modeling of De Vleeschouwer et al. (2017), was confirmed by the timing of the end-Frasnian Center Hill tephra horizon in Tennessee (several dozen cm below the conodont-dated boundary; Over, 2002), which yielded a date of 371.91 ± 0.15 Ma (Ver Straeten et al., 2020). I take the new U–Pb-derived age of the F–F boundary (estimated as 371.9 Ma) as the principal reference in this article. The main divergence still concerns the age of the LKW Event, which could be either 374.5 Ma (Becker et al., 2012) or 372.7 Ma (Percival et al., 2018b); accordingly to the second concept, the main UKW Event was initiated 372.1 Ma. However, an age of ~375 Ma was ascribed by Lanik et al. (2016) to tephra from the Middle Frasnian (= early *hassi* Zone), making the KW Crisis a lot younger (Fig. 3). If so, the timescale reference points are still tentative because the duration of the Frasnian age can in fact be ~5 Ma, which is half of that presently accepted (Fig. 1).

3. Updated volcanic press-pulse (greenhouse/icehouse) scenario

The primary triggers of global cataclysms and the immediate extermination factors forced by them should be clearly distinguished (McLaren, 1983), but they are often still mixed in so-called "multicausal scenarios" (Racki, 2020a). For example, the F–F cooling pulse was recently discussed in opposition to the disastrous volcanism by Wang et al. (2018). However, only three principal groups of primary processes were given to introduce the global sources of the stress varieties (Racki, 2020b): (1) *extraterrestrial causes*, particularly meteorite/cometary impacts, (2) *terrestrial volcanic causes*, as discussed below; and (3) *terrestrial non-volcanic causes*, associated with sudden climate and sea-level changes, exemplified by paleogeographic/oceanographic turning points (e.g., the Late Devonian closure of the ocean between Laurussia and Gondwana; Copper, 1986), in addition to biotic interactions and bioevolutionary consequences for the global ecosystem (e.g., the Devonian–Carboniferous forest expansion, McGhee, 2013; D'Antonio et al., 2019).

Ernst et al. (2018b, p. 1-2) summarized that there is "an increasing recognition of the role of LIPs and their silicic counterparts, Silicic LIPs (SLIPs), in rapid environmental and climate changes, including global warming (Hothouse events), global cooling (Icehouse events, i.e. Snowball Earth or regional glaciations), anoxia, stepwise oxygenation, acid rain/ocean acidification, enhanced hydrothermal and terrestrial

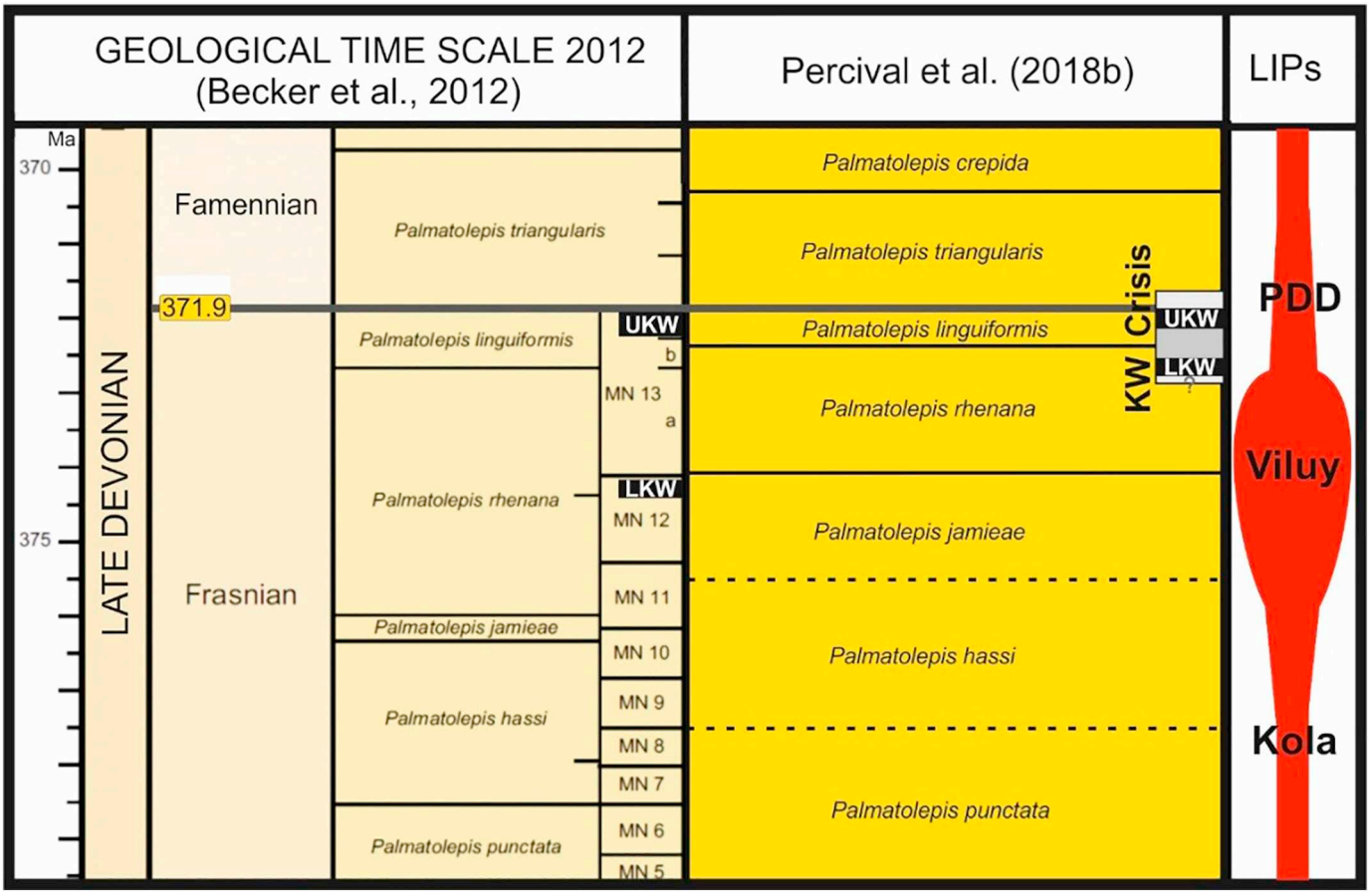

Fig. 3. Comparison of the recent two timescales of the F–F transition from GTS 2012 (modified fig. 12.10 in Becker et al., 2012) and the astrochronogically calibrated scheme compiled from Percival et al. (2018b), fig. 5) and De Vleeschouwer et al. (2017), fig. 3). The generalized timing of LIP eruptive activity, as shown in Fig. 1, refers to the revised timescale after Percival et al. (2018b).

nutrient fluxes, and mercury poisoning, leading, in many cases, to mass extinctions". The decisive role of volcanic cataclysms and the hyperthermal climate setting of mass extinctions have been addressed in many recent reviews (Kidder and Worsley, 2010; Bond and Wignall, 2014; Rampino and Self, 2015; Wignall, 2016; Emsbo et al., 2018; Ernst and Youbi, 2017; Clapham and Renne, 2019; Font and Bond, 2020). This concept was reinforced by the discovery of Hg anomalies in all five major extinctions horizons (Clapham and Renne, 2019; Racki, 2020a).

An extremely broad meaning of ultimate volcanic triggers of biosphere turnovers should be applied to encompass the associated tectonic phenomena (Racki, 2020b). In words of Rampino and Self (2015, p. 1050), "LIPs may represent only one facet of a host of geological factors (e.g., changes in seafloor-spreading rates, rifting events, tectonism, and sea-level variations)." By combining the distinguished volcanic summer/greenhouse model with the lesser known volcanic icehouse hypothesis of Cather et al. (2009), two pairs of opposing climatic and eustatic factors in dynamic equilibrium can be explained by the volcanic-induced loops of diverse processes (Fig. 4; see discussion in Racki, 2020b, and references therein), as described below:

1. *Climatic warming*: The volcanic-forced runaway greenhouse, promoted by intermittent excess CO_2, mostly promoted by thermogenic degassing in contact aureoles, is the most commonly accepted and well proved attribute of the recent mass extinction paradigm, particularly when used in combination with oceanic stagnation (and the resulting global O_2 depletion) and acidification.
2. *Climatic cooling*: The basic anti-greenhouse feedbacks include (1) the rapid chemical weathering rate of freshly erupted or tectonically lifted and exhumed flood basalt series ("weathering/chemical pump") and (2) volcanic-sourced oceanic fertilization and increased primary production leading to a highly efficient biological pump (Cather et al., 2009). Only a brief-term effect can be promoted by the traditionally considered factor, i.e., ejected sulfuric acid aerosol and dust impacts, but Tabor et al. (2020) stressed a key role of soot emission from catastrophic firestorms in triggering the climate deterioration. The short-lasting climatic shifts driven by explosive volcanism have been recently discussed by Lee and Dee (2019), who concluded the following: "It may be possible for individual eruptions to perturb the carbon cycle on timescales of 1–10 k.y…These effects would be manifested as short-term cooling events superimposed upon on an otherwise warmer baseline." In addition, climatic swings, driven by competing carbon and sulfur degassing by continental LIP eruptions, were also modeled, among others, by Fendley et al. (2019) for Deccan Traps flood basalt eruptions (see McKenzie and Jiang, 2019; Clapham and Renne, 2019, and Racki, 2020b). As highlighted by Macdonald et al. (2019), p. 1), "Low-latitude arc-continent collisions are hypothesized to drive cooling by exhuming and eroding mafic and ultramafic rocks in the warm, wet tropics, thereby increasing Earth's potential to sequester carbon through chemical weathering… Earth's climate state is set primarily by global weatherability, which changes with the latitudinal distribution of arc-continent collisions."

The long-term tectonoeustasy, in millions of years, traditionally associated primarily with changes in the spreading rate and volume of oceanic ridges, still cannot explain brief sea-level changes of less than 1 Ma that occur so frequently in the major biocrisis times. Therefore, the eustatic fluctuations can be more easily explained by variations in

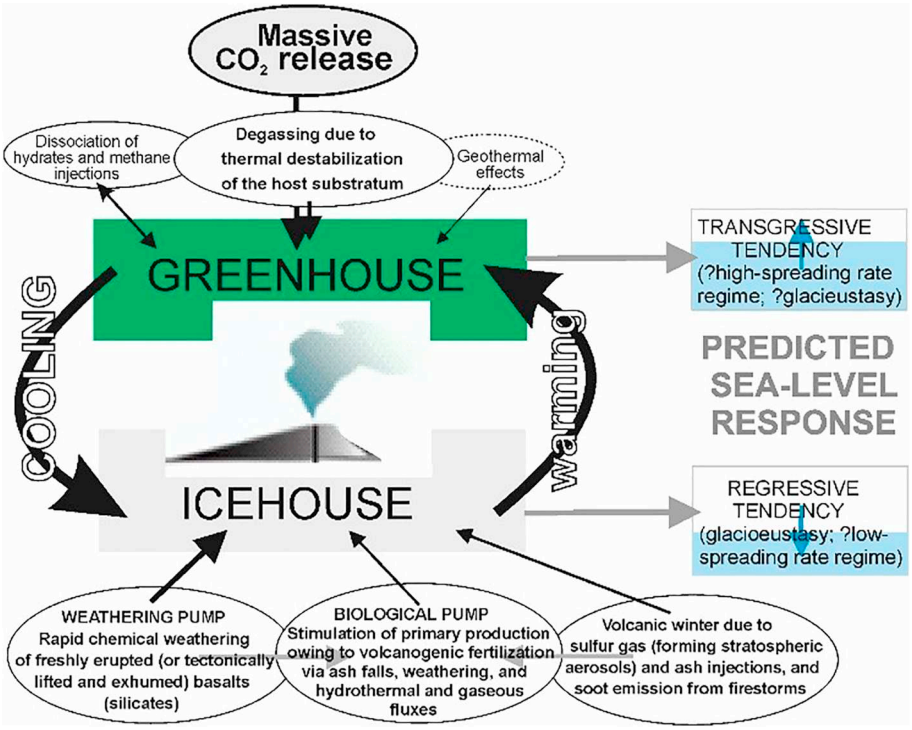

Fig. 4. Volcanism-related cause-and-effect interplaying links that can finally lead to change (shown by the thickest arrows) from (1) an amplified long-term greenhouse stimulus to (2) an intervening/ending climate cooling interlude/trend due to an anti-greenhouse effect, against the anticipated sea-level changes (augmented by Milankovitch-type cyclicity modulation; Elrick et al., 2009); the competing interactions (thinner arrows) are highlighted as immanent attribute of the dynamic model of punctuated volcanic summer in the general press-pulse scenario; arrow thicknesses reflect the alleged influence magnitude (modified fig. 12 from Racki, 2020b; see the complete models of volcanic greenhouse catastrophe in Kidder and Worsley, 2010; Bond and Wignall, 2014; Rampino and Self, 2015; Wignall, 2016; Ernst and Youbi, 2017; Clapham and Renne, 2019; and Font and Bond, 2020).

glacial ice volume and a glacioeustatic response to volcanically promoted climatic change (Fig. 4), i.e. toward more prolonged greenhouse mode (transgression) and toward icehouse interlude (regression).

In the general context of the Devonian greenhouse world (see McGhee, 2014), the glaciation-driven eustasy was discussed by Elrick et al. (2009, p. 170) in the case of third-order depositional sequences; "A plausible climate driver for these My-scale paleoclimate changes is long-period eccentricity (~2.4 My) and obliquity (~1.2 My) variations". In summary, all volcanism- and tectonism-driven anti-greenhouse feedbacks may be assumed as operative factors in the Devonian global events and are marked by cooling/glaciation episodes in an overall greenhouse setting (Averbuch et al., 2005; McGhee, 2005, 2013, 2014; Winter, 2015; Zhang et al., 2020). The comparable scenario was outlined for the KW Crisis already by Buggisch (1991); see Fig. 5A). Widespread anoxia and other ecosystem turnovers are recently difficult to interpret without a volcanic/greenhouse trigger (Kidder and Worsley, 2010; Knoll, 2013; Rampino and Self, 2015; Racki, 2020b), which is particularly clear in relation to Cretaceous oceanic anoxic events (OAEs; Weissert, 2019).

3.1. Towards the volcanism-driven press–pulse theory of mass extinction

Arens and West (2008), p. 456) in their press–pulse theory explained that "the global extinction power of flood basalts comes not from the eruptions themselves, but from secondary effects," such as climate change, C cycle disruption, and sea-level fluctuation when the LIP is paired with tectonism. Thus, volcanism-generated "press disturbances need not kill outright but can instead exert extinction power through curtailed reproduction, lost habitat, geographic range contraction, and the long-term decline of population size" (Arens and West, 2008, p. 464). The delayed ecosystem response owing to cumulative stress is demonstrated by the fact that LIPs typically preceded the main extinction intervals (the lag-time model of McGhee, 2005), and magmatic activity lasted much longer compared to consequent biotic collapse (Burgess et al., 2019, fig. 1 therein). For example, in the Late Cretaceous stressed ecosystem, volcanic activity was influencing pCO_2 levels up to 500 kA before the onset of OAE2 (Barclay et al., 2010).

The press–pulse mass extinction scenario, however, may include sole volcanic activity as a driver of both press and pulse disturbances, as considered in Racki (2020b). The most important factors in this respect are the frequency, composition, and magnitude of eruptions, associated primarily with and the type of thermally affected substratum and magma plumbing system (Clapham and Renne, 2019; Ernst et al., 2019). In particular, a highly discontinuous pulsed pattern characterizes plume-generated giant lava flows, on the diversity of orders from 10 Ma to 10 years (Courtillot and Fluteau, 2014). The worldwide pulse response can be attributed to multiple paroxysms in a suitably brief period and, as quoted above, recently simulated for rapid climate oscillations driven by LIPs and continental arc magmatism (McKenzie and Jiang, 2019). In this shifting greenhouse/icehouse context, additional puzzle includes LIP-associated alkaline magmatism, especially carbonatites, owing to tremendous expulsive potential of the rapid eruptions for large volumes of CO_2 and SO_2 (Ray and Pande, 1999; Isozaki, 2007; Ernst and Bell, 2010; cf. 'diatreme volcanoes' - Lorenz et al., 2017). Similarly, the critical role of initial emplacement pulse of the extensive Siberian Trap sill intrusions against the background of flood lava eruptions has recently been proposed by Burgess et al. (2019) for the end-Permian mass extinction (EPME). Ernst et al. (2019) demonstrated that the evolving LIP plumbing system varied between dyke- and sill-dominated, with the switches depending, among others, on the regional stress state and upper crustal structure/rheology.

4. Principal elements of present-day Earth-born multicausal KW crisis scenario

Many recent studies have emphasized that a complex combination of profound climatic and sea-level changes, including the concomitant imbalance of nutrient sources and the related anoxia levels, was the key factor in the multicausal scenario for the KW Crisis (e.g., Averbuch et al., 2005; Chen et al., 2005; Copper, 2011; Carmichael et al., 2014, 2019; Becker et al., 2016b; Ma et al., 2016; Lash, 2017, b; Zhang et al., 2020). Conversely, the evidence of coeval CO_2-driven oceanic acidification is meager (Veron, 2008; Kiessling and Simpson, 2011), even though coral bleaching was inferred from the skeletal record (Zapalski et al., 2017).

McGhee (2014) reported that the end-Famennian glaciation "erased the trace of the initial late Frasnian glaciers" and therefore propagated

the search for "ice-rafted debris in late Frasnian marine strata deposited offshore from Gondwana." Considering the lack of conclusive proof for the F–F glacial deposits, however, a leading factor of the lethal cooling has finally been resolved in a high-resolution paleotemperature signature on the basis of O_2 isotope systematics in conodont apatites (Joachimski and Buggisch, 2002; Joachimski et al., 2009; Huang et al., 2018). The runaway greenhouse-type climate mode, with surface seawater temperatures above 30 °C, was interrupted by two brief cooling pulses of ~7 °C during the KW episodes (Fig. 2).

Ma et al. (2016) clarified that large-scale regression existed on carbonate shelves in the latest Frasnian and was continued in earliest Famennian. However, this eustatic pattern is still highly debated (e.g., Dopieralska et al., 2015). For example, tectonic uplift control on the development of a paleokarst surface contradicts the simple eustatic sea-level fall in the Canning Basin of Western Australia (Chow et al., 2004; see similar data in Mizens et al., 2015, and Mottequin and Poty, 2015). Nevertheless, the 'classic' scenario of double large sea-level rise and fall (Johnson et al., 1985; Sandberg et al., 2002) is still the commonly accepted pattern.

The rapid eustatic changes suggest that polar ice caps may have ephemerally developed during the Late Devonian greenhouse climate (McGhee, 2014). Complex interplay of the orbital and volcanogenic drivers combined with expansion of vascular plants on land, particularly during Late Devonian humid episodes (Chen et al., 2005; Rattelack and Huang, 2011; Zhang et al., 2020), offers a more comprehensive explanation. An alternative aquifer-eustasy model (Sames et al., 2020) seems inapplicable in light of returning cooling episodes (Elrick et al., 2009; Pisarzowska and Racki, 2012; McGhee, 2014). Nevertheless, as outlined by Kabanov and Jiang (2020), changing the paradigm of Devonian sea level changes is an upcoming challenge.

4.1. Eutrophication and anoxia

Following Buggisch (1991) and Joachimski and Buggisch (1996), the KW-type organic-rich deposition episodes and associated distinctive CIEs can be explained by transgressive marine anoxia reaching the shelf setting and the enhanced burial of organic matter (OM; Fig. 5A). The spread of O_2 deficiency, even in shallow-shelf domains (Bond et al., 2013), was biogeochemically linked with a drawdown of atmospheric CO_2 and cooling pulses. Thus, owing to a continuous influx of multiple proxies of geochemical and ecological data, an array of research has discussed various aspects of the interplay among eutrophication, productivity and anoxia (e.g., van de Schootbrugge and Gollner, 2013; Carmichael et al., 2014, 2019; Formolo et al., 2014; Large et al., 2015; Whalen et al., 2015; Lash, 2017, b; Crasquin and Horne, 2018; Thornton et al., 2019; White et al., 2018; Kelly et al., 2019).

With respect to the available evidence, the term "anoxic event" should be substituted by "intermittent anoxic event" or "seasonal anoxic event" (Murphy et al., 2000; Racki et al., 2002). Oscillating redox states have been recently confirmed by the ichnological record (Stachacz et al., 2017; Haddad et al., 2017), and by the proliferation of benthic cyanobacterial mats (Marynowski et al., 2011; Kazmierczak et al., 2012). Paleogeographic variation in the anoxia onset and duration (Copper, 2002; Bond and Wignall, 2008; Thornton et al., 2019; Kelly et al., 2019; Percival et al., 2020) and even the persistency of mostly oxic refugia across the KW intervals is evident in some domains (George et al., 2014; Mizens et al., 2015; Racki et al., 2019). On the other hand, the thin pyrite horizon in the Bavarian slate succession (Silberberg) at the top of UKW BS (see SM 1), reported also from Rhenish and Appalachian basin sections (Over, 2002; Gereke and Schindler, 2012), suggests even euxinic conditions in the oceanic setting (Kump et al., 2005; Formolo et al., 2014). Euxinia in the photic zone has played a destructive role at least episodically (Joachimski et al., 2001).

Geochemical evaluation of the evolving weathering regimes and consequent terrigenous fluxes overall supports the punctuated greenhouse scenario (Whalen et al., 2015; Lash, 2017, b; Percival et al., 2019; Racki et al., 2019). Averbuch et al. (2005) discussed this aspect in detail by using a tectonic uplift model of the EFME (Fig. 5B). The anomalously high rate of continental weathering is proved by osmium isotope data in both KW events (Percival et al., 2019; Liu et al., 2020). This factor varies greatly in particular domains, which implies multiple triggers of spreading anoxia/euxinia (Percival et al., 2020; see also Large et al., 2015).

4.2. Undervalued tectonic control?

Tectonic factors and the plate tectonic setting have been rarely discussed in the causal context of the EFME, in particular the climate change. The trigger role of orogenic uplift, that progressed since the middle Frasnian in the tropical zone due to the developing collision of Gondwana and Laurussia (after Averbuch et al., 2005; Fig. 5B), was questioned by Copper (2011). He claimed that "the Acadian orogeny and mountain building in eastern Laurentia had started already in the Early Devonian, leaving a long lag time for such cooling. In addition, reefs can easily grow alongside coastal mountains on the eastern sides of continents (or volcanic peaks), and such effects would at best be noted only on the western margins of continents (bathed by cooler currents)" (Copper (2011, p. 26).

Frizon de Lamotte et al. (2013) developed the Eovariscan scenario of extensional-magmatic setting for the EFME. They considered "the geodynamical processes inducing the coeval development of collision along continental margins and nearby intraplate rifting and/or thermal doming" (Frizon de Lamotte et al., 2013, p. 14), analogous to lithosphere response in the foreland of Alpine compressive deformation (compare Golonka, 2020). On the other hand, Becker et al. (2018) quoted evidence of widespread seismic and tectonic events, mainly during the earliest Famennian interval. The tsunamite origin of event beds needs to be considered again (Racki, 1998; Sandberg et al., 2002; Du et al., 2008; Mottequin and Poty, 2015), as well as a question of purported oceanic overturn (Schindler, 1993).

4.3. Role of biotic factors and interactions

The Wilder–Algeo model links the F–F reef collapse to the first forests because the tree roots might have increased the weathering rate on land to mobilize nutrient elements, particularly phosphorus (Wilder, 1994; Algeo et al., 2001; Algeo and Scheckler, 2010). Although it has been accepted as a general secular trend, this scenario of "killer trees" cannot plausibly explain the recurring short-term KW episodes of less than 150 Ka (Fig. 3), as noted by Murphy et al. (2000), Racki (2005) and Percival et al. (2019, see also Lu et al., 2019; D'Antonio et al., 2019, Stein et al., 2020).Thus, a completely modified ("extrinsic") plant–climate feedback was postulated by Retallack and Huang (2011). Multiple transient expansions of intertidal to estuarine and riparian forests at times of episodic CO_2-greenhouse spikes were caused by extrinsic atmospheric perturbations. Eventually, the volcanic, Milankovitch, and other disturbance impacts toward the extreme hyperthermal state were "repaired by woodland expansion", owing to a highly effective CO_2 sink by this biological pump and anti-greenhouse feedback.

Another scarcely constrained biotic factor in the Phanerozoic mass extinctions concerns toxin-producing cyanobacterial blooms promoted by heightened temperatures, sea-level fluctuations, and eutrophication (Castle and Rodgers, 2009; van de Schootbrugge and Gollner, 2013). "Red tide" hypotheses were indeed proposed for the EFME (Ma et al., 2016), and benthic cyanobacterial communities surely proliferated (Kazmierczak et al., 2012). In addition, the spread of invasive species during the KW deepening events was postulated by Stigall (2012) as a critical cause. Even if supported by some examples among brachiopods, this proposal has not been exhaustively confirmed. Veron (2008) emphasized that "there is no credible case that supports the argument that mass extinctions had a biological cause."

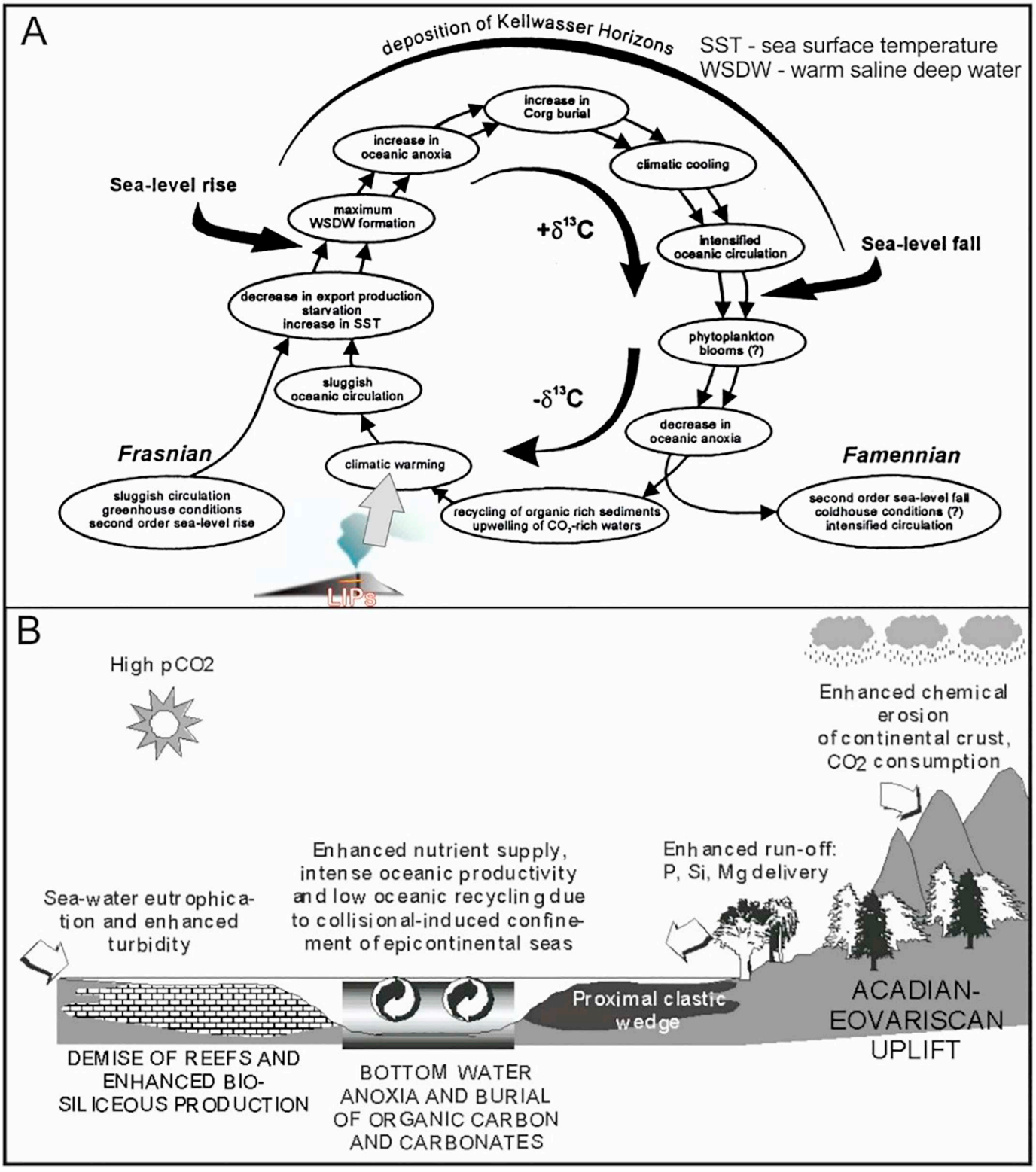

Fig. 5. Two crucial Earth-born multicausal scenarios of the Kellwasser Crisis. A – Autocyklic model of Joachimski and Buggisch (1996, fig. 3; used by permission from Georg-August-Universität Göttingen), with added volcanic trigger of climate warming (after Buggisch, 1991). B - Endogenous/tectonic scenario of Averbuch et al. (2005, fig. 8); used by permission from John Wiley and Sons.

4.4. Summary

A combination of the following broadly synchronous processes and circumstances can be demonstrated as occurring in the key EFME timespan:

- The Devonian eustatic highstand, corresponding to a long-term tectonoeustatic sea-level rise owing to a mid-oceanic thermal activity (Johnson et al., 1985; Buggisch, 1991), probably combined with the extreme interglacial epoch. The super-greenhouse ice-free climate mode, with temperatures peaking transiently up to 34 °C

(Fig. 2), ultimately led to nutrient stress (as recorded in the earliest Triassic - Bond et al., 2019; Large et al., 2015).

- Dramatic facies change including collapses of the reef biota paired with condensation and hiatuses as well as the spread of anoxia and silica-secreting biota in the basin habitats (e.g., Racki et al., 2002). A "carbonate crisis" marked an abrupt collapse in the calcite-mode epeiric carbonate factory, and a "dying stage" marked the destruction of the middle Paleozoic metazoan reefs of stromatoporoids–corals; the total $CaCO_3$ production dropped about 60–90% (Copper, 2002, 2011).
- Chen et al. (2005) and De Vleeschouwer et al. (2017) highlighted the stimulus of orbital tuning at the F-F climatic turning point. Such that the sudden orbitally tuned climate and eustatic variance is considered below to be a potentially important stress factor in the already disrupted global ecosystem.

5. Why has Late Devonian volcanic trigger been rejected thus far?

The attractive extraterrestrial scenario of the EFME finally failed as the cause of worldwide species destruction (Racki, 2012; McGhee, 2013), and therefore volcanically-driven cataclysm has slowly emerged as the leading "smoking gun" (as suspected for many years: Johnson, 1988; Racki, 1998, 2005; Courtillot, 1999; p. 95-96; Mahmudy Gharaie et al., 2004; Chen et al., 2005; Pujol et al., 2006; Courtillot et al., 2010; Kravchinsky, 2012; Ricci et al., 2013). In fact, already Sobolev (1928) gave the earliest scenario of a volcanic greenhouse-type climate for the Late Devonian evolutionary catastrophe. Buggisch (1991) postulated that the submarine "Schalstein" volcanism in the Rhenohercynian domain induced a progressive greenhouse effect that finally led to the climate-eustatic cyclicity that occurred during the KW Crisis (Fig. 5A). However, this basaltic and rhyolitic eruptions lasted only intermittently into early Frasnian time (Konigshof et al., 2010; see also Freyer, 1957; Timmerman, 2008). Alternatively, the intraplate oceanic (Panthalassan) volcanic center, consumed in subduction zones, has been guessed by Becker and House (1994).

Nevertheless, the volcanic trigger has been frequently heavily disputed owing particularly to the suppressed pyroclastic signature present in the well-studied F–F successions, in contrast to the well-known tuffite-rich beds of the D–C passage (Pisarzowska et al., 2020a). The magmatism has been considered to have rather negligible importance (Walliser, 1996; Hallam and Wignall, 1997; Becker et al., 2012), even relative to the assumed strictly tectonic controls (Averbuch et al., 2005; Riquier et al., 2006). McGhee (2013, p. 148) summarized that "both the magnitude and timing of that volcanism remain at present unproved", and this 'prejudice' is continued till now (DeLena et al., 2019; Shen et al., 2019a, b).

In fact, the following three main characteristics of the volcanic scenario remained in question.

1. *Recognition of Late Devonian LIPs*. In the only comprehensive review of the potential causal links between tectono–volcanic processes and the EFME in Anglophone literature presented by Racki (1998), global extensional pulses owing to tectonic plate rearrangement were highlighted after Veimarn and Milanovsky (1990). An alleged diverse record of mantle plume activities was indeed reported from several regions, particularly in Kazakhstan, eastern Siberia, the East European Platform, and South China. In modern synopses (fig. 1.6 and table 1.2 of Ernst, 2014; Ernst et al., 2020), two major LIPs have been reported from the Late Devonian interval: Yakutsk–Viluyi and Kola–Dnieper (see also Kravchinsky, 2012).
2. *Correlation of eruptive pulses with the KW Crisis phases*. The uncertain correlation was influenced by imprecise dating of activity in potential volcanic centers (Bond and Wignall, 2014) and that of the F–F stage boundary itself (Racki, 2005). An incompleteness of available radioisotope age ranges in LIPs has been highlighted by Kabanov (2018), who unsuccessfully attempted to link Frasnian anoxic levels with LIP activity. Nevertheless, this equivocal state has been altered by more precise timing of the stage boundary, at 371.9 Ma (Fig. 3), and by significant improvement in the radiometric geochronology of flood basalts and other magmatic records including kimberlites (Fig. 1).
3. *Reliability of geochemical proxies*. The abundance of several elements and elemental ratios are considered to reflect volcanic signals, particularly in the composition of wind-blown dust (Sageman and Lyons, 2003). These proxies, studied in the context of concurrent F–F tectono–magmatic activation, include Zr/Al, Ti/Al, Al/(Al + Fe + Mn), Mn, and Fe_2O_3 enrichments, as well as Sr isotope ratios (Racki et al., 2002, 2019; Yudina et al., 2002; Chen et al., 2005; Pujol et al., 2006; Weiner et al., 2017). These supposed tracers have been paired with scarce mineralogical data supporting volcanoclastic admixtures (Zimmerle, 1985; Yudina et al., 2002). However, alternative interpretations have been conclusively presented for these signatures, including those that contain aspects of climate, sedimentation, and provenance (Sageman and Lyons, 2003; Racki et al., 2019).

In summary, potential candidates for the F–F volcanic trigger have been recognized, and progress made during the past five years has enabled constraint of several of the doubts quoted previously. The state-of-art is discussed in sections 7 and 8 below. However, even the crude geochronological data of volcanic paroxysm must be precisely verified by a reliable volcanic signature in the conodont-dated marine successions in relation to the KW levels. Recently, Hg chemostratigraphy has emerged as a useful tool (Grasby et al., 2019). Since Racki et al. (2018a, b) published the first data on Hg chemostratigraphy applied across the F–F transition, the traditional concept of subordinate volcanic stimulus, relative to other possible causes, has been propagated with various viewpoints in three recent studies, discussed briefly below. These counterarguments serve as a starting point to discuss more proper methodology of Hg event chemostratigraphy (see section 6d).

5.1. Inconclusive Sr–Zn isotope counterevidence (Wang et al., 2018)

In a noteworthy study of Zn and Sr isotope records, conducted by Wang et al. (2018), based on the well-known F–F succession at Fuhe, South China, the volcanic scenario was rejected as a leading cause of the KW crisis, and therefore only a climatic (cooling) evidence was emphasized. However, in the work of Zhang et al. (2020), based on Sr isotope systematics in conodont bioapatites from the same section, this causal context was reinterpreted, and abrupt climate cycles are postulated in causal link with volcanic trigger. Thus, two general only aspects are outlined below in partial reference to paper of Wang et al. (2018):

1. An important question in the discussed geochemical record is the extreme (two-order) difference in residence time of the studied isotopes. Sr isotopes are thought to have long oceanic residence times of millions of years, which should make lower-resolution (not bed-by-bed) sample sets, exemplified by this study, less problematic. Nevertheless, the presented δ^{66}Zn time series is certainly biased by this sampling strategy owing to its brief residence time of 5–50 Ka (Fig. 6B). Thus, the perfectly parallel systematic variation of Sr and Zn isotope ratios is puzzling. Conversely, the presumed delay of Sr isotope ratios by more than 1 Ma, comparing with the Nd isotope values (Swanson-Hysell and Macdonald, 2017), is indeed well documented for the Late Ordovician mass extinction (LOME). Without precluding a type of regional geochemical decoupling (awaited by Wang et al., 2018; Zhang et al., 2020), however, the following alternative simpler explanations can be considered: (1) such precise chemostratigraphical coincidence is only an artifact of low sampling density and/or many discontinuities owing to intermittent event deposition (Fig. 6A), and (2) the enigmatic rapid $^{87}Sr/^{86}Sr$ positive excursions are signatures of the flux of radiogenic Sr

from the venting of hydrothermal (sedex) brines, as proposed by Emsbo et al. (2018).

2. Wang et al. (2018) assumed that negative Sr isotope shifts are diagnostic for large-scale volcanic activity. Numerous processes affect Zn and Sr isotopes, as the authors noted; however, the dominance of one process in the two systems does not negate the occurrence of other processes, such as volcanic and hydrothermal activity. Rather, this implies simply that silicate weathering had a stronger influence on the Zn and Sr cycles during the KW Crisis that overwhelmed the volcanic signal (see Figs. 7 and 11). This reservation concerns also crucial osmium isotopes, providing arguable data for the KW Crisis (Percival et al., 2019; Liu et al., 2020). In brief, volcanism as the cause of the KW Crisis cannot be ruled out on the basis of Sr and Zn data alone.

5.2. Bioevolutionary trigger only? (Shen et al., 2019b)

Shen et al. (2019b) focused on Hg chemostratigraphy in marine Ordovician–Silurian boundary sections of South China that had key implications for the EFME causes. The authors inferred that the Hg enrichments were due to the occurrence of Hg-rich sulfides, and provide no evidence of any volcanic signal. However, later Algeo and Li (2020, p. 26) concluded from compiled global geochemical database, that neither Hg/TOC nor Hg/S significantly linked with the organic and sulfide fractions, and "This is good news for the research community making use of Hg as a volcanic proxy because it demonstrates that these ratios are not significantly influenced by redox conditions and, therefore, have the potential to record other environmental information (i.e., volcanic Hg fluxes)". This conclusion corresponds well with the data from the Devonian Hg dataset (see below), and the obvious interpretation limitation can no longer be a principal contradiction (even if it is of regional importance - see also Figs. 8 and 10, LOLP environments).

In the EFME context, two arguments are quoted to preclude LIPs as a common cause of all Big Five mass extinctions because the LOME and EFME "being more protracted in duration, associated with long-term cooling rather than warming, and lacking any association to a known major LIP" (Shen et al., 2019b, p. 138). As previously discussed, the cooling interludes, that occurred during these Paleozoic biocrises, are explainable by the volcanic scenario (Cather et al., 2009; Racki, 2020b). On the other hand, it is difficult to negate any temporal links to presently known Late Devonian LIPs in the light of current datings (Fig. 1; Ernst et al., 2020). Finally, Shen et al. (2019b) reported that "these features suggest primary causes linked to massive organic carbon burial, triggered by bioevolutionary mechanisms (e.g., appearance of vascular land plants) rather than endogenic causes". As noticed above, so simple scenario is of limited significance, at least in Devonian terrestrial ecosystems.

5.3. "Weathering" Hg/TOC spikes only? (Charbonnier et al., 2020)

In state-of-the-art pioneering research on the effects of weathering and synsedimentary degradation of organic matter on the Hg/TOC volcanic proxy, Charbonnier et al. (2020, fig. 12 therein) implied that the F-F record of mercury, presented by Racki et al. (2018a, b), proves only episodes of OAE) or "environmental perturbation". The hypothesis of „weathering" Hg/TOC anomaly at Moroccan (Lahmida) locality is questionable because:

- Charbonnier et al. (2020) omitted the fact that not only OM preferentially sequestered Hg, but also clay and Fe minerals (see below). In addition, Hg can be extraordinaly enriched due to seafloor volcanic activity adjacent to the eruption site (Jones et al., 2019), and Hg-rich and TOC-poor samples can not be suspected *a priori* as recorded only the post-sedimentary factors. Thus, the Hg/TOC ratio is not the sole volcanic proxy, and it appears as indeed risky marker in light of new data.
- Post-depositional Hg redistribution and substantial enrichment in the precipitation front (Smit et al., 2016) is unlikely to be applicable to the Moroccan succession, that is marked by carbonate clay- and TOC-poor lithologies (for more about metals adsorption see Derkowski and Marynowski 2018). Thus, a specific surface desert-type (arid) weathering, supposed by Charbonnier et al.(2020), would lead to several extremely puzzling Hg enrichments (above 1 ppm), especially in the crucial biocrisis interval. Of course, the Hg/TOC ratios are certainly more (e.g., in the limestone bed LA 24/25N; Table 1) or less exaggerated due to weathering, but these 'anomalous peaks' result mainly from the high original Hg content, and not due to the secondary factors in random layers. Curiously, the Hg/TOC range between 400 and 1000 ppb/wt. %), proposed by Charbonnier et al. (2020, fig. 12) as a reliable volcanic guide for mass extinctions, only applies to Famennian horizons in the specifically Hg-enriched succession (Table 1 and SM 2).

- More importantly, any standard Hg/TOC threshfolds for "specific" mass extinction times are very risky, since the Hg cycle was differently disturbed even during increased LIP activity (Percival et al., 2018a; Fig. 8). In the context, the Hg contents and Hg/TOC ratios were disproportionately higher during episodes in the major Paleozoic biocrises than younger examples (see Racki et al., 2018a, b, DR 4). This constraint is evidenced also by very limited applicability (see SM 1 and SM 3) of the Hg/TOC anomaly threshold, i.e., 71.9 ppb/wt. %, estimated by Grasby et al. (2019).

6. When can Hg enrichment be a conclusive volcanic proxy?

The topic of anomalous Hg enrichment surprisingly flourished several years ago in the context of a new uniquely applicable volcanic marker. As discussed by Percival et al. (2018a), in contrast to Sr or Os isotopes, this proxy was notably less affected than many other elements by weathering or by marine redox chemistry. Sanei et al. (2012) were the first to introduce the Hg/TOC component which has proved vital for tracing sedimentary Hg enrichments. Many subsequent studies have reported anomalous Hg-enriched horizons from major and second-order global events, including four mass extinctions (e.g., Grasby et al., 2015; Percival et al., 2015, 2017; Jones et al., 2017; De Lena et al., 2019; Faggetter et al., 2019; Jones et al., 2019; Shen et al., 2019a, b; Them et al., 2019; Sial et al., 2020), as reviewed by Bergquist (2017), Clapham and Renne (2019) and Grasby et al. (2019). Prior to the report by Racki et al. (2018b), the EFME continued to be an ambiguous "missing link" in this chain of volcanic calamities, even if volcanogenic Hg anomalies were reported from Late Devonian black shales of Pay Khoy (north-central Russia) already by Yudovich et al. (1986).

6.1. Volcanic participation in the recent Hg cycle

Volcanic emissions are estimated to have contributed up to 20–40% of the Hg delivered to the modern Earth volatile budget, and widely distributed Hg-enriched event horizons are dictated by the explosiveness of eruptions (Pyle and Mather, 2003; Amos et al., 2014; for details see Fig. 8A). Volcanic-sourced Hg is contained mainly in gaseous injections that reach the stratosphere; extremely low contents of Hg at less than 6 ppb are found in basalts and pyroclastics owing to its incompatibility in magmatic melts (Coufalik et al., 2018). Prior to the deposition of oxygenated reactive Hg formed via rain, it can be distributed worldwide in the atmosphere because of the Hg residence time of about 0.5–2 years (Blum et al., 2014).

Hg binds readily with sedimentary OM during depositional processes, with particular effectiveness in soils and peats. However, Hg is also absorbed onto clay minerals such as montmorillonite, as well as sulfides and hydrous Fe oxides (Yudovich et al., 1986; Kongchum et al., 2011; Uddin, 2017). In marine basins, a sufficiently short residence

Table 1
Geochemical characteristics of the five samples most enriched in Hg from Lahmida, Morocco (see SM 1 and Fig. 16A). Note the different stratigraphic position and lithologic setting of the Hg excess, as well as the varied relationships of TOC and weathering-sensitive elements, combined with mostly average $\delta^{13}C$ values.

SAMPLE Lithology (position)	Hg (ppb)	TOC (%)	Hg/TOC	CaO	Al_2O_3	Fe_2O_3	S	Mo	As	V	$\delta^{13}C_{org}$
LA 14: CM (pre-KW)	1144.9	0.56	**2044**	40.2	3.49	1.93	0.09	4.6	96.8	37	-25.76
LA 24/25N: AL (UKW)	1136.4	0.16	**7103**	47.6	2.33	0.86	0.03	0.9	2.6	40	-27.06
LH 27A2 C (post-KW)	569.1	0.93	**612**	2.8	20.7	4.59	0.04	1.9	5.4	4.4	-27.29
LA 26/27: C (post-KW)	481.2	0.86	**560**	2.6	21.02	4.47	0.03	2.3	7.5	256	-27.28
LH 22: AL (UKW)	464.2	0.41	**1132**	46.2	2.08	4.48	0.07	15	23	52	-28.78
Median value in the section (n = 41)	*153.2*	*0.48*	***341***	*46.2*	*2.93*	*1.76*	*0.05*	*1.6*	*10.9*	*60*	*-27.63*

C – claystone, CM – calcareous marl, AL – argillaceous limestone

time of about 100–1000 years resulted in the stable Hg signal recorded in sediments via organo-Hg complexes (Ravichandran, 2004; Barnes, 2015). Hydrothermal venting is an additional Hg source, but mostly in areas of relatively close proximity to the source (Fig. 9 see also Scaife et al., 2017). It should be noted that hot spring precipitates contain extremely high amounts of Hg, with a maximum of 7,000 ppm reported (table 5.1 in Barnes, 2015). Percival et al. (2018a, p. 800) revealed that not all Cretaceous LIPs yield sufficiently large Hg release to perturb the global cycle, and key factors include: "submarine versus subaerial volcanism, volcanic intensity or explosivity, and the potential contribution of thermogenic mercury from reactions between ascending magma and surrounding organic-rich sediments."

6.2. Origin of Hg enrichments

Stratigraphical horizons characterized by Hg spikes have been studied intensively in geochemical terms against comparative analyses of background low-Hg sediments in particular successions. The Hg

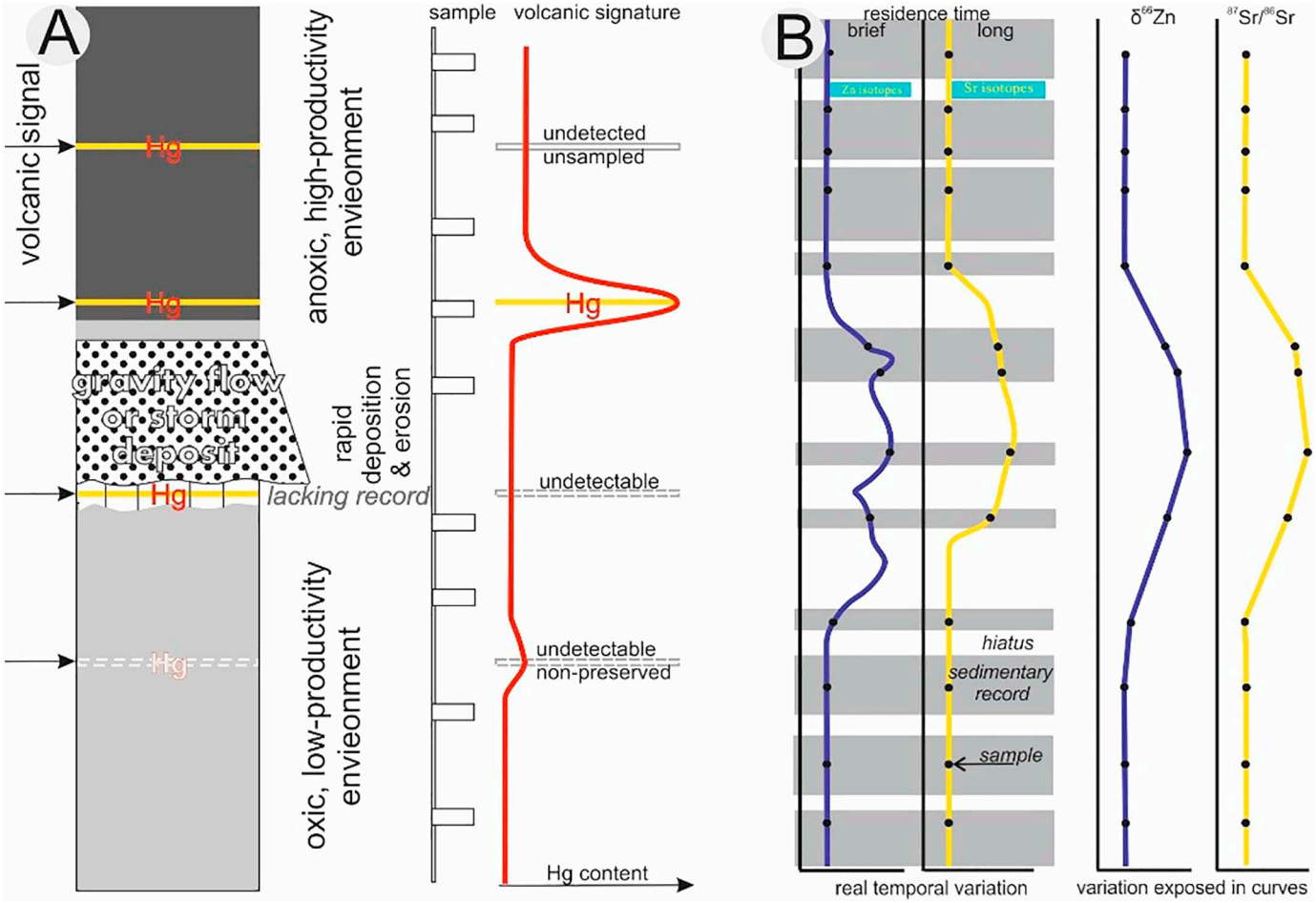

Fig. 6. Diagrammatic presentation of various constraints of the idealized geochemical record (= its interpretative potential), focused on possible detectability of volcanic signals, both Hg and paired Zn and Sr isotopes (see Wang et al., 2018), partly referred to the factual Fuhe succession (after Chen et al., 2005). A. Dominating unrecognizable volcanogenic Hg enrichments because of low-resolution sampling (compare fig. 9 in Trabucho-Alexandre, 2015), paired with unfavorable oxic environment (see below) and gravity flow deposition. B. Radically different residence time, recorded in a delay of slowly mixed isotopes (e.g., Sr; see Wang et al., 2018, table 1), cannot be clearly revealed in isotope curves in the case of essential differences of the stratigraphic completeness between background and event sediments, paired with extensive hiatuses in the critical intervals (the preserved record marked by grey fields).

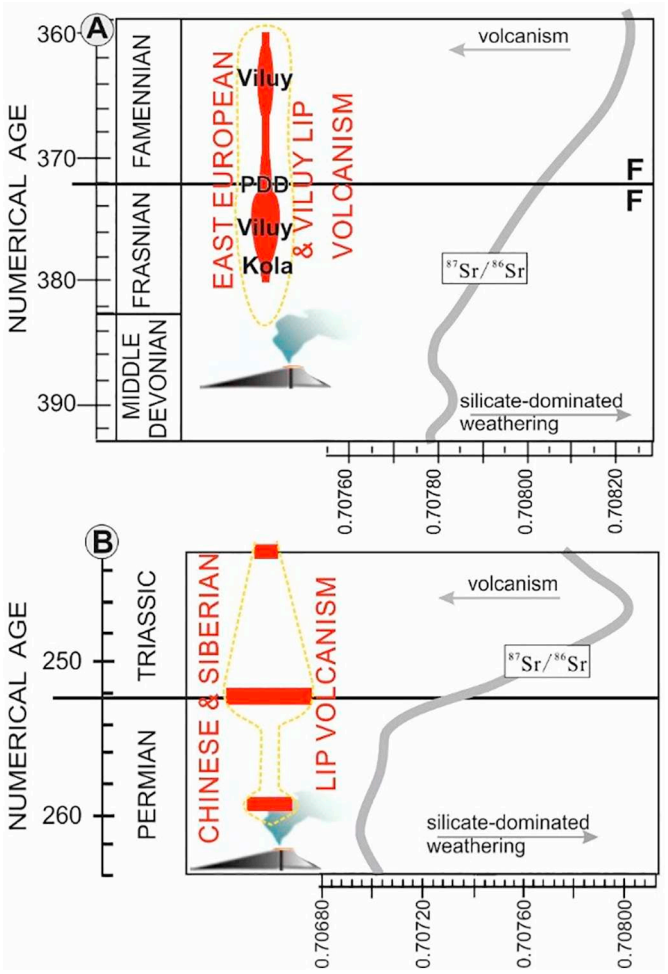

Fig. 7. Time relationships between the LIP volcanism and Sr isotope trends for (A) the Middle–Upper Devonian, and (B) Permian–Triassic transition slices. The standard oceanic $^{87}Sr/^{86}Sr$ curves are based on McArthur et al. (2012, fig. 7.2); the LIP ages in (A) and (B) are based on data from Tomshin et al. (2018) and Chen and Xu (2019), respectively. Note that even the largest Phanerozoic LIP activity of Siberian traps resulted in dubious temporal correlations with the reversal in the positive Sr isotope trend ~6 Ma after this large-scale volcanic cataclysm.

enrichments may have dissimilar origins and record not only volcanic source (Bergquist, 2017). Thus, specific features paired with greatly increased Hg accumulation can be established, particularly on host phases, as reported in the literature. The following major origins of extraordinary Hg enrichment are analysed (Fig. 10; see other Hg deposition processes in Grasby et al., 2019 and Jones et al., 2019):

- Atmospheric fallout from LIP-generated clouds and other volcanic sources (Figs. 8B and 9).
- Terrestrial delivery via runoff from weathered rocks in mercuriferous area, Hg-enriched sediments and soils. However, Kalvoda et al. (2019, p. 9) assumed the explanation that Hg, hosted primarily by clay particles, has been enriched in the marine sediments due to "an increased flux of volcanic-derived Hg from the landmass."
- Low-temperature hydrothermal activity in marine settings, exemplified by complex, multiphase origin of the giant Almadén-type cinnabar ore (Fig. 10); such unique Hg accumulation differs from that produced by a simple venting episode because was additionally associated with mafic sea-floor eruptions (Higueras et al., 2005). Excessive accumulations of several other elements (Pb, Zn, As, Co, Sb, Ni, among others) have commonly been reported in hydrothermal precipitates (Yudovich et al., 1986; Gurvich, 2006; Bagnato et al., 2017; Emsbo et al., 2018; see the D-C examples in Section 10).
- Post-sedimentary re-distribution and re-precipitation at a diagenetic front, formed by a contrast in lithology, was proposed by Smit et al. (2016) for the end-Cretaceous Hg anomaly, but never described in detail. Derkowski and Marynowski (2018) showed that the partially weathered zone exhibits different adsorption properties, compared to a pristine black shale, and when Hg is weakly only (2-3 times) enriched, Hg/TOC ratios can be increased by more than ten times; however, the Hg signal is almost completely reduced in the 'completely weathered' rock (see also Charbonnier et al., 2020).

Only the first two genetic types are considered below, and, as a prerequisite, sedimentary Hg abundances should be normalized against the TOC and other host contents (see Section 6.4). Relatively low correlation indices and elevated values of Hg/TOC and other proxies may provide evidence for the excess Hg concentrations, particularly those produced by an external Hg source such as volcanism, rather than the promotion of additional Hg burial into sediments by an increased flux of OM or other host material (Sanei et al., 2012; Grasby et al., 2015, 2019; Percival et al., 2015, 2018a). The latter case is referred to as a *pseudo-enrichment* (Figs. 10-11). Pruss et al. (2019) reported a Cambrian example of this in which abundances of redox-sensitive mineral, glauconite, and low bioturbation fabrics correlate exclusively with the Hg enrichments, what indicates oscillating redox conditions as the major controlling process of the burial. However, for reliable exclusion of the volcanic signal due to atmospheric deposition, coeval Hg spikes should be confirmed in different facies and in distant regions.

6.3. Environmental control of Hg signatures

Local or even regional Hg pseudo-enrichments may record only specific depositional conditions, which can bias the initial volcanic Hg fallout (see Fig. 11). This control is visible in varying lateral reproducibility of Hg signals in crucial crisis intervals (see the variable 'chemo-correlations' in Percival et al., 2015, Faggetter et al., 2019; Shen et al., 2019a; Sial et al., 2020). Noteworthy varying "effectiveness of different sediment types" in preservation of the Hg signal is known, "with lithologically homogeneous records documenting more clear Hg enrichments than sections with major changes in lithology such as limestones to claystones or organic-rich shales" (Percival et al., 2018a, p. 799).

Thus, the distinction between local and global Hg records is a prerequisite in event-chemostratigraphic analysis. Terrestrial Hg delivery was clearly indicated by relative Hg enrichment solely in nearshore domains (Fig. 10; see the alleged Toarcian example in Them et al., 2019). On the other hand, autochthonous marine OM could be substituted by allochtonous terrestrial organic detritus and recorded in palynofacies with an effect on Hg signature (Fig. 10; Menor-Salván et al., 2010; Jones et al., 2019). A bias by post-depositional degradation of OM is highlighted by Charbonnier et al. (2020).

Therefore, the final deductive step encompasses the different fates of the excessive Hg signal in three basic marine settings characterized by different redox and primary productivity states, including elevated bioproductivity versus enhanced preservation related to O_2 deficiency (LOHP-type vs. LOLP-type basins in Fig. 10; Sinninghe Damsté and Köster, 1998; Tyson, 2005; Brumsack, 2006; Algeo and Liu, 2020). As explicitly explained by Percival et al. (2018a): "In well-oxygenated environments where there is little organic matter, sulfide, or clays, mercury drawdown is likely to be limited." Other Hg sinks such as absorption by sulfides or clay minerals also influence the Hg sequestration, particularly in euxinic basins containing sulfidic water and in nearshore zones (e.g., Kongchum et al., 2011), but in general terms, redox conditions had minor control over Hg sequestration (as implied by Algeo and Liu, 2020). Furthermore, Sanei et al. (2012, p. 65; see also Ravichandran, 2004) clarified that "Normally the strong Hg-OM association prevents highly insoluble Hg sulfide from precipitating in marine sediments.... with the absence of adequate organic fixing

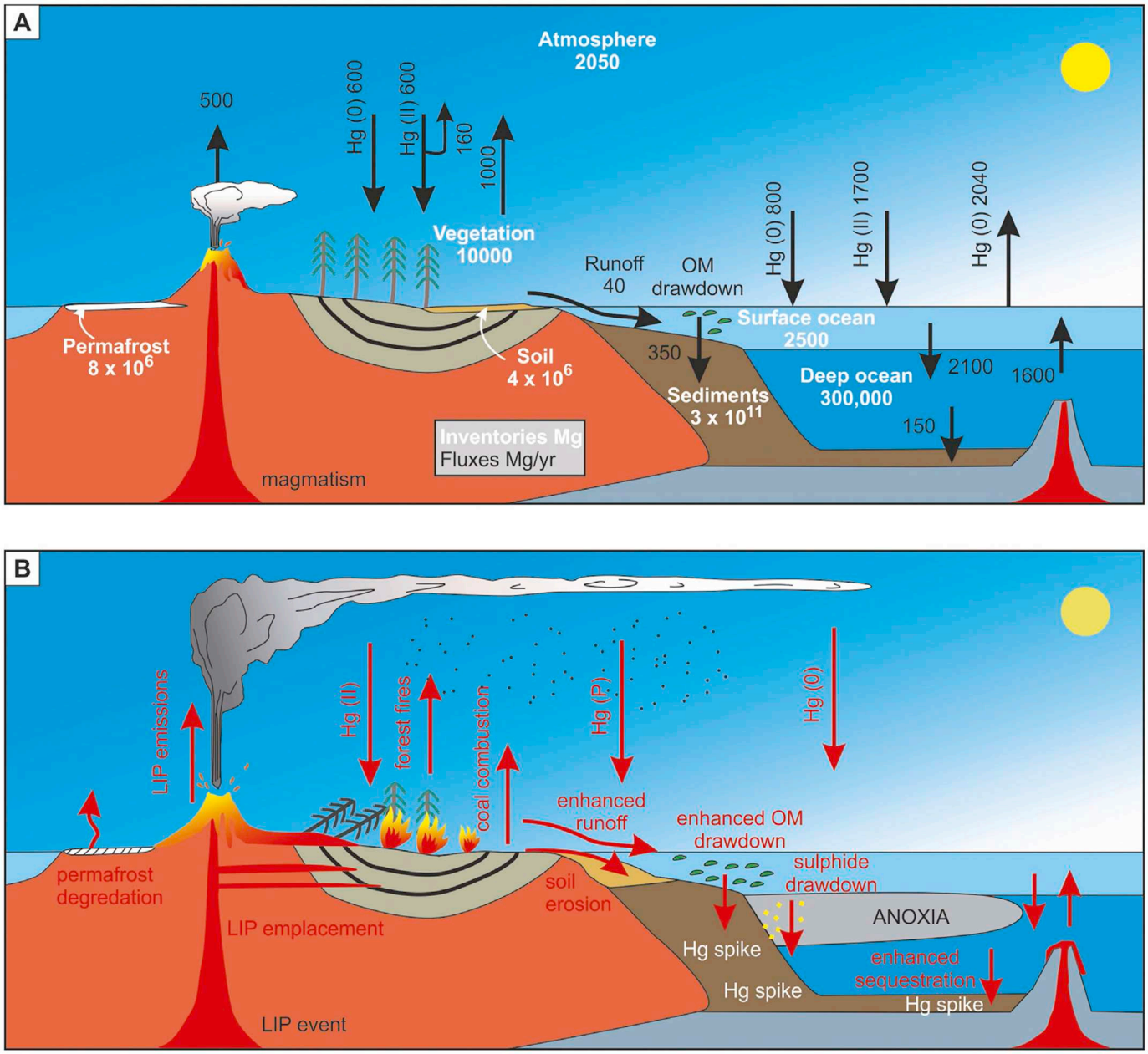

Fig. 8. The global mercury cycle under normal conditions (A) and affected by LIP eruption (B), according to Grasby et al. (2019, Fig. 1) and references therein; assesment of Hg inventories (white text) and fluxes between reservoirs (black text; see also Percival et al., 2018a, fig. 2) are shown, as well as the disruptive impact of volcanic activity (red text; see also Figs. 9-10).

capacity, and a continued accumulation of dissolved Hg, a tipping point would be reached where development of euxinic conditions allows sulfide deposition to become the dominant Hg fixation process to compensate for the failing OM Hg drawdown."

Thus, a distinction between pseudo-anomalous and real Hg enrichments requires a comparative lateral analysis (via normalization procedure) in coeval successions to trace facies overprint on the Hg signal (Fig. 11). Geochemical characteristics and elemental correlations are another useful tool because different redox states are recognizable in trace metal signatures (Brumsack, 2006; Tribovillard et al., 2006; Algeo and Liu, 2020).

6.4. Normalization procedures

The OM overload resulted in sedimentary burial of excess Hg in seawater (Fig. 11), as indicated by decreased Hg/TOC ratios (Sanei et al., 2012; Grasby et al., 2015, 2019; Percival et al., 2015; Jones et al., 2019). To evaluate other possible 'pseudo-enrichment' effects of the host, similar normalization against Al from clay minerals and Mo, S, or Fe for a potential Fe-sulfide sink is optional (SM 1).

The normalization values for TOC-poor samples (<0.2%) are unreliable owing to possible analytical errors (Grasby et al., 2019), and best treated with caution. However, the elimination of samples with such low TOC values, proposed by Grasby et al. (2019), may lead to omission of Hg enrichment cases hosted by non-OM phases Thus, another approach is preferred herein for samples with such depletion in TOC, in which the maximum acceptable value of 0.2% is arbitrarily used, to approximate the *minimum value* of the Hg/TOC ratios (SM 1 and SM3).

6.5. Recommendations for determining F–F volcanic Hg signals

In summary, individual levels rich in Hg may be heterogeneous in

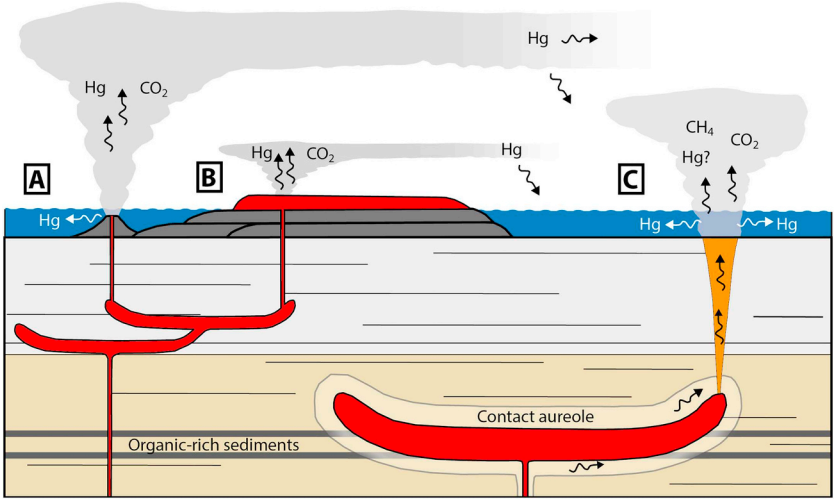

Fig. 9. Patterns showing the scale and distribution of volcanic Hg emission as controlled by various styles of emplacement within LIPs (based on the Paleogene North Atlantic case shown in fig. 2 in Jones et al., 2019, and referencs therein). Differentiation is shown between (A) shallow marine, highly explosive eruptions, resulting in wide atmospheric dispersal of Hg-rich gases and worldwide Hg signal, (B) dominant effusive flood basalt (LIP-type) volcanism, and (C) hydrothermal venting from the peripheries of sill intrusions in OM-rich strata mainly to the overlying water mass, for which only localized Hg dispersal is predicted.

individual sections, and their original origin more or less obliterated. Thus, on the basis of critical discussion on the approaches presented in recent literature, the following recommendations are proposed for more accurate recognition of volcanic Hg signals.

- *How much should the timing of LIPs overlap with the dates of global crises and events*? The definite ('robust') temporal correlation has been intensively researched (e.g., Percival et al., 2018b, 2019), and DeLena et al. (2019, p. 5) downgraded the marine Hg enrichments of Racki et al. (2018b) exclusively because their "temporal connection to any LIP activity is unclear and remains speculative". This oversized attribute of the volcanic scenario could be significantly weakened for the following three principal reasons:
  (1) The volcanic activity was not principally a direct factor of worldwide catastrophe; rather, it triggered only disastrous climatic changes and related feedbacks to generate a cascading calamity (press disturbance) effect that led to postponement in the final collapse of the ecosystem. Thus, some delay between the eruptive activity and the following global change toward ecological catastrophe is predicted (see Section 3.1).
  (2) Late Devonian intraplate and arc magmatisms are still scarcely known and understood, especially that some LIPs are inferred from only dolerite dykes (Carmichael et al., 2019; Ernst et al., 2020; Golonka, 2020). One can speculate how many LIPs have not yet been recognized, and this is also considered for subducted oceanic plateau basalts (Kaiser et al., 2016). Thus, Hg spikes can be only traceable fingerprint of 'lost' LIP activity in the stratigraphic record (Racki et al., 2018b). Partial or only conjectural temporal correlation between the LIP activity and biotic crisis is therefore sufficient rationale for hypothetical volcanic cataclysm.
  (3) Increasing causal potential of magmatic activity other than continental flood basalts is recently emphasized (Racki, 2020b; see below).
- *Only high-resolution sampling of relatively continuous successions supplies reliable Hg chemostratigraphical data*. When detecting cataclysmic episodes such as meteorite impacts or volcanic eruptions, samples should be taken at intervals of several centimeters because the signature occurs as very thin horizons on this scale (see Winter, 2015; Fig. 6A). Only sufficiently dense sampling was a prerequisite for the discovery of several Hg spikes directly below the F–F boundary in the Russian Syv'yu section, in horizons with a maximum thickness of 5 cm (see Racki et al., 2018b). Thus, the Hg anomalies are frequently detected as one-point spikes. This trivial pre-condition is frequently overlooked, but low-resolution ("lottery") analytical data preclude any negative conclusion on the volcanic stimulus. In addition, the inherent resolution flaw is controlled by the nature of the stratigraphic record; this constraint should be elucidated for each succession before planning a sampling strategy. Interpretation of hypothetical events should first consider the probability of their signal recognition for each geochemical dataset (see also Trabucho-Alexandre, 2015). Its interpretative potential is determined by both the sampling pattern and completeness degree of the stratigraphic record (Fig. 6; Miall, 2015).
- *Synchronous and worldwide real Hg enrichments occur in different facies settings*. Not all coeval localities can reveal the true abundances of excessive Hg because the dynamic interplay between volcanic signal (as a result of atmospheric Hg deposition) and the OM sequestration in particular depositional conditions (Figs. 10-11). However, at least some sections from paleogeographically separated regions and those developed in different facies should provide the real anomalous enrichments as conclusive proof of the external Hg delivery. The atmospheric source resulting from volcanic paroxysm, based on the Occam's razor, is a far more simple explanation than the alternatives offered by oceanic anoxia and/or simultaneous short-lived weathering pulses at the global scale (see Percival et al., 2019; Algeo and Liu, 2020).
- *Other indicators of magmatic activity in the key intervals are welcomed*. Mineralogical evidence is not easily provided owing to severe burial alterations of pyroclastic material such as the black shale paradox highlighted by Zimmerle (1980). In fact, Cretaceous and Late Devonian volcanic ashes are variably enriched in Hg (see Yudovich et al., 1986; Scaife et al., 2017; Pisarzowska et al., 2020a, b; SM 1 and SM3). The cryptic markers of explosive activity can be in fact present in many F–F successions (Winter, 2015). In addition, Δ^{199}Hg values close to zero, coinciding with Os- and Sr-isotope positive spikes, and C-isotope negative excursions, may be an additional tool in event–stratigraphy correlations (Emsbo et al., 2018; Grasby et al., 2019; Percival et al., 2019; Shen et al., 2019a; Schobben et al., 2019), as well as weak platinum group enrichments (Racki, 2012; Tankersley et al., 2018). The tectono–magmatic activation may in fact be manifested in a diversity of local and regional signatures (see Grasby et al., 2015), including intensive hydrothermal venting and plume dispersal of mineralizing brines, recorded primarily in sedimentary/exhalative Zn–Pb–Ba ore deposits (Figs. 9-10; Emsbo et al., 2018), but also e.g., in positive Eu anomaly (Zeng et al., 2011).

For the most cases, the proposed steps and terminology toward determination of samples evidencing volcanic signal are follow (Racki et al., 2018b; Fig. 10): (a) Hg excess above 3, (b) among them, enrichment factor for Hg/TOC above 3, and (c) among them, *Hg volcanic*

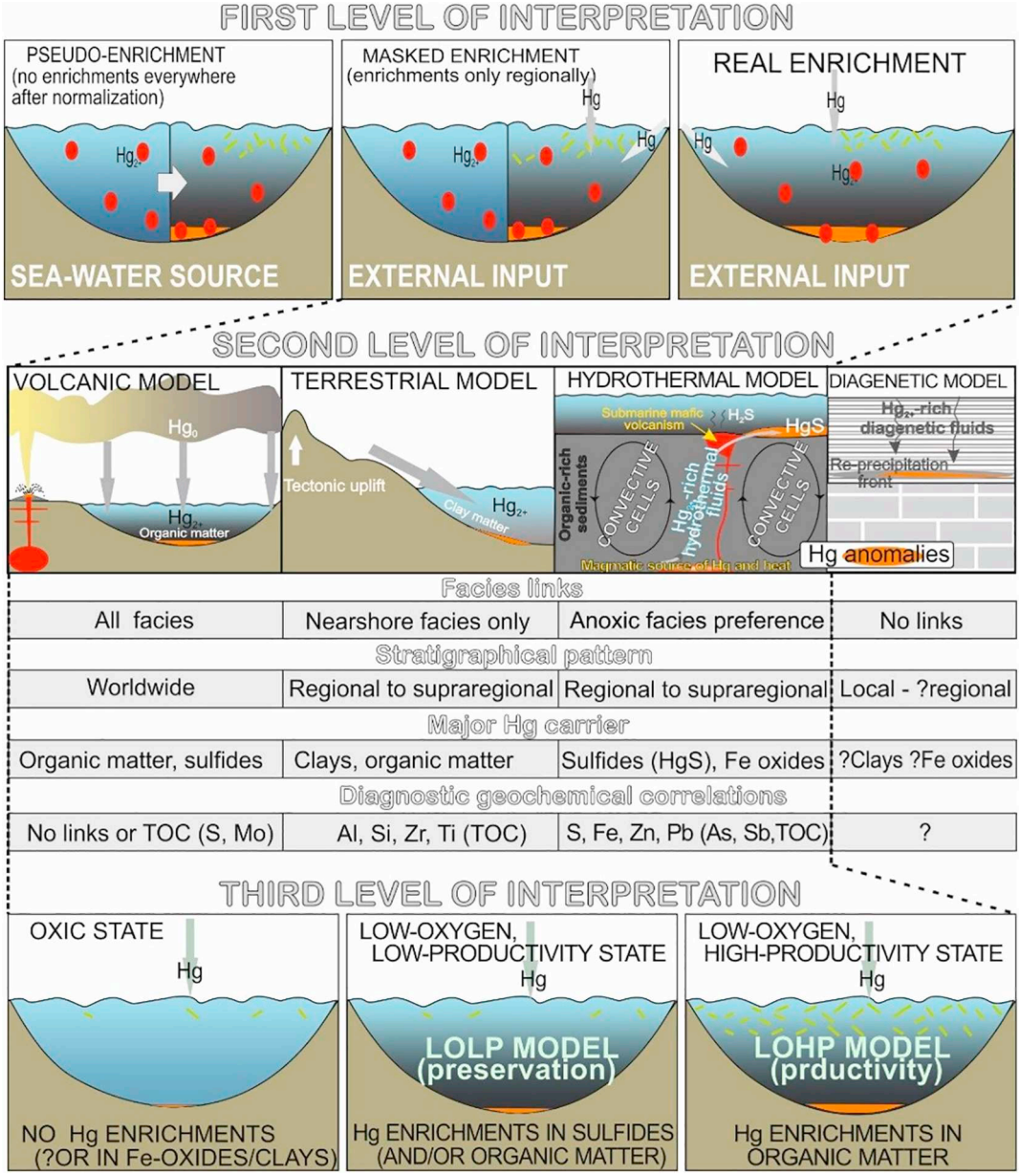

Fig. 10. Scheme of the three successive levels in the interpretation of sedimentary Hg enrichments. A key starting distinction includes (1) *pseudo-enrichments/anomalies* including also *masked enrichments/anomalies*, promoted mostly by bioproduction acme in photic zone (marked as a greening), and *real enrichment/anomalies* that recorded excess Hg sinks owing to external input; (2) main environmental models of sedimentary Hg enrichment as depicted in Figs. 8B and 9, including Almadén-type hydrothermal Hg ores (Higueras et al., 2005); and (3) a final distinction of the different Hg signatures in the three contrasting marine settings.

enrichment identified in worldwide, euryfacies and synchronous horizons (*Hg volcanic anomaly* for Hg/TOC above 10; cf. Algeo and Tribovillard, 2009). In the last steps, *Hg pseudo-enrichments*, i.e. displaying Hg /TOC enrichment less than 3, can be treated as *a masked volcanic enrichment* if this Hg/TOC impoverishment would be at most regionally recorded.

7. Current account regarding the Late Devonian LIPs

7.1. Viluy LIP

The mid-Paleozoic Siberian flood-basalt succession of the large high-latitude volcanic domain, referred to also as the Vilyui LIP by Russian authors and the Yakutsk–Vilyui LIP by Ernst (2014; Fig. 12). The traps have been considered as causal links to Late Devonian global events for almost three decades (Veimarn and Milanovsky, 1990; Racki, 1998). The current radiometric dating enables outlining of two main eruptive phases (Figs. 1 and 12B), dated by Polyansky et al. (2018) as 374.1 ± 3.5 Ma and 363.4 ± 0.7 Ma. However, Tomshin et al. (2018) reported three-step basalt emplacements corresponding to 380 Ma, 373–376 Ma (?prolonged to 368 Ma), and 362–364 Ma. An erosional Middle–Upper Devonian unconformity has recorded widespread domal uplift of ~ 500 m prior to the LIP outpouring as layered intrusions, dykes and sills, but also as subaerial lava outflows (Kiselev et al., 2012). All of the data support specifically the pre-KW eruptions in the Siberian volcanic-rift system(s), for which the total basalt volume has been roughly estimated as more than 1×10^6 km^3 (Courtillot et al., 2010), with lavas forming ~ 95 % of the volume (Masaitis, 2007).

The felsic to mafic marine volcanics of adjoined Kolyma-Omolon superterrane, described as the Kedon Formation (e.g., Gagiev, 2009; Fig. 12C), are interpreted as a record of a short-lived discontinuous continental-margin arc by Nokleberg et al. (2004), but also as a silicic-

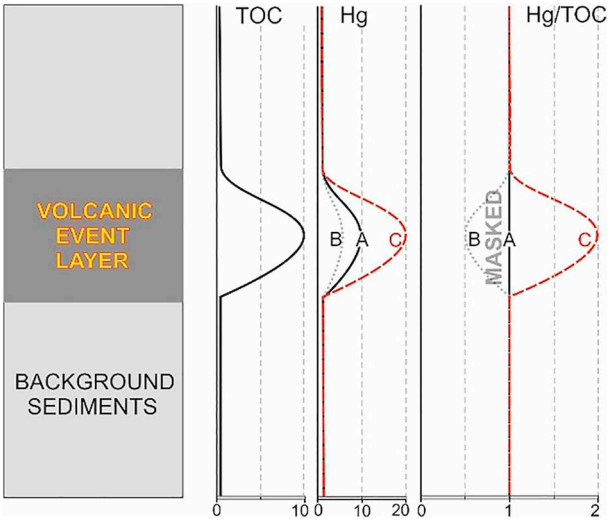

Fig. 11. Relations of Hg/TOC ratios and dynamic equilibrium between Hg and TOC content changes in the Hg-enriched volcanically overprint level. Three variants of the Hg enrichment scale are presented against the stabilized bioproductivity, approximated by the TOC. However, this volcanic signal is in fact exposed by the Hg/TOC proxy only when this increase has overwhelmed the concomitant TOC increase (variant C); conversely, decreasing ratios are promoted ('masked') by relatively large TOC abundances (variant B). The relations refer to dynamically varying processes revealed in geochemical markers such as those in the Sr and Os isotope ratios (see Section 5.1).

dominated LIP by Gagieva (2016). In the basin succession in the Stolb Island, Lena River delta, where the UKW BS level was recognized for the first time in Arctic Siberia (Yazikov et al., 2013; (Fig. 12A), no obvious volcanic evidence exists in the F–F transition. Submarine effusive activity has been reported in the Middle Frasnian in this region, which differs from the Early Famennian siliciclastic–pyroclastic delivery. In fact, in a conodont-dated limestones of the southeastern Siberian Platform, thick basaltic lavas already occur in the basal Frasnian (Baranov, 2007).

7.2. Kola LIP

The diverse alkaline complexes associated with plume magmatism, referred to as the Kola/Kontegoro LIP by Kravchinsky (2012), were emplaced in the Kola Peninsula within a total range of 387–362 Ma (Fig. 1). Considering the data of Arzamastsev et al. (2017), the basalt floods extruded between the Givetian and the Late Frasnian at 375–387 Ma, with a main pulse likely occurring at ~380 Ma. This extrusive phase was followed only by intrusive and related hydrothermal-ore activities. However, Arzamastsev (2018) distinguished also "several pulses of dyke emplacement and formation of diatremes of alkali picrite, kimberlite, olivine melanephelinite, nephelinite, and phonolite" in Late Devonian rocks between 377 and 362 Ma. Thus, the basalt effusions either signaled or coincided with the onset of the alkaline melting in the magmatic-rift system, in contrast to other LIPs (Arzamastsev et al., 2017). The Late Devonian effusive rocks were likely much less voluminous than other Late Devonian traps (Kravchinsky, 2012; Bond and Wignall, 2014), although they were also widely distributed as submarine volcanism in the basement of the Barents Sea (Nikishin et al., 1996; Puchkov et al., 2016).

7.3. Pripyat–Dnieper–Donets (PDD) LIP

The total amount of basalt in large-scale rift systems in the southwestern East European Platform is estimated be 1.5 × 10^6 km^3, and occurs as effusions in two phases in the Dnieper–Donets segment between the late Frasnian and late Famennian (Fig. 13A; Nikishin et al., 1996; Wilson and Lyaskovitch, 1996; Kravchinsky, 2012). Explosive volcanism was dominant at the Frasnian emplacement stage, with pyroclastic material forming 70–90% of the igneous succession (Wilson and Lyaskovitch, 1996). In fact, the basal Famennian pyroclastics in Central Europe, specifically the Scorpius group of Winter (2015), are linked with the westward ash dispersal from the PDD LIP (Fig. 14). This prolonged intermittent tectono–magmatic reactivation, associated largely with carbonate–evaporitic sedimentation, may be uniquely correlated with conodont zonation. In the Pripyat Trough, the Middle Devonian to Frasnian intrusive bodies are followed in succession by differentiated volcanics including Yevlanovo to Petrikov regional stages (Aizberg et al., 2001), containing Late *rhenana* to *rhomboidea* zones (Strelchenko and Kruchek, 2013). The Upper Frasnian volcanics "are

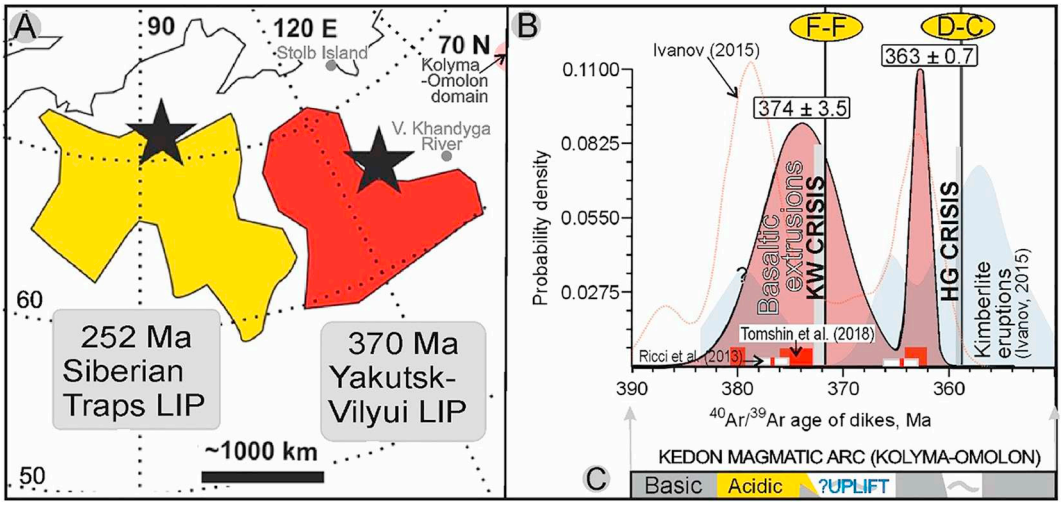

Fig. 12. (A) Regional distribution of the EFME- (Yakutsk–Vilyui) and EPME-related Siberian LIPs (plume centers marked by stars; after Ernst et al., 2018a, fig. 7B), and location of nearby conodont-dated sedimentary Upper Devonian sections (grey circles; Baranov, 2007; Yazikov et al., 2013). (B) Statistical analysis of radiometric Ar isotope dating of the Viluy dykes, exposing the bimodal temporal distribution of trap-type eruptions after Polyansky et al. (2018, fig. 3B; Fig. 1), against the LIP timing after Ricci et al. (2013), Ivanov (2015, fig. 2), and Tomshin et al. (2018), and kimberlite dating after Ivanov (2015, fig. 2), respectively. (C) Evolving igneous activity (continental arc or SLIP?) in the Kolyma-Omolon domain (see Fig. 12A), interpreted from fig. 3 of Gagiev (1997), against the eruptive phases of Viluy LIP.

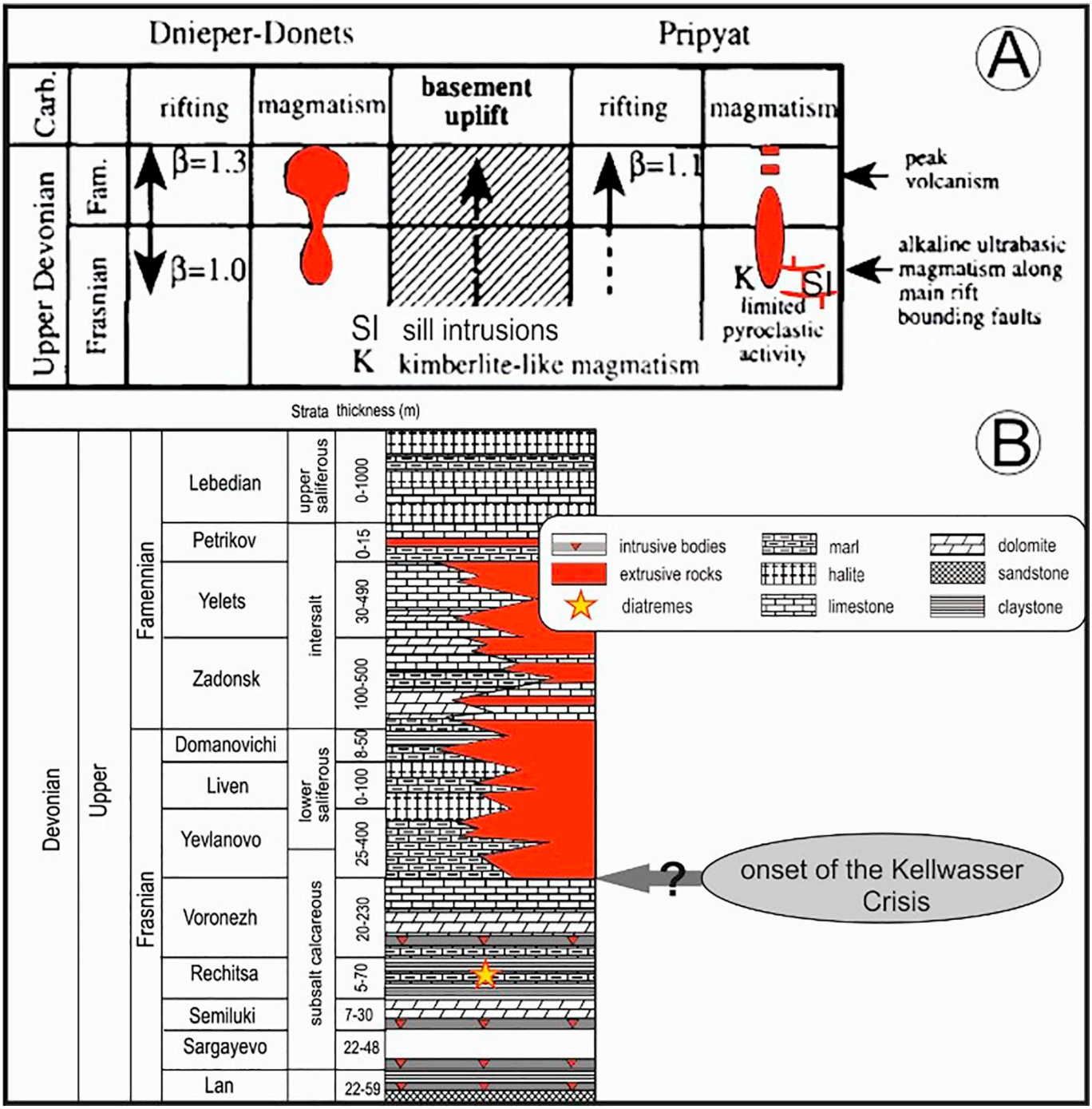

Fig. 13. (A) Timing of rifting, volcanism, and basement uplift in the PDD rift system, showing secular differentiation of the phenomena between the Pripyat and Dnieper–Donets segments (adapted fig. 2 of Wilson and Lyashkevich, 1996, modified after data from Aizberg et al., 2001). (B) Lithostratigraphic log of the Upper Devonian succession in the Pripyat Trough; note extrusive eruptions across the F-F boundary interval, preceded by pre-KW intrusive activity (modified fig. 3 of Aizberg et al., 2001). The initial outpouring of flood basalts likely correlates with the onset of the KW Crisis (Figs. 1 and 3; for conodont datings see Narkiewicz and Narkiewicz, 2008).

mainly of intermediate composition (subalkaline and alkaline trachytes, trachybasalts and syenite porphyrites) and are represented by explosion, effusive, pipe and subvolcanic facies" (Aizberg et al., 2001, p. 352). Abundance of intrusive bodies, mainly sills up to several tens of meters thick, is another notable character of the Pripyat rift, with two maxima in Givetian to early Frasnian and in late Frasnian (Rechitsa-Voronezh horizons, mostly Early *rhenana* Zone; Aizberg et al., 2001).

The PDD rift–volcanic system is usually linked with a mantle plume with its center located at the intersection of the Dnieper–Donets rift and the Uralian swarms (Puchkov et al., 2016). The last structure of the 370–377 Ma age is possibly even ~2300 km long because it can be traced along the Ural Mountains to the Pay–Khoy–Novaya Zemlya fold belt. According to Stepanenko (2016), the ages of the traps in the northern Timan–Pechora region correspond to the F–F transition interval at 374–367 Ma. At the northern Arctic ending, the sea-floor basalt lavas occur in the lower half of the Frasnian stage in Novaya Zemlya and are hosted by shallow-marine clastics (Guo et al., 2010). Yutkina et al. (2017) summarized other Givetian to the Late Frasnian

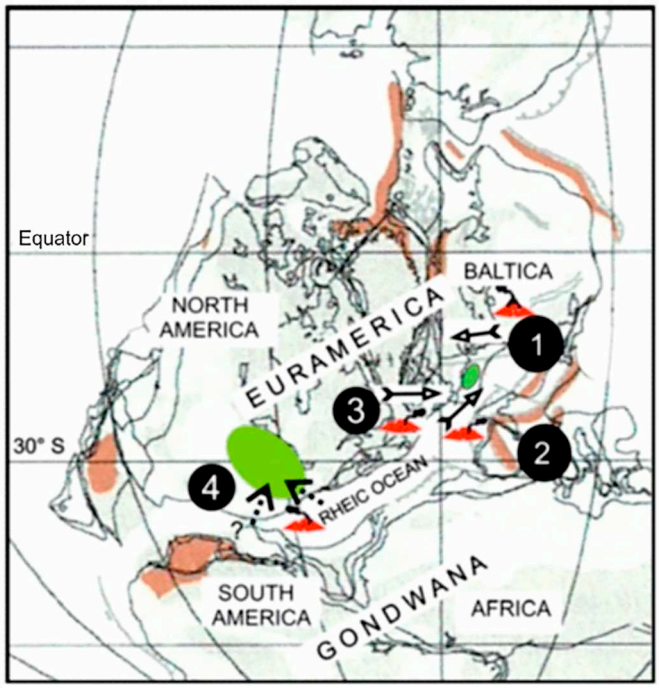

Fig. 14. Geotectonic setting of Late Devonian volcanic ashes in Central Europe (fig. 17 from Winter, 2015; used by permission from E. Schweizerbart'sche Verlagsbuchhandlung; see also Fig. 15); paleogeography modified from Golonka (2000); collision belts (brownish), distribution areas of air-fall ash layers (green), eruption centres and directions of aeolian transport (black arrows); ash chronohorizons (= eruptive events; Fig. 2): 1 = Scorpus, 2 = Sextans, 3 = Pegasus, 4 = Center Hill Ash, USA (Over, 2002).

magmatic centers from the central and eastern East European Platform, particularly in the Vyatka (Kirov–Saratov) trough (see also fig. 10 in Nikishin et al., 1996).

Thus, the igneous domain was undoubtedly the largest Late Devonian LIP. Puchkov et al. (2016) reinterpreted the Kola–Dnieper and Yakutsk–Vilyui LIPs as a joint record of a single superplume mega-eruptions (see also Ernst et al., 2020).

7.4. Other alleged LIPs

Several Late Devonian igneous domains of different types may be considered (Racki, 1998, 2005; Veimarn and Korneeva, 2007; Ernst et al., 2020), as listed below.

- Laurentian Maritime (Magdalen) LIP, a conjectural continental/silicic LIP "fragment" in eastern Canada (Ernst, 2014), dated roughly as 360–370 Ma. The Famennian age was confirmed by palynostratigraphy (Murphy and Keppie, 2005; Dessureau et al., 2007). Ernst et al. (2020) distinguished two magmatic pulses at 380-370 Ma and 360 Ma.
- Several occurrences of poorly dated basaltic series in central Asia. For example, rift-related sub-alkaline magmatism during the tectonic rebuilding of the Kazakhstan plate was initiated in the Late *rhenana* zone. This activation was recorded by extensive uplift, volcanogenic deposition, and giant stratiform Fe–Mn and polymetallic ores (Veimarn et al., 1997; Racki, 1998; Veimarn and Korneeva, 2007).
- Thick submarine basalt series occur in northern Iran (Wendt et al., 2005; Ghomalian, 2007). For example, lava flows up to 400 m in thickness occur in the Late Devonian carbonate–siliciclastic Geirud Formation in the central Elburz Mountains and in Azerbaijan.
- A complex rift system is assumed to be the tectonic setting for the South China shelf basin (Bai et al., 1994). Various forms of volcanic activity include basaltic effusion associated with the opening of the Paleotethys Ocean (Guo et al., 2004) as well as hydrothermal-exhalative venting and mineralization (Chen et al., 2005; Zeng et al., 2011; Ma et al., 2016).

7.5. Magmatic arc activity

Probably four domains of arc explosive eruptions in the Late Devonian are recognizable in Central European volcanic signatures (Fig. 14). Winter (2015) described numerous metabentonites that appear to constitute a record of intensified alkaline volcanism during the KW Crisis. The ashes originated largely from "volcanic islands of a subduction front caused by the closing of the Rheic Ocean between Gondwana and Euramerica" (Winter, 2015, p. 228). Graham et al. (1995) reported Late Devonian silicic and alkaline volcanic activity in the Munster Basin in southwest Ireland. Supplementary unidentified intra-oceanic(?) eastern source for the Late Frasnian Sextans pyroclastics is notable. In this context, the intensive mineralizing activity that occurred in the Rheic (Rhenohercynian) oceanic domain as a result of accelerated northward subduction is understandable (Raumer et al., 2017).

On the other hand, tuffite horizons in an interval dated as approximately late Frasnian have been reported in northwestern Turkey (Eastern Taurides) by Göncüoğlu et al. (2016) and Çimen (2018). The authors linked the pyroclastics with the South Urals, where coeval colliding arc island volcanism is widely regarded to have originated from the Magnitogorsk Zone (Pravikova et al., 2008). However, only rift basalts are reported from the conodont-dated F-F transition by Artyushkova and Maslov (2011, fig. 1).

Furthermore, different scales of hydrothermal venting along the back- and fore-arc spreading centers, resulted in well-known mineral resources occur in some other regions, e.g., in Kazakhstan (Racki, 1998) and Spain (Moreno et al., 2018). Emsbo et al. (2018) reported several Zn–Pb–Ba ore deposits of 379 to 373 Ma in the Selwyn Basin of Canada (see Ernst et al., 2020).

7.6. Carbonatite/kimberlite outbursts

Tremendously explosive carbonatite–alkaline magmatism and the associated kimberlite-type eruption blooms are potentially a far more effective factor in the volcanic cataclysm scenario than recurrent flood basalt extrusions (Ray and Pande, 1999; Isozaki, 2007). This rare variety of intraplate magmatic activity (Ernst, 2014; Ernst et al., 2019) occurred in all three main Frasnian LIPs (Fig. 1). Ray and Pande (1999) discussed the catastrophic impact of relatively minor carbonatite–alkaline activity within the Deccan LIP, whereas large-scale CO_2- and SO_2-rich expulsions from the huge Kola alkaline domain occurred undoubtedly during the Late Devonian (Wall and Zaitsev, 2004).

Kimberlite pipe swarms have been dated at 380–375 Ma in the Archangelsk diamond province (Yutkina et al., 2017), i.e., the pre-KW interval. The Livaara alkaline series of the Kola LIP intruded at 373–363 Ma (O'Brien et al., 2005), and Arzamastsev (2018) timed this magmatism as occurring between 377 and 362 Ma. Ivanov (2015) and Ernst et al. (2018a) placed the Viluy kimberlite intrusions in a prolonged Late Devonian interval although not at the EFME time (Fig. 12B). Onset of the KW crisis seemed to be close to alkali ultrabasic kimberlite-like eruptions in the Pripyat Trough (Fig. 15A; Sheremet, 2014); however, the conodont dating of diatreme-related Rechitsa Horizon appears rather poorly constrained, and this alkali ultrabasic event could precede the KW interval (Narkiewicz and Narkiewicz, 2008). In addition, Torsvik and Cocks (2017, p. 141, fig. 8.3) placed the East Australian intrusion of kimberlites at 382–367 Ma and sourced them from a Pacific mantle plume. Extrusive and intrusive activity is also shown for the western and southern North American segment of the Laurussian subduction zone, including kimberlite eruptions at ~370 Ma (fig. 8.6 in

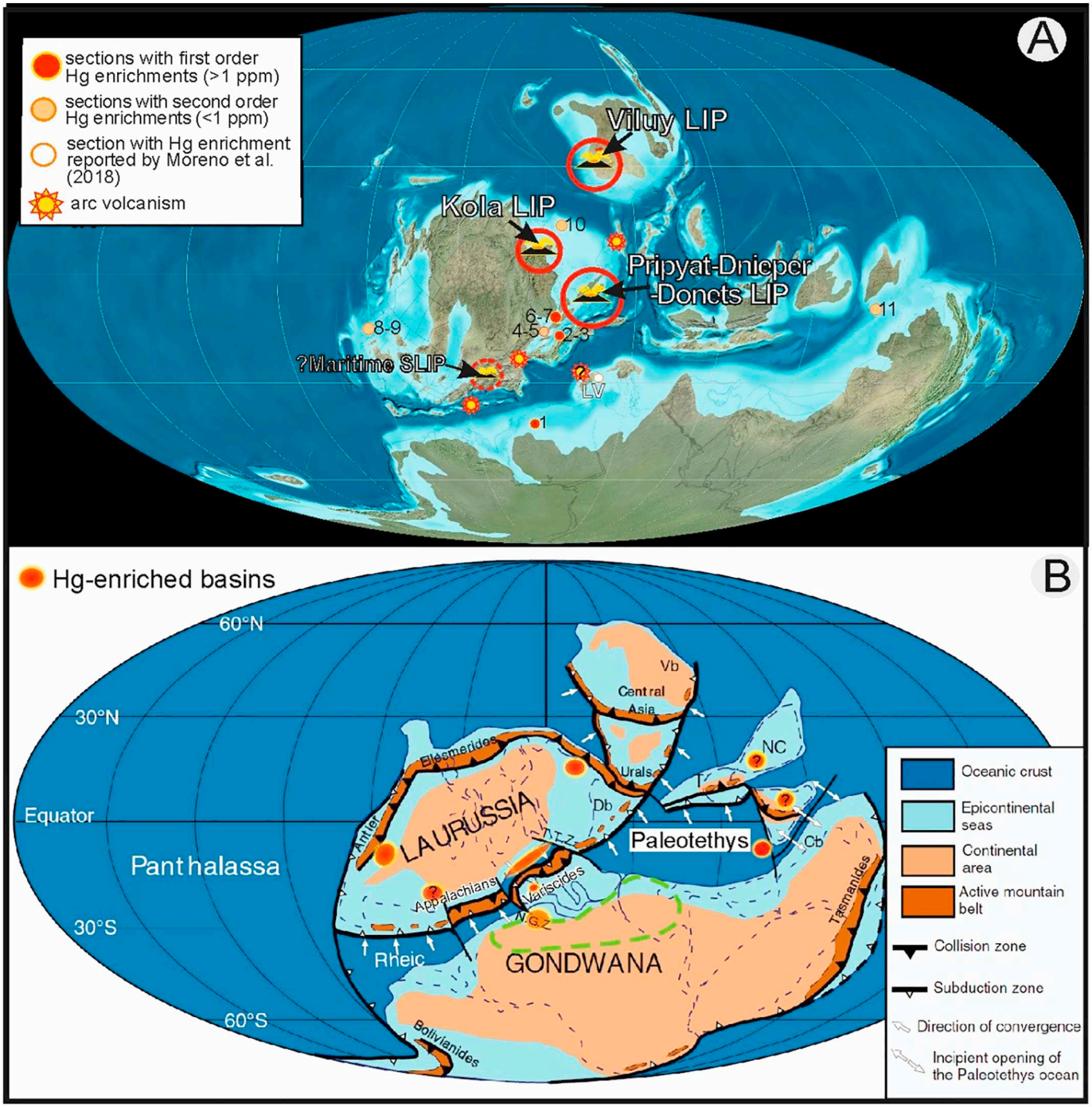

Fig. 15. A. Approximate location of the F–F sections (see Table 2 and SM 1), ranked in terms of Hg enrichment compared with assumed areas of coeval large-scale igneous activity (after Kravchinsky, 2012, and Ernst, 2014; paleogeography after Blakey, 2016; compare Golonka, 2020). 1. Lahmida (Anti-Atlas, Morocco), 2. Silberberg (Bavaria, Germany), 3. Kahlleite (Thuringia, Germany), 4. Junge Grimme (Rhenish Massif, Germany), 5. Wisenberg (Rhenish Massif, Germany), 6. Psie Górki (Holy Cross Mountains, Poland), 7. Kowala (Holy Cross Mountains, Poland, 8. White Rock Canyon (Nevada, USA), 9. Devil's Gate (Nevada, USA), 10. Syv'yu River (Subpolar Urals, Russia), 11. Mae Sariang (Thailand); LV: Less Vilelles (Spain; Moreno et al., 2018). B. Currently known Hg-enriched areas (undocumented data with question marks) against a global Late Devonian paleogeodynamic reconstruction (after Frizon de Lamotte et al., 2013, fig. 11 used by permission from John Wiley and Sons), showing the incipient collision of Gondwana and Laurussia and thermal uplift and coeval rifting (outlined with a green broken line) in north Gondwana (N.G.Z - Newfoundland–Gibraltar transfer zone, T.T.Z. - Teysseire-Tornquist Zone; T - Tarim block. NC - Northern China block, Db - Dnieper-Donets basin, Vb - Viluy basin, Cb - Canning basin).

Torsvik and Cocks, 2017). It brief, even if the dating and volume relations of intrusive versus extrusive eruptions remain inadequately understood, carbonatite/kimberlite paroxysms can tentatively be implied as a key to the EFME puzzle.

8. Hg anomalies in the worldwide F–F perspective

Can the elements of Earth-born scenarios of the KW Crisis, as summarized in Section 4, be explained by the volcanic press-pulse model? Becker et al. (2016b, p. 4), in their summary of the current multicausal model, recapitulated that "sudden climate change appears

to have been the most important common trigger, possibly linked with episodes of massive volcanism and times of significant drawdown of atmospheric CO_2." Benton (2019, p. 84) also presumed that the EFME was driven by "series of major volcanic events, where great volumes of lava were spewed out over parts of Russia." Therefore, this inescapable trigger has been clearly identified and requires only factual enhancement. The prerequisite involves reliable recognition of Hg enrichments (see Qie et al., 2019).

Since 2015, the University of Silesia, Sosnowiec, Poland, has established a collective database for Hg abundances determined initially by inductively coupled plasma mass spectrometry (ICP-MS) for 17 F–F sections in different regions of the world, and later refined for 9 sections by atomic absorption spectroscopy (AAS; Racki et al., 2018a). Eleven locations were taken into account because of the Hg enrichment pattern (see SM 1 for analitycal data).

Several variously recorded anomalous Hg spikes were found in 11 sites (Fig. 15A, Table 2). In four localities, first-order anomalies occurred above 1 ppm (Fig. 16), with a maximum value of 8 ppm recorded at the Psie Górki site in the Holy Cross Mountains, Poland. Moreno et al. (2018) also reported a highly enriched interval with 1.57 ppm Hg in the assumed UKW level in the Less Vilelles section in Catalan Spain; they interpreted this anomaly as a signature of hydrothermal activity. In addition, "high mercury signals (3x median) immediately preceding the Lower and Upper Kellwasser in multiple localities" have been signaled from northern Appalachian basin (Upstate New York) by Estrada et al. (2018); with the exception of one LKW enrichment, the Hg enrichments are obscured in Hg/TOC ratios.

Centimeter-sized sampling intervals enabled recognition of at least five Hg volcanic enrichments in the UKW interval only in the Syv'yu River section (Fig. 16B). Therefore, single Hg spikes in other Upper Frasnian successions are probably the manifestation, at least in part, of insufficient sample density and stratigraphic incompleteness (Table 2), what excludes any correlative attempt. Furthermore, the Syv'yu site represents stratigraphically continuous deep-shelf hemipelagic facies with high interpretative potential. Conversely, intra-regional Hg data from six sections in the South Polish-Moravian shelf (see Racki et al., 2002) revealed extremely high (Psie Górki) or low (Kowala) Hg excesses only at these two sites. This somewhat surprising pattern was definitely influenced either by sampling or stratigraphic record weaknesses, exemplified by the highly condensed UKW limestone of the Płucki section. Oscillating deoxygenation processes in localized Kowala basin (Racki et al., 2002), and in German parts of Rhenohercynian domain may have caused relative Hg impoverishment in bottom sediments (see SM 2). Two Asiatic F–F sections have not provided support for any volcanic signal owing to the dominantly oxic depositional regime at the Thai Thong Pha Phum site (see Fig. 10; Racki et al., 2019) or to the severe weathering imprint on the organic-rich biosiliceous strata at the Chinese Bancheng site. However, the coeval Hg spikes have recently been recognized in South and North China continental blocks as well (J. Shen, e-mail comm., 2019). Other volcanic tracers are likely related with the Hg spikes only at Kahlaite and Kowala, and are well evidenced in the Syv'yu locality only (Yudina et al., 2002).

Even if the sedimentary Hg excess can mostly be demonstrated around Paleotethyan oceanic domain, they have also been found widespread in distant shelves of the large Laurussian continent (Fig. 15). In addition, the facies spectrum is very wide, spanning from coastal and near-reef foreslopes of Less Vilelles and Psie Górki, respectively, to deep-shelf settings, including White Rock, Lahmida, Kahlaite, and Syv'yu, as well as to oceanic settings exemplified by the Silberberg locality.

The most frequently recognizable and prominent Hg volcanic anomaly occurs worldwide in the UKW level just prior to the F–F boundary, likely at nine localities studied (Fig. 16; Table 2). This key signal is tentatively referred to as the Center Hill (CH, Fig. 2) after the Laurentian explosive episode (= an initial event of longer-lasting Scorpius Group activity; Winter, 2015, fig. 2), which highlights the hypothesis of synchronous global LIP and arc magmatic pulse (see below). The results of normalization confirm the varying relations among primary productivity, anoxia, and Hg input (Fig. 11), although the CH volcanic signal is significantly masked by the rapidly increase in primary production in the LOHP basins at Silberberg (Fig. 16E) and Junge Gerimme. The Hg values also reveal different correlation links in particular sections, with more or less reliable determination of the major hosting phases in some sites, i.e., TOC (Silberberg) and sulfide-tracing S and Mo (Junge Grimme; ?Winsenberg), and with Al and Mo (both American sections; ?Kahleite). Unexpectedly, reef-derived talus may have preserved the large-scale Hg spike (Psie Górki; Fig. 16C), but maybe associated with geothermal venting in a seismically active area (Szulczewski et al., 1996; Szrek and Salwa, 2020). Such extreme Hg anomaly in pure limestone is somewhat enigmatic and requires more refined data (see the similar D-C case from Uzbekistan in Racki et al., 2018a), but note a pioneer insight in biogenic carbonate Hg in Meyer et al. (2019).

In brief, the proven worldwide and euryfacies distribution of the Hg enrichments has been preserved in particular stratigraphic intervals of KW Crisis (Table 2), even if the global volcanic signal has probably been biased or overwhelmed by more localized processes in some sites.

8.1. Eruptions, uplifts, and weathering fluxes versus climate modes

In light of the Hg spikes documented worldwide, other expected causal links and feedbacks may be considered in terms of the volcanism-forced greenhouse/icehouse model (Fig. 4). In the most simplified prediction, LIP outpouring should correspond to greenhouse episodes, while relative quiescence and outgassing decrease in the provinces resulted in an overall cooling trend and dominance of the non-volcanic feedbacks.

With two principal dates given as 371.9 Ma for the F–F boundary and 372.7 Ma for the commencement of the LKW, a peak in Frasnian igneous activity evidently occurred simultaneously in the three main LIPs before or at most near the onset of the KW Crisis, as noted already by Percival et al. (2018b; Figs. 1 and 3). More precisely, pulsed LIP activity lasted from ~ 380 Ma, and only PDD LIP and likely other less-known Eastern European centers were initiated near the onset of biocrisis (Fig. 13B). Racki (1998), Veimarn and Korneeva (2007), Frizon de Lamotte et al. (2013) and Golonka (2020) summarized the literature on tectonic activation in the KW interval, focusing on rifting phenomena and related tectonic uplifts in extensional regimes. The events were geodynamically linked to the Eovariscan orogenic phase due to initial Laurussia-Gondwana collision, also initiated in the pre-KW (*hassi-jamieae*) interval (Fig. 5B; fig. 2 in Averbuch et al., 2005). In the context, Koglin et al. (2018) reported the Frasnian (~ 375 Ma) stacking of the four Bavarian nappe units in accretionary wedge of the Rheic Ocean.

The combined uplift processes have conceptually been recently developed as a tectonically promoted rapid increase in weathering rates on continents and terrigenous input to the marine basins. The weathering pulses that overall preceded both KW events, were recently proved by osmium isotope signatures even though several processes may have contributed (Percival et al., 2019; Liu et al., 2020). In the EFME climatic context, runaway greenhouse simulation via volcanically emitted CO_2 may have been critical for the accelerated hydrologic cycle and the increased terrigenous delivery to marine basins (also characterizing other major crisis intervals, e.g., EPME - Cao et al., 2019). However, this volcanic summer loop may finally have reached a threshold level due to, e.g., kimberlite-like eruptions at least in the PDD (Fig. 13A). The assumed pulse disturbance on the already high pressed global ecosystem might have caused a reversed climatic trend combined with regressive sea-level change (Fig. 5A). If so, two major autocycles may explain the eustatic/climate pattern during the entire KW Crisis, with the final pacing due to orbital forcing, as postulated by De Vleeschouwer et al. (2017).

Nevertheless, the extrinsic stimulus by volcanic phenomena may

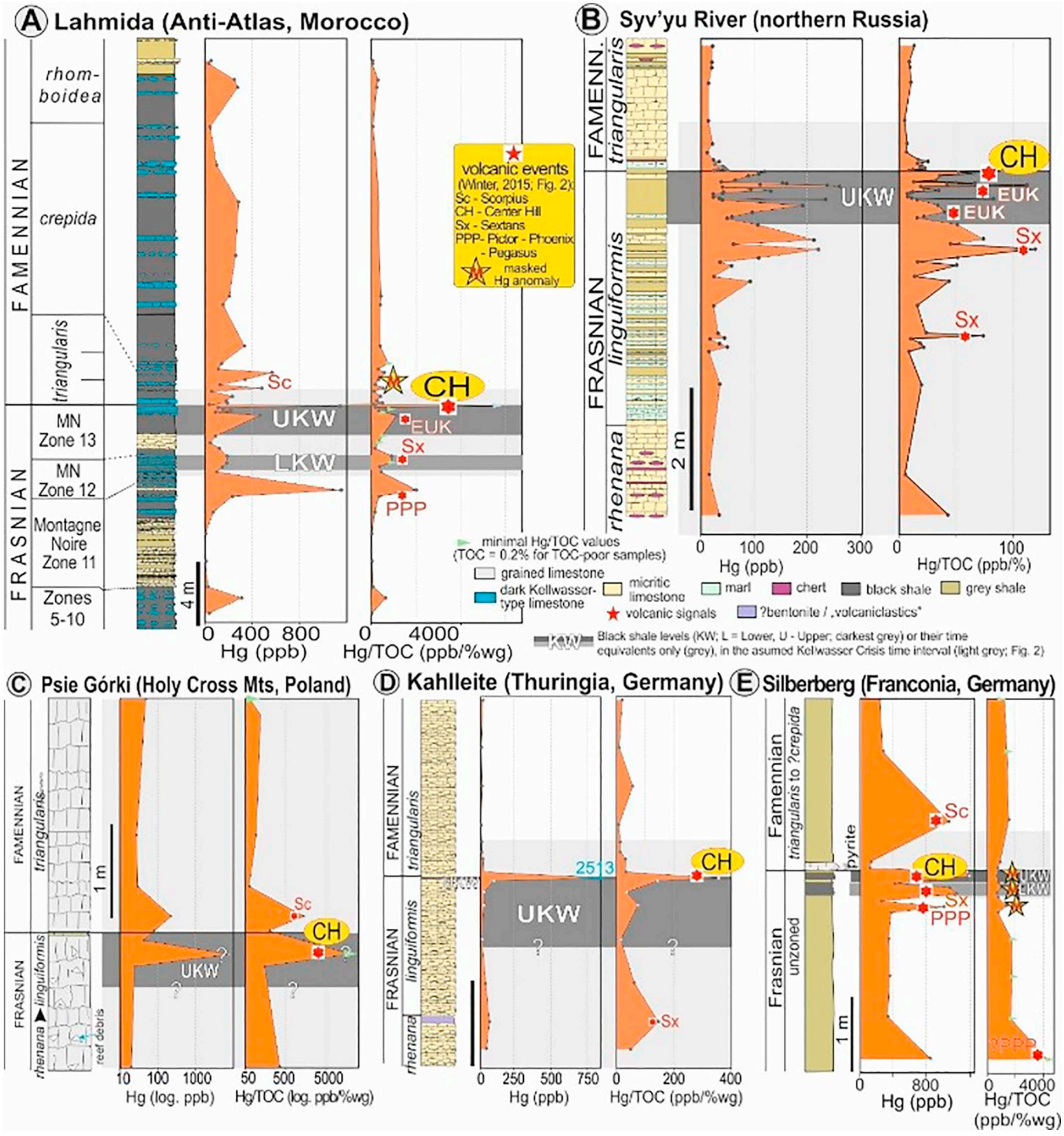

Fig. 16. Five reference F–F sections located in (A) Morocco (after Dopieralska, 2003), (B) north-central Russia (after Yudina et al., 2002), (C) Poland (after Bond et al., 2004), and (D-E) in Germany (see Gereke, 2004, and SM 1,respectively). Highlighted are the Hg enrichments in the KW Crisis interval (fig. 2 in Racki et al., 2018b) and their hypothetical correlation with volcanic events distinguished by Winter (2015; Fig. 2); in (C) the logarithmic scales of Hg and Hg/TOC are given. Very different lithologies and the widespread CH volcanic signal occur just prior to the crucial F–F boundary (note the masked Hg spike at the Silberberg succession; see Figs. 10-11).

also be assumed for the second half of the KW Crisis. In addition to the widespread CH volcanic signal, the hydrothermal mineralization pulses are also well evidenced by the key EFME interval (Racki, 1998, 2005; Veimarn and Korneeva, 2007; Emsbo et al., 2018). In particular, CO_2 spikes and greenhouse interludes during both KW episodes, postulated from soil archives by Retallack and Huang (2011), obviously may be seen as a response for magmatic degassing (see Chen et al., 2005 and Zhang et al., 2020). The anti-greenhouse feedback and climate balancing by recurrently expanding wetland forests has been proposed as an effective mechanism of CO_2 sink during the entire Late Devonian epoch (Retallack and Huang, 2011). Widespread wildfires and soot surplus as additional icehouse driver (Fig. 4) remain not reliably evidenced till now (L. Marynowski, e-mail. comm., 2020), conversely to inference of Liu et al. (2020).

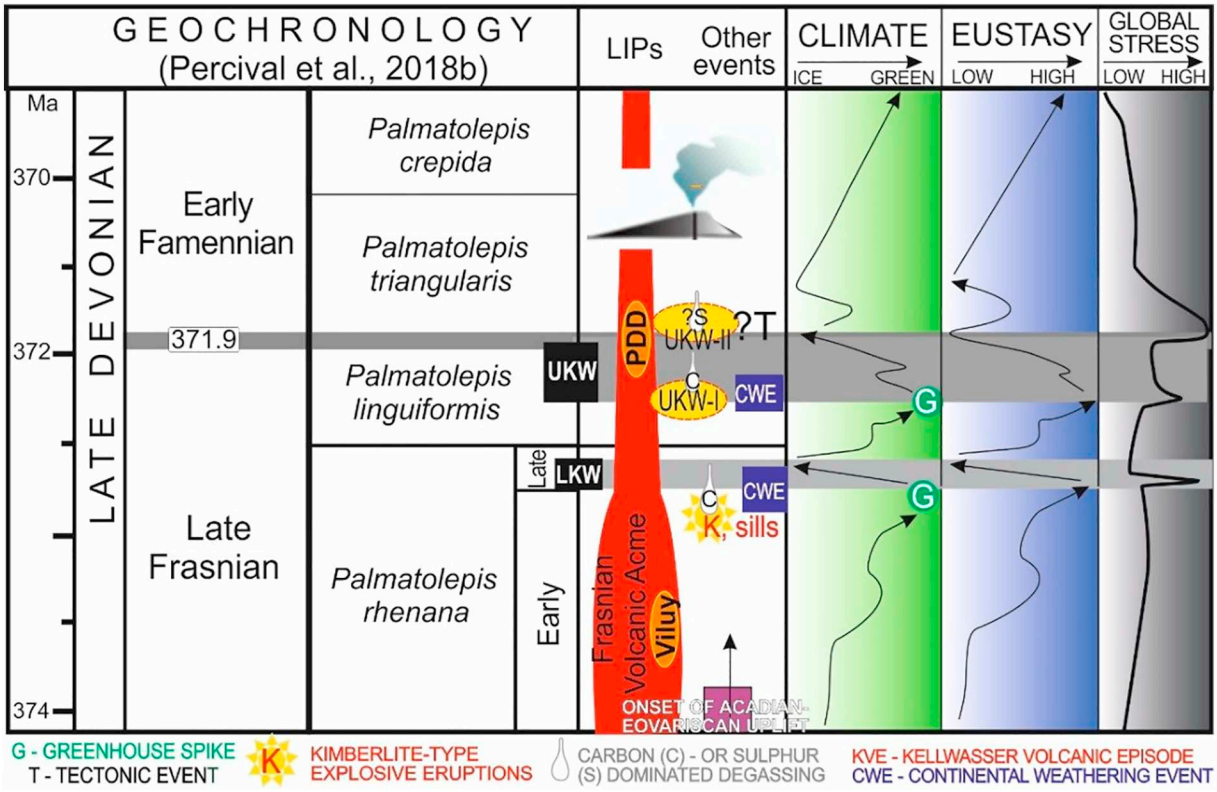

Fig. 17. Preliminary volcanic press-pulse model for the major F–F biocrisis, showing the main stimulus in pre-KW igneous activity in the LIPs, followed by a partly autocyclic two-step ecosystem turnover in the crisis interval (Fig. 5A; the folded arrows express fluctuating trend), strengthened by orbital forcing (De Vleeschouwer et al., 2017; see Fig. 2 for references). The doubled volcanic impact is implied also for the major extinction event at the F–F boundary, with a disastrous explosive event (CH signal) as the eventual pulse disturbance in the cascading catastrophic effect. The global stress pulses are guided by the extinction steps of Gereke and Schindler (2012); note that the main biodiversity collapse the major decline in biodiversity took place one step prior to the F-F boundary.

Abrupt sea-level fluctuation, driven by glacieustasy, was therefore an obvious consequence of the enhanced marine and terrestrial bioproduction. The additional albedo effect propagated for the LOME by Jones et al. (2017) was far more uncertain owing to conjectural growth of the Gondwanan ice sheets (McGhee, 2014). Clathrate dissociation remains a less probable stimulus in light of the known C-isotope record (but see Gharaie et al., 2007). On the other hand, amplified global weatherability trend, owing to successive Eovariscan arc–continent collisions in the tropical zone (Averbuch et al., 2005), strengthened this anti-greenhouse feedback (compare Swanson-Hysell and Macdonald, 2017; Ge et al., 2019; Macdonald et al., 2019).

The accelerated spreading rate in oceanic realms, combined with plume-generated extensional regimes over the continents, should have resulted in acceleration of the subduction processes, recorded in the pulsated intensification of arc-type explosive activity during the second half of Frasnian age (Winter, 2015; Zhang et al., 2020). A similar geodynamic setting is shown for the EPME in connection with Siberian Superplume activity and progressive arc volcanism along the growing subduction zones (Chen and Xu, 2019). Likewise, prolonged, subduction-related igneous activity is implied for the LOME (Ge et al., 2019; Yang et al., 2019). There were also notable references to the Late Cretaceous (to Early Paleogene) ocean-atmosphere system, profoundly disturbed by mantle superplume activity (Weissert, 2019). In particular, Barnett et al. (2019, p. 688) emphasized “heightened carbon cycle and climate sensitivity to orbital forcing”. Hence, “Volcanism is probably the ultimate driver of oceanic anoxia, but orbital periodicities determine the exact timing of carbon cycle perturbations” (Batenburg et al., 2016, p. 1).

9. Volcanic press-pulse scenario of the KW crisis

In summarizing all of the data discussed above, the volcanic scenario for the EFME is introductively proposed despite several constraints in the knowledge of distribution, magnitude, style, and timing of the magmatic phenomena. In part, this concept refers directly to the scenario of progressive two-step major rifting events of Racki (1998, fig. 7), based on the concepts of Veimarn and Milanovsky (1990) and Veimarn et al. (1997). In the last contribution of Veimarn and Korneeva (2007), this model was considered as two mantle superplume “impulses” at the base of the Late *rhenana* Zone and, most intensively, close to the F–F boundary.

9.1. Pre-KW volcanic acme in LIPs

Percival et al. (2018a, b, p. 6) concluded for the Viluy LIP that “The given ages of individual basalts do not coincide with the F-F boundary even once uncertainties in comparing the new U-Pb derived boundary age with Ar-Ar ages of volcanics are accounted for, although some may be closer in age to the Lower Kellwasser Event”. In fact, as summarized above, the Middle Frasnian subage experienced increased activity of mantle plume(s) and trap-type volcanism, lasting ~ 7 Ma in subaerial and submarine settings of the Viluy and Kola domains (Figs. 1 and Fig. 12B). This claim is surprising in light of the known stratigraphic and geochemical records of the pre-KW slice. However, the commonly assumed commencement ~ 380 Ma in the both LIPs should serve as a guide to more refined comparative studies of Early-Middle Frasnian anoxic events (Becker et al., 2016b; see below).

If this interpretation is correct, the pre-KW timespan should be marked by enhanced magmatic degassing, extensional regimes and widespread domal uplifts, particularly when paired with the first

Table 2
Volcanic events record in the studied F–F sections (see Fig. 2 and SM 1 – SM 2), as interpreted from recognized Hg excessive abundances as confirmed, probable, and non-evidenced, where x represents absent or non-sampled intervals, and **M** refers to masked enrichments (Figs. 10-11). The characteristics of Hg abundance data, sampling density, and interpretative potential are also given. Note that the average Phanerozoic Hg abundance varies from 30 ppb in limestone to 450 ppb in argillaceous shale (after Wedepohl, 1991; see SM 2).

Locality/paleogeographic location (Fig. 17) (G – Gondwana; L – Laurussia; ST – Saxo–Thuringian Ocean; P – Paleotethys)	**PPP** (Pictor-Phoenix-Pegasus) pre-KW	**Sx** (Sextans) Lower KW	**Sx** (Sextans) inter-KW	**LUK** earlier Upper KW	**CH** (Center Hill) Upper KW	**Sc** (Scorpius) post-KW	Background/peak Hg value	Sampling density/interpretative potential (**L**ow, **F**air, **H**igh)
Lahmida (G)						**(2)**	175/**1530**	F/H
Silberberg (ST)	**M** (1-2?)	**M** (2)		**M**	**M**		380/**1380**	H/F
Kahlleite (L-SE)	x	x					25/**2380**	L/H
Junge Grimme (L-SE)	x	x			**M**	?	120/330	L/H
Winsenberg (L-SE)	**M**	(2)		**M**			20/190	F/H
Psie Górki (L-SE)	x	x	x				27/**8024**	F/L
Kowala (L-SE)	x	x	**M** (5)	?			29/172	H/F
Whiterock Canyon (L-W)	x	x	**M** (3)				110/480	F/H
Devil's Gate (L-W)	x	**? (?3)**		?		(2)	20/230	F/L
Syv'yu (L-NE)	x	x		(?5)			39/260	H/H
Mae Sariang (P)	x					Multiple (?3)	21/383	H/L

Eovariscan orogenic episodes (Figs. 5B and 17). This trigger is recorded in the runaway greenhouse climate (Fig. 1) in the course of volcanic spasms (see the PPP signal in Fig. 16 and Table 2), followed by pulses of increased weathering and terrigenous delivery to marine basins. This supposition is on agreement with the reconstructed 'punctuated greenhouse' temperature trends, as well as the transgressive/anoxic Middlesex and Rhinestreet events (Pisarzowska and Racki, 2012; Becker et al., 2016b). Transient CO_2-greenhouse crises on continents have been correlated with Late Devonian marine anoxia by Retallack and Huang (2011, figs 2 and 9). However, only the cooling trend of 5°C is proved through the transgressive Middlesex interval (Pisarzowska and Racki, 2012). This conundrum may be explained by very brief warm/humid pulses promoted by assumed volcanic paroxysm that were unrecorded in oceanic archives because of their inert thermal nature of this reservoir, or were below the temporal resolution in O_2 isotope stratigraphy. If we accept the time correlations of Retallack and Huang (2011), a scenario of repetitive Frasnian hyperthemal episodes and resultant rapid weathering events on lands (recorded in soils) would be a common volcanically triggered causal link.

9.2. Two first-order climatic-eustatic cycles of the KW Crisis

The cascade of environmental stress factors has pre-conditioned the Frasnian biosphere for a major ecological crisis of carbonate biota, and finally approached the critical threshold recorded in the onset of the LKW event, as evidenced by the extreme greenhouse peak (Fig. 17). Unusually high-intensity flood basalt outpourings and arc magmatism paroxysm may also be a decisive pulse factor in the KW Crisis (see Section 3a). However, the conjectural progressive stimulus is believed rather to be to be carbonatite and/or kimberlite-type explosions (in the East European centres?), paired with or followed by sill-type intrusive activity, as recognized in the PDD LIP (Fig. 12B; see the EPME scenario of Burgess et al., 2019). This compound trigger rapidly enhanced the global warmth up to 34 °C (Fig. 2), as well as the chemical weathering rate. The unstable climate state was abruptly reversed toward the icehouse mode by a combination of diverse anti-greenhouse processes (Fig. 4). Thus, the intervals of KW events can unexpectedly correspond to periods of relative volcanic quietness when the loop of volcanic winter was the dominant operating mechanism. This paradox would explain the still unsuccessful search for 'robust' time correlation between LIP and EFME.

The regressive/cooling episode during ~100 Ka initiated an autocyclic response, followed by a gradual return to overall eustatic highstand and warming conditions that lasted ~600 Ka in the inter-KW interval. Similar autocyclic mechanisms operated more or less effectively during all 14 Devonian transgressive–regressive upward-shallowing cycles (Johnson et al., 1985; McGhee, 1996). Orbital cyclicity alone, controlled by eccentricity and obliquity, may be thought as sufficient for the precise timing of KW Crisis acme on the F-F boundary (De Vlesschouwer et al. (2017). However, the first-order control is speculatively linked with two-step eruptive stimulus also for the major UKW cycle, referred as subcycle UKW-I (Frasnian) and UKW-II (Famennian) in Fig. 17. Note that Zhang et al. (2020) indicated even three intra-UKW cycles, determined by volcanically-driven abrupt climate changes.

A temperature increase of ~3 °C was recorded near the onset of the UKW event (Fig. 2), as anticipated by Retallack and Huang (2011). The crucial F–F interval overlapped with the stepped extrusive spasms on the East European Platform, as recorded in multiple CH signals in Polar Urals (Fig. 16B), likely induced by the nearby Timan–Pechora traps. The worldwide CH signal suggests a global peak in arc magmatism close to the F-F boundary (see the non-plume scenario of Frizon de Lamotte et al., 2013), hypothetically paired with other non-trap volcanism.

Whilst the main peak of diversity loss occurred just prior the F-F

boundary (Ma et al., 2016, fig. 10; Gereke and Schindler, 2012), the maximum of carbon cycle perturbation (= the peak of bacterial bioproduction?; Joachimski et al., 2001), cooling (at least regionally – Joachimski et al., 2009, fig. 5) and marine sulfidic conditions took place after this biodiversity loss (cycle III of Zhang et al., 2020; see Fig. 2), with a basic impact on survival/recovery process. Coeval tectonic instability was recorded in the synsedimentary reworking, slope collapse, and mud flows related to seismicity and tsunami events in the earliest Famennian (Becker et al., 2018; Szrek and Salwa, 2020). The F-F tectonic-magmatic acme may be traced worldwide (Veimarn and Korneeva, 2007; Frizon de Lamotte et al., 2013; Golonka, 2020), exemplied by the East Australia (Torsvik and Cocks, 2017, p. 141, fig. 8.3), South America (Dahlquist et al., 2019) and Chukotka, Russian Arctic (fig. 11 in Ershova et al., 2016).

10. Applicability to other Late Devonian global events

In the University of Silesia database of Hg abundances, 11 localities straddling the D–C boundary in different parts of the world expose variously recorded Hg spikes, with a maximum value of 18.5 ppm recorded in the Kronhofgrabe section of the Carnic Alps, Austria (Racki et al., 2018a; Pisarzowska et al., 2020a; Rakociński et al., 2020). The numerous different-scale Hg enrichments are placed preferentially in the Hangenberg (HG) black shale, which exhibits criteria of masked anomalies (not only by OM, but also by other Hg carriers; Fig. 18). The Hg spikes have been also reported in different lithofacies in sections of Vietnam by Paschall et al., (2019) and in the Czech Republic and South China (Guangxi) by Kalvoda et al. (2019). Noteworthy, Hg spikes also occur below and above the HG level, as recognized in the carbonate strata at Novchomok, Uzbekistan, and in the mostly shaly succession at Kahleite, Germany (fig. 2 in Racki et al., 2018a; Pisarzowska et al., 2020a).

Supporting data are provided herein from the shaly–marly basinal succession of Bavaria in the Losau section, and from the exceptionally Hg-rich radiolarite succession of South China at the Shijia site (Fig. 18; SM 3). Accordingly, the criterion of synchronous, worldwide, euryfacies distribution is fulfilled, even if the volcanic Hg signal was mostly biased in LOPH sedimentary environments studied. In addition, spore malformations are the apparent response of the stressed vegetation to the widespread explosive volcanism, as proved by numerous pyroclastic horizons in the same Polish succession (Pisarzowska et al., 2020a). Highly elevated soot emission due to volcanism-promoted firestorms is well evidenced in the D-C passage as a possible icehouse stimulus (Fig. 4; Marynowski et al., 2012).

Surprisingly, the available LIP dates appear to preclude more intensive flood basalt eruptions in the D–C transition (e.g., at most a vaning stage in Siberia; Fig. 12B; Ernst et al., 2020), nonetheless data from the East European LIPs are uncertain (Nikishin et al., 1996, p. 49; Narkiewicz, 2020, fig. 11 see also 360 Ma major magmatic event in the Variscan internal domain, Pochon et al., 2019). This volcanism may again be seen as a press factor leading finally to delayed disastrous climatic and oceanographic responses. On the other hand, Percival et al. (2019) discussed the correlation between the last eruptive phase in the Viluy LIP and the anoxic *Annulata* event (both occurring at ~364 Ma), which was confirmed by the enhanced weathering rate determined through Os isotope trend. This inference awaits support by Hg data.

In the HG Crisis time of alleged LIP quiescence, correlative with a final of Bretonian orogenic phase and main rifting/volcanic stage in the PPD rift system (Narkiewicz, 2020, fig. 11), kimberlite explosive activity peaked on Siberian land, and also possibly carbonatites erupted in NE Poland sector (Ivanov, 2015; Pisarzowska et al., 2020a; Fig. 12B). In addition to diverse pyroclastic horizons, hydrothermal and mineralization signatures were reported from many regions (reviewed by Kaiser et al., 2016; Emsbo et al., 2018; Pochon et al., 2019 and Pisarzowska et al., 2020a; Fig. 18). The hydrothermal peak is recorded particularly in the Iberian domain by the massive sulfide event (Menor-Salván et al., 2010) and the last Hg mineralization episode of ~360 Ma in the Almadén cinnabar ore (Higueras et al., 2005). In the context, in the preliminary survey for the Hg content in the D-C hydrothermal precipitates of the Holy Cross Mountains, Poland, at the Ostrówka locality (Szulczewski et al., 1996), the radical Hg content differentiation between hematite at 50.6 ppm and sulfide at a maximum of 1.5 ppm is particularly noteworthy for localized Hg anomalies generated this way.

Kaiser et al. (2016, p. 412) noted that "An ultimate volcanogenic trigger of the warming, associated with a significant outgassing of carbon and sulphur dioxide, can be postulated, but there is no preserved record of a major DCB volcanic province. If it was positioned in the giant Panthalassia Ocean the evidence may have been lost. Interference ('nodes') of Milankovitch cycles was possibly a different/additional but decisive trigger for climate warming in the lower crisis interval." Correspondence with the volcanic EFME scenario (Fig. 17) is hence obvious, at least in overall conceptual terms (compare Pisarzowska et al., 2020a).

Moderate Hg enrichments up to 600 ppb have also been traced in an initial phase of the Early–Middle Frasnian Middlesex/*punctata* event in the Padberg section of the Rhenish region (Pisarzowska et al., 2020b). This fourth-order global biotic event (*sensu* Becker et al., 2016b) was also marked by oceanic cooling and weathering pulses, as well as greenhouse-type soil formation (Retallack and Huang, 2011). Even if only partly approved as real Hg enrichments, it provides promising evidence, as highlighted above based on the LIP dating (Fig. 1).

11. Final remarks and challenges for further research

The press-pulse volcanic scenario, proposed herein (Fig. 17), is subsequent conceptual step resulting from models developed by Veimarn and Milanovsky (1990), Buggisch (1991), Racki (1998) and Winter (2015). The documented worldwide Hg enrichments in the KW Crisis time (Figs. 15-16) can be used as a significant argument for the prime volcanic trigger (Racki et al., 2018b). In combination with the tectonic model of Averbuch et al. (2005), it offers the next possibility for testing its principal 'multicausal' elements in the context of global tectono-magmatic activation. It is hoped that the volcanic hypothesis (Fig. 17) offers at least partial answers to the EFME questions and dilemmas as set out in Racki's (2005) eight issues. Further testing of the F–F model will verify the three types of pending evidence given below (compare Becker et al., 2016b; Kaiser et al., 2016).

- Data from unknown unique successions that have become accessible, e.g., as a result of borehole works. Marine Siberian successions (see Baranov, 2007; Izokh et al., 2009; Yazikov et al., 2013) and from other LIP vicinities should provide particularly significant results.
- An event record with greater time resolution owing to very dense sampling and more precise field observations can lead to the identification of crucial volcanic characters. In particular, a reliable correlation between global biotic events and allegedly extremely explosive eruptions requires the findings of accompanying carbonatite and kimberlite pyroclasts in the conodont-dated successions.
- The application of more advanced analytical methods is needed, as exemplified by orbitally modulated astrochronology (De Vleeschouwer et al., 2017). Additionally, pervasive methylo-Hg toxicity resulting from volcanic-sourced Hg input to O_2-deficient basins has been considered by Clapham and Renne (2019). This extremely destructive factor has for first time been confirmed in the fossil record by Rakociński et al. (2020) for the HG Crisis, and can offer new insight into the recurring concept of the substantial Hg toxicity.

For individual LIPs, analysis of the host geology, in terms of the potential and composition of thermogenic degassing (Fig. 9), is another key question (Racki, 2020b), and it seems that gas-producing carbonate

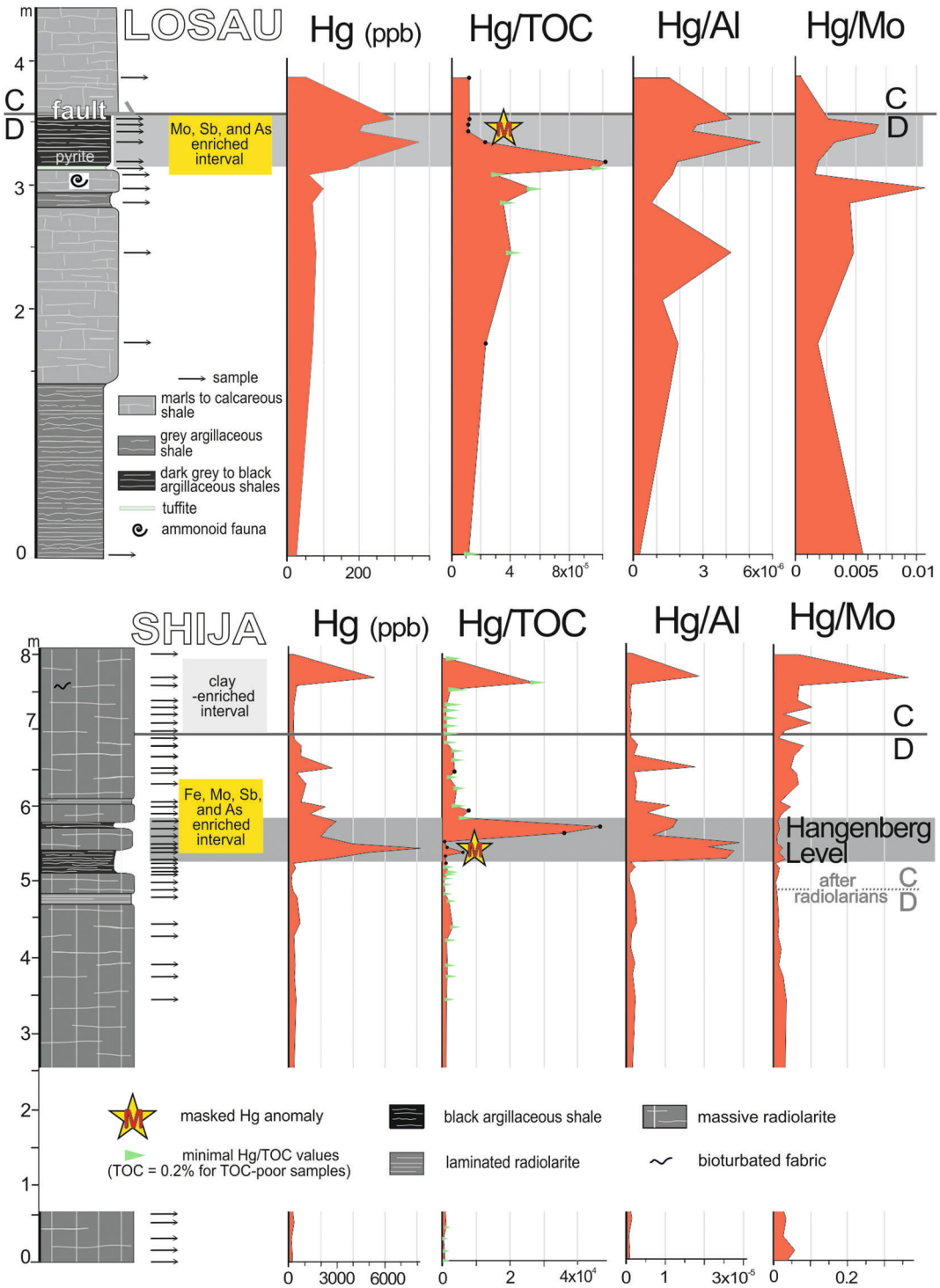

Fig. 18. Very different scales of Hg enrichment in deep-water successions of Germany and China across the D–C boundary beds (see SM 3), characterized by the metal enrichment levels (in orange boxes), suggestive of the widespread hydrothermal signature. Note extreme Hg anomalies and two versions of the D-C boundary location at Shija (cf. Shiti Reservoir East Section, fig. 1 in Wang et al., 2007, logged by M. Stachacz and P. Łapcik) and verified Hg/TOC curve.

lithologies (with evaporites) prevail in contact halos (see Fig. 12B). In addition, the Hg anomalies requires refined mineralogical research, in combination with Hg, Sr and C isotope systematics, as a starting point to their chemo-correlation. Recognition of their primary vs. secondary origin as well as local/regional vs. global distribution would be the final step towards a high-resolution volcanic model.

The applicability of the proposed volcanic press-pulse model (Figs. 4 and 17) to other global events is an obvious research perspective, implicitly outlined by Racki (2020a, 2020b). Thus, the conceptually expanding model of volcanic cataclysm as the main cause of global changes and evolutionary catastrophes (Courtillot, 1999; Bond and Wignall, 2014; Ernst, 2014; Wignall, 2016) has inevitably become an updated neocastrophic paradigm in 21st century geology.

Declaration of Competing Interest

The author declares that he does no know competing financial interests or personal relationships that could have appeared to influence

the work reported in this paper.

Acknowledgments

The study based on results of the MAESTRO grant 2013/08/A/ST10/00717 from the National Science Centre – Poland (to Grzegorz Racki). The manuscript benefited from constructive discussions and comments by Lawrence Percival, Zdzisław Bełka, Rich Ernst, Jun Shen, Leszek Marynowski and Morgan Jones. I thank also an anonymous journal reviewer and, in particular, Paul Wignal, who served as the guest editor. Many peoples participated in field work program during the MAESTRO grant realization (see SM 1 and SM 3), especially Michał Rakocinski (also kindly provided the draft of part of Fig. 16), Leszek Marynowski and Michał Stachacz. Zdzisław Bełka, Harald Tragelehn, Tom Becker, Manfred Gereke, Dave Bond, Xueping Mao and Daizhao Chen were guides of foreign field trips. Katarzyna Narkiewicz kindly contributed to the conodont dating of the some F-F sections studied.

Appendix A. Supplementary data

Supplementary data to this article can be found online at https://doi.org/10.1016/j.gloplacha.2020.103174.

References

Aizberg, R.Y., Beskopylny, V.N., Starchik, Y.A., Tsekoyeva, T.K., 2001. Late Devonian magmatism in the Pripyat Palaeorift: a geodynamic model. Geol. Quart. 45, 349–358.
Algeo, T.J., Scheckler, S.E., 2010. Land plant evolution and weathering rate changes in the Devonian. J. Earth Sci. 21 (Special Issue), 75–78.
Algeo, T.J., Liu, J., 2020. A re-assessment of elemental proxies. for paleoredox analysis. Chem. Geol. https://doi.org/10.1016/j.gca.2020.01.055. in press.
Algeo, T.J., Tribovillard, N., 2009. Environmental analysis of paleoceanographic systems based on molybdenum–uranium covariation. Chem. Geol. 268, 211–225.
Algeo, T.J., Scheckler, S.E., Maynard, J.B., 2001. Effects of the Middle to Late Devonian spread of vascular land plants on weathering regimes, marine biotas, and global climate. In: Gensel, P.G., Edwards, D. (Eds.), Plants Invade the Land. Columbia University Press, New York, pp. 213–236.
Amos, H.M., Jacob, D.J., Kocman, D., Horowitz, H.M., Zhang, Y., Dutkiewicz, S., Horvat, M., Corbitt, E.S., Krabbenhoft, D.P., Sunderland, E.M., 2014. Global biogeochemical implications of mercury discharges from rivers and sediment burial. Environ. Sci. Technol. 9514–9522.
Arens, N., West, I.D., 2008. Press-pulse: a general theory of mass extinction? Paleobiology 34, 456–471.
Artyushkova, O.V., Maslov, V.A., 2011. Devonian volcanism and conodont biodiversity in the South Urals. In: IGCP 596 Opening Meeting Graz, Abstract Volrme, Ber. Inst. Erdwiss. K.-F.-Univ. Graz. 16. pp. 23–25.
Arzamastsev, A.A., 2018. Geochronology and isotope geochemistry of the Kola alkaline intrusions, northeastern Fennoscandian Shield: what we can do more? In: XXXV International Conference "Magmatism of the Earth and related strategic metal deposits", Moscow, pp. 23–26. https://pureportal.spbu.ru/ru/publications/geochronology-and-isotope-geochemistry-of-the-kola-alkaline-intru.
Arzamastsev, A.A., Vesolovskiy, R.V., Travin, A.V., Yudin, D.S., Belyatsky, B.V., 2017. Paleozoic tholeiitic magmatism of the Kola Province: spatial distribution, age, and relation to alkaline magmatism. Petrology 25, 42–65.
Averbuch, O., Tribovillard, N., Devleeschouwer, X., Riquier, L., Mistiaen, B., Van Vliet-Lanoe, B., 2005. Mountain building-enhanced continental weathering and organic carbon burial as major causes for climatic cooling at the Frasnian–Famennian boundary (c. 376 Ma)? Terra Nova 17, 25–34.
Bagnato, E., Oliveri, E., Acquavita, A., Covelli, S., Petranich, E., Barra, M., Italiano, F., Parello, F., Sprovieri, M., 2017. Hydrochemical mercury distribution and air-sea exchange over the submarine hydrothermal vents off-shore Panarea Island (Aeolian arc, Tyrrhenian Sea). Marine Chem. 194, 63–78.
Bai, S.L., Bai, Z.Q., Ma, X.P., Wang, D.R., Sun, Y.L., 1994. Devonian Events and Biostratigraphy of South China. Peking University Press, Beijing 303 p.
Baliński, A., Olempska, E., Racki, G. (Eds.), 2002. Biotic responses to the Late Devonian global events. Acta Palaeont. Pol. 47, 186–404.
Bambach, R.K., 2006. Phanerozoic biodiversity mass extinctions. Annu. Rev. Earth Planet. Sci. 34, 127–155.
Baranov, V.V., 2007. The Middle and Upper Devonian in southeastern flank of the Siberian Platform (southern Verkhoyansk Region, Sette-Daban Mountain Range). Stratigr. Geol. Correlation 15, 470–484.
Barclay, R.S., McElwain, J.C., Sageman, B.B., 2010. Carbon sequestration activated by a volcanic CO2 pulse during Ocean Anoxic Event 2. Nat. Geosci. 3, 205–208.
Barnes, H.L., 2015. Hydrothermal processes. Geochem. Perspect. 4, 1–93.
Barnet, J.S.K., Littler, K., Westerhold, T., Kroon, D., Leng, M.J., Bailey, I., Röhl, U., Zachos, J.C., 2019. A high-Fidelity benthic stable isotope record of late Cretaceous–early Eocene climate change and carbon-cycling. Paleoceanogr. Paleoclimatol. 34, 672–691.
Batenburg, S.J., De Vleeschouwer, D., Sprovieri, M., Hilgen, F.J., Gale, A.S., Singer, B.S., Koeberl, C., Coccioni, R., Claeys, P., Montanari, A., 2016. Orbital control on the timing of oceanic anoxia in the Late Cretaceous. Clim. Past 12, 1995–2009.
Becker, R.T., House, M.R., 1994. Kellwasser events and goniatite successions in the Devonian of the Montagne Noire with comments on possible causations. Cour. Forsch.-Inst. Senckenberg 169, 45–77.
Becker, R.T., Gradstein, F.M., Hammer, O., 2012. In: Gradstein, F.M., Ogg, J.G. (Eds.), The Devonian Period. Schmitz.
Becker, R.T., Königshof, P., Brett, P. (Eds.), 2016. Devonian climate, sea level and evolutionary events. Geological Society, London, Special Publications 423, 1–464.
Becker, R.T., Königshof, P., Brett, P., 2016b. Devonian climate, sea level and evolutionary events: an introduction. Geological Society, London, Special Publications 423, 1–10.
Becker, R.T., Aboussalam, Z., Hartenfels, S., 2018. The Frasnian-Famennian boundary mass extinction – widespread seismic events, the timing of climatic pulses, "pelagic death zones", and opportunistic survivals. In: The Fossil Week, Abstract Book, 5th International Paleontological Congress – Paris, 9th-13th July 2018, pp. 107.
Benton, M. (Ed.), 2019. Cowen's History of Life. John Wiley & Sons, Hoboken 400 p.
Bergquist, A.B., 2017. Mercury, volcanism, and mass extinctions. Proc. Nat. Acad. Sci. USA 114, 8675–8677.
Blakey, R., 2016. Devonian - 370 Ma, global paleogeography and tectonics in deep time series. In: Deep Time Maps™ Paleogeography.
Blum, J.D., Sherman, L.S., Johnson, M.W., 2014. Mercury isotopes in earth and environmental sciences. Annu. Rev. Earth Planet. Sci. Lett. 42, 249–269.
Bond, D.P.G., Wignall, P.B., 2008. The role of sea-level change and marine anoxia in the Frasnian-Famennian (Fate Devonian) mass extinction. Palaeogeogr. Palaeoclimatol. Palaeoecol. 263, 107–118.
Bond, D.P.G., Wignall, P.B., 2014. Large igneous provinces and mass extinctions: an update. Geological Society of America Special Paper 505, 339–352.
Bond, D.P., Wignall, P.B., Racki, G., 2004. Extent and duration of marine anoxia during the Frasnian– Famennian (Late Devonian) mass extinction in Poland, Germany, Austria and France. Geol. Mag. 141, 173–193.
Bond, D.P., Zatoń, M., Wignall, P.N., Marynowski, L., 2013. Evidence for shallow-water 'Upper Kellwasser' anoxia in the Frasnian–Famennian reefs of Alberta, Canada. Lethaia 46, 355–368.
Bond, D.P., Wignall, P.B., Joachimski, M.M., Sun, Y.D., Savov, I., Grasby, S.E., Beauchamp, B., Blomeier, D.P.G., 2019. An abrupt extinction in the Middle Permian (Capitanian) of the Boreal Realm (Spitsbergen) and its link to anoxia and acidification. Geol. Soc. Am. Bull. 127, 1411–1421.
Bottjer, D.J., 2016. Paleoecology: Past, Present and Future. John Wiley & Sons, Chichester 232 p.
Brumsack, H.J., 2006. The trace metal content of recent organic carbon – rich sediments: implications for Cretaceous black shale formation. Palaeogeogr. Palaeoclimatol. Palaeoecol. 232, 344–361.
Buggisch, W., 1991. The global Frasnian-Famennian "Kellwasser Event" Geol. Rundsch. 80, 49–72.
Burgess, S.D., Muirhead, J.D., Bowring, S.A., 2019. Initial pulse of Siberian Traps sills as the trigger of the end-Permian mass extinction. Nature Comm. 8 (164), 1–6.
Cao, Y., Song, H.Y., Algeo, T.J., Chu, D.L., Du, Y., Tian, L., Wang, Y.H., Tong, J.N., 2019. Intensified chemical weathering during the Permian-Triassic transition recorded in terrestrial and marine successions. Palaeogeogr. Palaeoclimatol. Palaeoecol. 519, 166–177.
Carmichael, S.K., Waters, J.A., Suttner, T.J., Kido, E., DeReuil, A.A., 2014. A new model for the Kellwasser Anoxia Events (Late Devonian): shallow water anoxia in an open oceanic setting in the Central Asian Orogenic Belt. Palaeogeogr. Palaeoclimatol. Palaeoecol. 399, 394–403.
Carmichael, S.K., Waters, J.A., Königsof, P., Suttner, T.J., Kido, E., 2019. Paleogeography and paleoenvironments of the Late Devonian Kellwasser event: a review of its sedimentological and geochemical expression. Glob. Planet. Change 183 (102984), 1–28.
Castle, J.W., Rodgers, J.H., 2009. Hypothesis for the role of toxin-producing algae in Phanerozoic mass extinctions based on evidence from the geologic record and modern environments. Environ. Geosci. 1–23.
Cather, S.M., Dunbar, N.W., McDowell, F.W., McIntosh, W.C., Scholle, P.A., 2009. Climate forcing by iron fertilization from repeated ignimbrite eruptions. Geosphere 5, 315–324.
Charbonnier, G., Adatte, T., Föllmi, K.B., Suan, G., 2020. Effect of intense weathering and post-depositional degradation of organic matter on Hg/TOC proxy in organic-rich sediments and its implications for deep-time investigations. Geochem., Geophys., Geosyst 21, 1–19 e2019GC008707.
Chen, J., Xu, Y.G., 2019. Establishing the link between Permian volcanism and biodiversity changes: insights from geochemical proxies. Gondwana Res. 75, 68–96.
Chen, D.Z., Qing, H.R., Li, R.W., 2005. The Late Devonian Frasnian–Famennian (F/F) biotic crisis: insights from $\delta^{13}C_{carb}$, $\delta^{13}C_{org}$ and $^{87}r/^{86}Sr$ isotopic systematics. Earth Planet. Sci. Lett. 235, 151–166.
Chow, T.N., George, A.A., Trinajstic, K.M., 2004. Tectonic control on development of a Frasnian–Famennian (Late Devonian) palaeokarst surface, Canning Basin reef complexes, northwestern Australia. Austral. J. Earth Sci. 51, 911–917.
Çimen, O., 2018. The new findings on the Late Devonian volcanism in the Eastern Taurides (Develi, Kayseri): preliminary data. Geol. Bull.Turkey 61, 75–90.
Clapham, M.E., Renne, P.R., 2019. Flood basalts and mass extinctions. Annu. Rev Earth Planet. Sc. 47, 275–303.
Copper, P., 1986. Frasnian-Famennian mass extinctions and cold water oceans. Geology 14, 835–838.
Copper, P., 2002. Reef development at the Frasnian/Famennian mass extinction boundary. Palaeogeogr. Palaeoclimatol. Palaeoecol. 181, 27–65.
Copper, P., 2011. 100 million years of reef prosperity and collapse: Ordovician to Devonian interval. Paleontological Society Papers 17, 15–32.

Coufalík, P., Krmíček, L., Zvěřina, O., Meszarosová, N., Hladil, J., Komárek, J., 2018. Model of mercury flux associated with volcanic activity. Bull. Env. Contam. Toxicol. 101, 549–555.
Courtillot, V., 1999. Evolutionary Catastrophes: the Science of Mass Extinctions. Cambridge University Press, Cambridge 188 p.
Courtillot, V., Fluteau, F., 2014. A review of the embedded time scales of flood basalt volcanism with special emphasis on dramatically short magmatic pulses. Geological Society of America Special Paper 505, 301–317.
Courtillot, V., Kravchinsky, V.A., Quidelleur, X., Renne, P.R., Gladkochub, D.P., 2010. Preliminary dating of the Viluy traps (Eastern Siberia): eruption at the time of Late Devonian extinction events? Earth Planet. Sci. Lett. 300, 239–245.
Crasquin, S., Horne, D.J., 2018. The palaeopsychrosphere in the Devonian. Lethaia 51, 547–563.
Dahlquist, J.A., Grande, M.C., Alasino, P.H., Basei, M.A.S., Morales Cámera, M.M., 2019. New geochronological and isotope data for the Las Chacras – Potrerillos and Renca batholiths: a contribution to the Middle-Upper Devonian magmatism in the pre-Andean foreland (Sierras Pampeanas, Argentina), SW Gondwana. J. South Am. Earth Sci. 93, 348–363.
D'Antonio, M.P., Ibarra, D.E., Boyce, C.K., 2019. Land plant evolution decreased, rather than increased, weathering rates. Geology 48, 29–33.
De Lena, L.F., Taylor, D., Guex, J., Bartolini, A., Adatte, T., van Acken, D., Spangenberg, J.E., Samankassou, E., Vennemann, T., Schaltegger, T., 2019. The driving mechanisms of the carbon cycle perturbations in the late Pliensbachian (Early Jurassic). Sci. Rep. 9 (18430), 1–12.
De Vleeschouwer, D., da Silva, A.C., Sinnesael, M., Chen, D.Z., Day, J.E., Whalen, M.T., Guo, Z.H., Claeys, P., 2017. Timing and pacing of the Late Devonian mass extinction event regulated by eccentricity and obliquity. Nat. Commun. 8 (2268), 1–11.
Derkowski, A., Marynowski, L., 2018. Binding of heavy metals by oxidised kerogen in (palaeo)weathered black shales. Chem. Geol. 493, 441–450.
Dessureau, G., Piper, D.J.W., Pe-Piper, G., 2007. Geochemical evolution of earliest Carboniferous continental tholeitic basalts along a crustal-scale shear zone, southwestern Maritimes basin, eastern Canada. Lithos 50, 27–50.
Dopieralska, J., 2003. Neodymium isotopic composition of conodonts as a palaeoceanographic proxy in the Variscan oceanic system. Justus-Liebig-University, Giessen 111 p.
Dopieralska, J., Belka, Z., Walczak, A., 2015. Nd isotope composition of conodonts: an accurate proxy of sea-level fluctuations. Gondwana Res. 22, 1102–1109.
Du, Y.S., Gong, Y.M., Zeng, X.W., Huang, H.W., Yang, J.H., Zhang, Z., Huanh, Z.Q., 2008. Devonian Frasnian-Famennian transitional event deposits of Guangxi, South China and their possible tsunami origin. Sci. China D - Earth Sci. 5, 1570–1580.
Elrick, M., Berkyová, S., Klapper, G., Sharp, Z., Joachimski, M., Frýda, J., 2009. Stratigraphic and oxygen isotope evidence for My-scale glaciation driving eustasy in the Early–Middle Devonian greenhouse world. Palaeogeogr. Palaeoclimatol. Palaeoecol. 276, 170–181.
Emsbo, P., Premo, W.R., McLaughlin, P.I., Neymark, L.A., Vandenbroucke, T.R.A., Day, J.E., du Bray, E.A., Manning, A.H., Bancroft, A.M., 2018. Impact of sedimentary-exhalative hydrothermal systems on marine chemistry and mass extinctions: applications for ore genesis research and mineral exploration. Soc. Econ. Geol. Spec. Publ. 21, 75–87.
Ernst, R.E., 2014. Large Igneous Provinces. Cambridge University Press, Cambridge 653 p.
Ernst, R.E., Bell, K., 2010. Large Igneous Provinces (LIPs) and carbonatites. Mineral. Petrol. 98, 55–76.
Ernst, R.E., Youbi, N., 2017. How Large Igneous Provinces affect global climate, sometimes cause mass extinctions, and represent natural markers in the geological record. Palaeogeogr. Palaeoclimatol. Palaeoecol. 478, 30–52.
Ernst, R.E., Davies, D.R., Jowitt, S.M., Campbell, I.H., 2018a. When do mantle plumes destroy diamonds? Earth Planet. Sci. Lett. 502, 244–252.
Ernst, R.E., Wang, Q., Mishenina, Y., 2018b. Linking paleo-surface characteristics and deep crustal processes caused by mantle plumes. In: International Symposium on Deep Earth Exploration and Practices Beijing, China - October 24-26, 2018, pp. 1–2.
Ernst, R.E., Liikane, D.A., Jowitt, S.M., Buchan, K.L., Blanchard, J.A., 2019. A new plumbing system framework for mantle plume-related continental Large Igneous Provinces and their mafic-ultramafic intrusions. J. Volcanol. Geothermal Res. 384, 75–84.
Ernst, R.E., Rodygin, S.A., Grinev, O.M., 2020. Age correlation of Large Igneous Provinces with Devonian biotic crises. Glob. Planet. Change 185 (103097), 1–13.
Ershova, V.B., Prokopiev, E.V., Khudoley, A.K., 2016. Devonian–Permian sedimentary basins and paleogeography of the Eastern Russian Arctic: an overview. Tectonophysics 691, 234–255.
Estrada, L., Pippenger, K., Boyer, D.L., Jones, D.S., Cohen, P., 2018. Mercury and microfossil trends during end-Devonian extinction events. GSA Abstracts with Programs 50 (6). https://doi.org/10.1130/abs/2018AM-319352.
Faggetter, L.E., Wignall, P.B., Pruss, S.B., Jones, D.S., Grasby, S., Widdoson, S., Newton, R.J., 2019. Mercury chemostratigraphy across the Cambrian Series 2 – Series 3 boundary: evidence for increased volcanic activity coincident with extinction? Chem. Geol. 510, 188–199.
Fendley, I.M., Mittal, T., Sprain, C.J., DiPasqualec, M.M., Tobind, T.S., Renne, P.R., 2019. Constraints on the volume and rate of Deccan Traps flood basalt eruptions using a combination of high-resolution terrestrial mercury records and geochemical box models. Earth Planet. Sci. Lett. 524 (115721), 1–11.
Font, E., Bond, D.P.G., 2020. Volcanism and Mass Extinction. Reference Module in Earth Systems and Environmental Sciences 1–11. https://doi.org/10.1016/b978-0-12-409548-9.12108-6.
Formolo, M.J., Riedinger, N., Gill, B.C., 2014. Geochemical evidence for euxinia during the Late Devonian extinction events in the Michigan Basin (U.S.A.). Palaeogeogr. Palaeoclimatol. Palaeoecol. 414, 146–154.
Freyer, G., 1957. Neue Untersuchungen im Oberdevon des Vogtlandes auf Ggrund des Fossilinhaltes der Kalke im Bereich der Vogtländischen Mulde. In: Freib Forsch, H. (Ed.), Geologie. C 27. pp. 1–100.
Frizon de Lamotte, D., Tavakoli-Shirazi, S., Leturmy, S., Averbuch, O., Mouchot, N., Raulin, C., Leparmentier, F., Blanpied, C., Ringenbach, J.C., 2013. Evidence for Late Devonian vertical movements and extensional deformation in northern Africa and Arabia: integration in the geodynamics of the Devonian world. Tectonics 32, 1–16.
Gagiev, M.H., 1997. Sedimentary evolution and sea-level fluctuations in the Devonian of North-east Asia. Cour. Forsch.–Inst Senckenberg 199, 75–82.
Gagiev, M.H., 2009. Stratigraphy of Devonian and Lower Carboniferous of the Prikolymian Uplift (Northeastern Asia). NEISRI FEB RAS, Magadan (290p In Russian).
Gagieva, A.M., 2016. The Kedon series volcanics of the Middle Paleozoic as the Large Igneous 528 Province (LIP) of the Omolon Massif. In: The 3rd Russian Conference in Commemoration 530 of A.P. Vaskovsky and in Dedication of his 105th Birthday Date (Magadan, October 12-14), pp. 118–120 (In Russian).
Ge, X., Mou, C., Wang, C., Men, X., Chen, C., Hou, Q., 2019. Mineralogical and geochemical characteristics of K-bentonites from the Late Ordovician to the Early Silurian in South China and their geological significance. Geol. J. 54, 514–528.
George, A.D., Chow, N., Trinajstic, K., 2014. Oxic facies and the Late Devonian mass extinction, Canning Basin, Australia. Geology 42, 327–330.
Gereke, M., Schindler, E., 2012. Time-specific facies and biological crises—the Kellwasser event interval near the Frasnian/Famennian boundary (Late Devonian). Palaeogeogr. Palaeoclimatol. Palaeoecol. 367–368, 19–29.
Gharaie, M.H.M., Matsumoto, R., Racki, G., Kakuwa, Y., 2007. Chemostratigraphy of Frasnian-Famennian transition: possibility of methane hydrate dissociation leading to mass extinction. Geological Society of America Special Paper 424, 109–125.
Gholamalian, H., 2007. Conodont biostratigraphy of the Frasnian-Famennian boundary in the Esfahan and Tabas areas. Central Iran. Geol. Quart 51, 453–476.
Golonka, J., 2000. Cambrian-Neogene plate tectonic maps. Wyd. Uniwersytetu Jagiellońskiego, Kraków 125 p.
Golonka, J., 2020. Late Devonian paleogeography in the framework of global plate tectonics. Glob. Planet. Change 186 (103129), 1–19.
Göncüoğlu, M.C., Günal-Türkmenoğlu, A., Bozkaya, Ö., Ünlüce-Yücel, Ö., 2016. Geological features and geochemical characteristics of Late Devonian–Early Carboniferous K-bentonites from northwestern Turkey. Clay Minerals 51, 539–562.
Graham, J.R., Russell, K.J., Stillman, C.J., 1995. Late Devonian magmatism in West Kerry and its relationship to the development of the Munster Basin. Irish J. Earth Sci. 14, 7–23.
Grasby, S.E., Beauchamp, B., Bond, D.P.G., Wignall, P., Talavera, C., Galloway, J.M., Piepjohn, K., Reinhardt, L., Blomeier, D., 2015. Progressive environmental deterioration in northwestern Pangea leading to the latest Permian extinction. Geol. Soc. Am. Bull. 127, 1331–1347.
Grasby, S.E., Them, T.R., Chen, Z., Yin, R.S., Ardakani, O.H., 2019. Mercury as a proxy for volcanic emissions in the geologic record. Earth-Sci. Rev. 196 (102880), 1–16.
Guo, F., Fan, W.M., Wang, Y.J., Li, C.W., 2004. Upper Paleozoic basalts in the southern Yangtze block: geochemical.
Guo, L., Schekoldin, R., Scott, R., 2010. The Devonian succession in northern Novaya Zemlya, Arctic Russia: sedimentology, palaeogeography and hydrocarbon occurrence. J. Petrol. Geol. 33, 105–122.
Gurvich, E., 2006. Metalliferous Sediments of the World Ocean: Fundamental Theory of Deep-Sea Hydrothermal Sedimentation. Springer, Berlin 416 p.
Haddad, E.F., Boyer, D.L., Droser, M.L., Love, Gordon, 2017. Ichnofabrics and chemostratigraphy argue against persistent anoxia during the Upper Kellwasser Event in New York State. Palaeogeogr. Palaeoclimatol. Palaeoecol. 490, 178–190.
Hallam, A., Wignall, P., 1997. Mass Extinctions and Their Aftermath. Oxford University Press, Oxford 320 p.
Higueras, P., Munha, J., Oyarzun, R., Tassinari, C.C.G., Ruiz, I.R., 2005. First lead isotopic data for cinnabar in the Almadćn district (Spain): implications for the genesis of the mercury deposits. Mineral. Deposita 40, 115–122.
Huang, C., Michael, M.J., Gong, Y.M., 2018. Did climate changes trigger the Late Devonian Kellwasser Crisis? Evidence from a high-resolution conodont record from South China. Earth Planet. Sci. Lett. 495, 174–184.
Isozaki, Y., 2007. Plume winter scenario for biosphere catastrophe: The Permo-Triassic boundary case. In: Yuen, D.A., Maruyama, S., Karato, S.I., Windley, B.F. (Eds.), Superplumes: Beyond Plate Tectonic. Springer, Dordrecht, pp. 409–440.
Ivanov, A.V., 2015. Why volatiles are required for cratonic flood basalt volcanism: two examples from the Siberian craton. Geological Society of America Special Paper 514, 325–338.
Izokh, O.P., Izokh, N.G., Ponomarchuk, V.A., Semenova, D.V., 2009. Carbon and oxygen isotopes in the Frasnian-Famennian section of the Kuznetsk basin (southern West Siberia). Russian Geol. Geoph. 50, 610–617.
Joachimski, M.M., Buggisch, W., 1996. The Upper Devonian reef crisis - insights from the carbon isotope record. Göttinger Arb. Geol. Paläont. Spec. 2, 365–370.
Joachimski, M.M., Buggisch, W., 2002. Conodont apatite $\delta^{18}O$ signatures indicate climatic cooling as a trigger of the Late Devonian mass extinction. Geology 30, 711–714.
Joachimski, M.M., Ostertag-Henning, C., Pancost, R.D., Strauss, H., Freeman, K.H., Littke, R., Damste, J.S.S., Racki, G., 2001. Water column anoxia, enhanced productivity and concomitant changes in $\delta^{13}C$ and $\delta^{34}S$ across the Frasnian–Famennian boundary (Kowala—Holy Cross Mountains/Poland). Chem. Geol. 175, 109–131.
Joachimski, M.M., Breisig, S., Buggisch, W., Talent, J.A., Mawson, R., Gereke, M., Morrow, J.R., Day, J., Weddige, K., 2009. Devonian climate and reef evolution: insights from oxygen isotopes in apatite. Earth Planet. Sci. Lett. 284, 599–609.
Johnson, J.G., 1988. Volcanism, eustacy, and extinctions. Geology 16, 573–574.

Johnson, J.G., Klapper, G., Sandberg, C.A., 1985. Devonian eustatic fluctuations in Euramerica. Geol. Soc. Am. Bull. 96, 567–587.
Jones, D.S., Martini, A.M., Fike, D.A., Kaiho, K., 2017. A volcanic trigger for the Late Ordovician mass extinction? Mercury data from south China and Laurentia. Geology 45, 631–634.
Jones, M.T., Percival, L.M.E., Stokke, E.W., Frieling, J., Mather, T.A., Riber, L., Schubert, B.A., Schultz, B., Tegner, C., Planke, S., Svensen, S.H., 2019. Mercury anomalies across the Palaeocene–Eocene Thermal Maximum. Clim. Past 15, 217–236.
Jourdan, F., Reimold, W.U., 2012. Age of the Siljan impact structure. In: 75th Annual Meteoritical Society Meeting (2012), 5093.pdf. http://www.lpi.usra.edu/meetings/metsoc2012/pdf/5093.pdf.
Kabanov, P., 2018. Devonian (c. 388–375 Ma) Horn River Group of Mackenzie Platform (NW Canada) is an open-shelf succession recording oceanic anoxic events. J. Geol. Soc. 176, 29–45.
Kabanov, P., Jiang, C., 2020. Photic-zone euxinia and anoxic events in a Middle-Late Devonian shelfal sea of Panthalassan continental margin, NW Canada: changing paradigm of Devonian ocean and sea level fluctuations. Glob. Planet. Change. https://doi.org/10.1016/j.gloplacha.2020.103153. in press.
Kaiser, S.I., Aretz, M., Becker, R.T., 2016. The global Hangenberg Crisis (Devonian–Carboniferous transition): review of a first-ordermass extinction. Geological Society, London, Special Publications 423, 387–439.
Kalvoda, J., Kumpan, T., Qie, W., Frýda, J., Bábek, O., 2019. Mercury spikes at the Devonian-Carboniferous boundary in the eastern part of the Rhenohercynian zone (central Europe) and in the South China block. Palaeogeogr. Palaeoclimatol. Palaeoecol. 531, 1–12 A; 109221.
Kazmierczak, J., Kremer, B., Racki, G., 2012. Late Devonian marine anoxia challenged by benthic cyanobacterial mats. Geobiology 10, 371–383.
Kelly, A.A., Cohen, P.A., Boyer, D.L., 2019. Tiny keys to unlocking the Kellwasser events: detailed characterization of organic walled microfossils associated with extinction in Western New York State. Palaios 34, 96–104.
Kidder, D.L., Worsley, T.R., 2010. Phanerozoic Large Igneous Provinces (LIPs), HEATT (Haline Euxinic Acidic Thermal Transgression) episodes, and mass extinctions. Palaeogeogr. Palaeoclimatol. Palaeoecol. 295, 162–191.
Kiessling, W., 2008. Sampling-standardized expansion and collapse of reef building in the Phanerozoic. Fossil Record 11, 7–18.
Kiessling, W., Simpson, C., 2011. On the potential for ocean acidification to be a general cause of ancient reef crises. Global Change Biol. 17, 56–67.
Kiselev, A.I., Ernst, R.E., Yarmolyuk, V.V., Egorov, K.N., 2012. Radiating rifts and dyke swarms of the middle Paleozoic Yakutsk plume of eastern Siberian craton. J. Asian Earth Sci. 45, 1–16.
Knoll, A.H., 2013. Systems paleobiology. Geol. Soc. Am. Bull. 125, 3–13.
Koglin, N., Zeh, A., Franz, G., Schüssler, U., Glodny, J., Gerdes, A., Brätz, H., 2018. From Cadomian magmatic arc to Rheic ocean closure: the geochronological-geochemical record of nappe protoliths of the Münchberg Massif, NE Bavaria (Germany). Gondwana Res. 55, 135–152.
Kongchum, M., Hudnall, W.H., Delaune, R.D., 2011. Relationship between sediment clay minerals and total mercury. J. Envir. Sci. Health A 46, 534–539.
Königshof, P., Nesbor, H.D., Flick, H., 2010. Volcanism and reef development in the Devonian: a case study from the Lahn syncline, Rheinisches Schiefergebirge (Germany). Gondwana Res. 17, 264–280.
Kravchinsky, V.A., 2012. Paleozoic large igneous provinces of Northern Eurasia: correlation with mass extinction events. Glob. Planet. Change 86–87, 31–36.
Kump, L.R., Pavlov, A., Arthur, M.A., 2005. Massive release of hydrogen sulfide to the surface ocean and atmosphere during intervals of oceanic anoxia. Geology 33, 397–400.
Lanik, A., Over, D.J., Schmitz, M., Kirchgasser, W.T., 2016. Testing the limits of chronostratigraphic resolution in the Appalachian Basin, Late Devonian (middle Frasnian), eastern North America: new U-Pb zircon dates for the Belpre Tephra suite. Geol. Soc. Am. Bull. 128, 1813–1821.
Large, R.R., Halpin, J.A., Lounejeva, E., et al., 2015. Cycles of nutrient trace elements in the Phanerozoic Ocean. Gondwana Res. 28, 1282–1293.
Larionova, Y.O., Sazonova, L.V., Lebedeva, N.M., Nosova, A.A., Tretyachenko, V.V., Travin, A.V., Kargin, A.V., Yudin, D.S., 2016. Kimberlite age in the Arkhangelsk Province, Russia: isotopic geochronologic Rb–Sr and $^{40}Ar/^{39}Ar$ and mineralogical data on phlogopite. Petrology 24, 562–593.
Lash, G.G., 2017. A multiproxy analysis of the Frasnian-Famennian transition in western New York State, U.S.A. Palaeogeogr. Palaeoclimatol. Palaeoecol. 473, 108–122.
Lee, C.T., Dee, S., 2019. Does volcanism cause warming or cooling? Geology 47, 687–688.
Liu, Z.Y., Selby, D., Hackley, P.C., Over, D.J., 2020. Evidence of wildfires and elevated atmospheric oxygen at the Frasnian–Famennian boundary in New York (USA): implications for the Late Devonian mass extinction. Geol. Soc. Am. Bull. https://doi.org/10.1130/B35457.1. in press.
Lorenz, V., Suhr, P., Suhr, S., 2017. Phreatomagmatic maar-diatreme volcanoes and their incremental growth: a model. Geological Society, London, Special Publications 446, 29–59.
Lu, M., Lu, Y.H., Ikejiri, T., Hogancamp, N., Sun, Y.G., Wu, Q.H., Carroll, R., Çemen, I., Pashin, J., 2019. Geochemical evidence of first forestation in the southernmost Euramerica from Upper Devonian (Famennian) black shales. Sci. Reports 9 (7581), 1–15.
Ma, X.P., Gong, Y.M., Chen, D.Z., Racki, G., Chen, X.Q., Liao, W.H., 2016. The Late Devonian Frasnian–Famennian event in South China — patterns and causes of extinctions, sea level changes, and isotope variations. Palaeogeogr. Palaeoclimatol. Palaeoecol. 448, 224–244.
Macdonald, F.A., Swanson-Hysell, N.L., Park, Y.E., Lisiecki, L., Jagoutz, O., 2019. Arc-continent collisions in the tropics set Earth's climate state. Science 364, 181–184.
Mahmudy Gharaie, M.H., Matsumoto, R., Kakuwa, Y., Milroy, P.G., 2004. Late Devonian facies variety in Iran: volcanism as a possible trigger of the environmental perturbation near the Frasnian-Famennian boundary. Geol. Quart. 48, 323–332.
Marynowski, L., Rakociński, M., Borcuch, E., Kremer, B., Schuber, T.B.A., Jahren, A.H., 2011. Molecular and petrographic indicators of redox conditions and bacterial communities after the F/F mass extinction (Kowala, Holy Cross Mountains, Poland). Palaeogeogr. Palaeoclimatol. Palaeoecol. 306, 1–14.
Marynowski, L., Zatoń, M., Rakociński, M., Filipiak, P., Kurkiewicz, S., Pearce, T.J., 2012. Deciphering the Upper Famennian Hangenberg Black Shale depositional environments based on multi-proxy record. Palaeogeogr. Palaeoclimatol. Palaeoecol. 346–347, 66–86.
Masaitis, V.L., 2007. Devonian basalts of Siberian platform, and their heterogeneous mantle sources. In: International Symposium "Large Igneous Provinces of Asia, Mantle Plumes and Metallogeny", Novosibirsk, Russia, 13-16 August 2007, pp. 39–42.
McArthur, J.M., Howarth, R.J., Shields, G.A., 2012. Strontium isotope stratigraphy. In: Gradstein, F.M., Ogg, J.G., Schmitz, M., Ogg, G. (Eds.), The Geologic Time Scale 2012. Elsevier, Amsterdam, pp. 127–144.
McGhee, G.R., 1996. The Late Devonian Mass Extinction. In: The Frasnian/Famennian Crisis. Columbia University Press, New York 303 p.
McGhee, G.R., 2005. Modelling Late Devonian extinction hypotheses. In: Over, D.J., Morrow, J.R., Wignall, P.B. (Eds.), Understanding Late Devonian and Permian-Triassic Biotic and Climatic Events: Towards an Integrated Approach, Developments in Paleontology and Stratigraphy, pp. 37–50.
McGhee, G.R., 2013. When the Invasion of Land Failed: The Legacy of the Devonian Extinctions. Columbia University Press, New York 356 p.
McGhee, G.R., 2014. The search for sedimentary evidence of glaciation during the Frasnian/Famennian (Late Devonian) biodiversity crisis. Sediment. Rec. 6, 5–8.
McGhee, G.R., Clapham, M.E., Sheehan, P.M., Bottjer, D.J., Droser, M.L., 2004. Ecological ranking of Phanerozoic biodiversity crises: ecological and taxonomic severities are decoupled. Palaeogeogr. Palaeoclimatol. Palaeoecol. 211, 289–297.
McKenzie, N.R., Jiang, H.H., 2019. Earth's outgassing and climatic transitions: the slow burn towards environmental "catastrophes"? Elements 15, 325–330.
McLaren, D.J., 1959. The role of fossils in defining rock units with examples from the Devonian of Western and Arctic Canada. Am. J. Sci. 257, 734–751.
McLaren, D.J., 1970. Presidential address: time, life and boundaries. J. Paleontol. 48, 801–815.
McLaren, D., 1983. Bolides and biostratigraphy. Geol. Soc. Am. Bull. 94, 313–324.
Menor-Salván, C., Tornos, F., Fernández-Remolar, D., Amils, R., 2010. Association between catastrophic paleovegetation changes during Devonian-Carboniferous boundary and the formation of giant massive sulfide deposits. Earth Planet. Sc. Lett. 299, 398–408.
Meyer, K.W., Petersen, S.V., Lohmann, K.C., Blum, J.D., Washburn, S.J., Johnson, M.W., Gleason, J.D., Kurz, A.I., Winkelstern, I.Z., 2019. Biogenic carbonate mercury and marine temperature records reveal global influence of Late Cretaceous Deccan Traps. Nature Comm. 10 (5356), 1–8.
Miall, A.D., 2015. Updating uniformitarianism: stratigraphy as just a set of 'frozen accidents' Geological Society, London, Special Publications 404, 11–36.
Mizens, G.A., Kuleshov, V.N., Stepanova, T.I., Kucheva, N.A., 2015. Evidence for global Famennian and Tournaisian geologic events in the section of an isolated carbonate platform in the eastern Urals. Russ. Geol. Geophys. 56, 1531–1543.
Moreno, C., Gonzalez, F., Sáez, R., Melgarejo, J.C., Suárez-Ruiz, I., 2018. The Upper Devonian Kellwasser event recorded in a regressive sequence from inner shelf to lagoonal pond, Catalan Coastal Ranges, Spain. Sedimentology 65, 2055–2087.
Mottequin, B., Poty, E., 2015. Kellwasser horizons, sea-level changes and brachiopod–coral crises during the late Frasnian in the Namur–Dinant Basin (southern Belgium): a synopsis. Geological Society, London, Special Publications 423, 235–250.
Murphy, J.B., Keppie, J.D., 2005. The Acadian orogeny in the Northern Appalachians. Int. Geol. Rev. 47, 663–687.
Murphy, A.E., Sageman, B.B., Hollander, D.J., Lyons, T.W., Brett, C.E., 2000. Black shale deposition and faunal overturn in the Devonian Appalachian Basin: Clastic starvation, seasonal water-column mixing, and efficient biolimiting nutrient recycling. Paleoceanogr. 15, 280–291.
Narkiewicz, M., 2020. The Variscan foreland in Poland revisited: new data and new concepts. Geol. Quart. 64 (2). https://doi.org/10.7306/gq.1511. in press.
Narkiewicz, K., Narkiewicz, M., 2008. The mid-Frasnian subsidence pulse in the Lublin Basin (SE Poland): sedimentary record, conodont biostratigraphy and regional significance. Acta Geol. Pol. 58, 287–301.
Nikishin, A.M., Ziegler, P.A., Stephenson, R.A., et al., 1996. Late Precambrian to Triassic history of the East-European craton: dynamics of sedimentary basin evolution. Tectonophysics 268, 23–63.
Nokleberg, W., Bundtzen, T.K., Ereminand, R.A., et al., 2004. Metallogenesis and Tectonics of the RussianFar East, Alaska, and the Canadian Cordillera. U.S. Geol. Surv. Prof. Pap. 1697, 1–397.
O'Brien, H.E., Peltonen, P., Vartiainen, H., 2005. Kimberlites, carbonatites, and alkaline rocks. In: Lehtinen, M., Nurmi, P.A., Rirab, O.T. (Eds.), Precambrian Geology of Finland – Key to the Evolution of the Fennoscandian Shield. Elsevier B.V, Amsterdam, pp. 605–644.
Over, J., 2002. The Frasnian/Famennian boundary in central and eastern United States. Palaeogeogr. Palaeoclimatol. Palaeoecol. 181, 153–169.
Paschall, O., Carmichael, S., Königshof, P., Waters, J., Ta, H.P., Komatsu, T., Dombrowski, A., 2019. The Devonian-Carboniferous boundary in Vietnam: sustained ocean anoxia with a volcanic trigger for the Hangenberg Crisis? Glob. Planet. Change 175, 64–81.
Percival, L.M.E., Witt, M.L.I., Mather, T.A., Hermoso, M., Jenkyns, H.C., Hesselbo, S.P., Al-Suwaidi, A.H., Storm, M.S., Xu, M., Ruhl, M., 2015. Globally enhanced mercury deposition during the end-Pliensbachian extinction and Toarcian OAE: a link to the Karoo–Ferrar Large Igneous Province. Earth Planet. Sci. Lett. 428, 267–280.

Percival, L.M.E., Ruhl, M., Hesselbo, S.P., Jenkyns, H.C., Mather, T.A., Whiteside, J.H., 2017. Mercury evidence for pulsed volcanism during the end-Triassic mass extinction. Proc. Natl. Acad. Sci. USA 114, 7929–7934.
Percival, L.M.E., Jenkyns, H.C., Mather, T.A., et al., 2018a. Does large igneous province volcanism always perturb the mercury cycle? Comparing the records of Oceanic Anoxic Event 2 and the end-Cretaceous to other Mesozoic events. Am. J. Sci. 318, 799–860.
Percival, L.M.E., Davies, J.H.F.L., Schaltegger, U., De Vleeschouwer, D., Da, Silva, Föllmi, A.C., K.B., 2018b. Precisely dating the Frasnian–Famennian boundary: implications for the cause of the Late Devonian mass extinction. Sci. Rep. 8 (9578), 1–10.
Percival, L.M.E., Selby, D., Bond, D.P.G., Rakociński, M., Racki, G., Adatte, T., Spangenberg, J.E., Föllmi, K.B., 2019. Osmium-isotope evidence for pulses of extreme continental weathering associated with multiple Late Devonian climate perturbations. Palaeogeogr. Palaeoclimatol. Palaeoecol. 524, 240–249.
Percival, L.M.E., Bond, D.P.G., Rakociński, M., Marynowski, L., Hood, A., Adatte, T., Spangenberg, J.E., Föllmi, K.B., 2020. Phosphorus-cycle disturbances during the Late Devonian anoxic events. Glob. Planet. Change 184 (103070), 1–19.
Pisarzowska, A., Racki, G., 2012. Isotopic geochemistry across the Early-Middle Frasnian transition (Late Devonian) on the South Polish carbonate shelf: a reference for the global *punctata* Event. Chem. Geol. 334, 199–220.
Pisarzowska, A., Rakociński, M., Marynowski, L., et al., 2020a. Large environmental disturbances caused by magmatic activity during the Late Devonian Hangenberg Crisis. Glob. Planet. Change 188 (103155), 1–24.
Pisarzowska, A., Becker, R.T., Aboussalam, Z.S., Szczerba, M., Sobień, K., Kremer, B., Owocki, K., Racki, G., 2020b. Middlesex/*punctata* Event in the Rhenish Basin (Padberg section, Sauerland, Germany) – geochemical clues to the early-middle Frasnian global biogeochemical perturbation. Glob. Planet. Change; in revision.
Pochon, A., Branquet, Y., Gloaguen, E., et al., 2019. A Sb ±Au mineralizing peak at 360Ma in the Variscan belt. BSGF - Earth Sci. Bull. 190 (4), 1–12.
Polyansky, O.P., Prokopiev, A.V., Koroleva, O.V., Tomshin, M.D., Reverdatto, V.V., Babichev, A.V., Sverdlova, V.G., Vasiliev, D.A., 2018. The nature of the heat source of mafic magmatism during the formation of the Vilyui rift based on the ages of dike swarms and results of numerical modeling. Russian Geol. Geophys. 59, 1217–1236.
Pravikova, N.V., Matveeva, E.A., Tevelev, A.V., Veimarn, A.B., Rudakov, A.V., 2008. Volcanism of the transitional stage from the Late Devonian island arc to Early Carboniferous rifts in the Southern Ural. Moscow Univ. Geol. Bull. 63, 359–367.
Pruss, S.B., Jones, D.S., Fike, D.A., Tosca, N.J., Wignall, P.B., 2019. Marine anoxia and sedimentary mercury enrichments during the late Cambrian SPICE event in northern Scotland. Geology 47, 475–478.
Puchkov, V., Ernst, R.E., Hamilton, M.E., Söderlund, U., Sergeeva, N., 2016. A Devonian >2000-km-long dolerite dyke swarm-belt and associated basalts along the Urals-Novozemelian fold-belt: part of an East-European (Baltica) LIP tracing the Tuzo Superswell. GFF 138, 6–16.
Pujol, F., Berner, Z., Stüben, D., 2006. Palaeoenvironmental changes at the Frasnian/Famennian boundary in key European sections: chemostratigraphic constraints. Palaeogeogr. Palaeoclimatol. Palaeoecol. 240, 120–145.
Pyle, D.M., Mather, T.A., 2003. The importance of volcanic emissions for the global atmospheric mercury cycle. Atmos. Environ. 37, 5115–5124.
Qie, W.K., Algeo, T., Luo, G.M., Herrmann, A., 2019. Global events of the Late Paleozoic (Early Devonian to Middle Permian): A review. Palaeogeogr. Palaeoclimatol. Palaeoecol. 531, 1–15 A; 109259.
Racki, G., 1998. Frasnian-Famennian biotic crisis: undervalued tectonic control? Palaeogeogr. Palaeoclimatol. Palaeoecol. 141, 77–198.
Racki, G., 2005. Toward understanding Late Devonian global events: few answers, many questions. In: Over, D.J., Morrow, J.R., Wignall, P.B. (Eds.), Understanding Late Devonian and Permian-Triassic Biotic and Climatic Events: Towards an Integrated Approach. Developments in Paleontology and Stratigraphy 20. pp. 5–36.
Racki, G., 2012. The Alvarez impact theory of mass extinction; limits to its applicability and the "great expectations syndrome" Acta Palaeont. Pol. 57, 681–702.
Racki, 2020a. Big 5 Mass Extinctions. In: Encyclopedia of Geology, 2 ed. Elsevier. https://doi.org/10.1016/B978-0-12-409548-9.12028.7. in press.
Racki, 2020b. Volcanism as a prime cause of mass extinction: retrospectives and perspectives. In: Geological Society of America Special Paper 544, pp. 1–34.
Racki, G., Racka, M., Matyja, H., Devleeschouwer, X., 2002. The Frasnian/Famennian boundary interval in the South Polish-Moravian shelf basins: integrated event-stratigraphical approach. Palaeogeogr. Palaeoclimatol. Palaeoecol. 181, 251–297.
Racki, G., Marynowski, L., Rakociński, M., 2018a. Anomalous Upper Devonian mercury enrichments - comparison of Inductively Coupled Plasma-Mass Spectrometry (ICP-MS) and Atomic Absorption Spectrometry (AAS) analytical data. Geol. Quart. 62, 487–495.
Racki, G., Rakocinski, M., Marynowski, L., Wignall, P.B., 2018b. Mercury enrichments and the Frasnian-Famennian biotic crisis: a volcanic trigger proved? Geology 46, 543–546.
Racki, G., Königshof, P., Belka, Z., Dopieralska, J., Pisarzowska, A., 2019. Diverse depositional and geochemical signatures of the Frasnian-Famennian global event in western Thailand reveal Palaeotethyan vs. Western Australian geotectonic affinities. J. Asian Earth Sci. X 2 (100010), 1–23.
Rakociński, M., Marynowski, L., Pisarzowska, A., Bełdowski, J., Siedlewicz, G., Zatoń, M., Perri, M.C., Spalletta, C., Schönlaub, H.P., 2020. Volcanic related methylmercury poisoning as the possible driver of the end-Devonian Mass Extinction. Sci. Reports, in revision.
Rampino, M.R., Self, S., 2015. Large Igneous Provinces and biotic extinctions. In: Sigurdsson, H. (Ed.), The Encyclopedia of Volcanoes, 2nd edit. Elsevier, Amsterdam, pp. 605–644.
Raup, D.M., Sepkoski, J.J., 1982. Mass extinctions in the marine fossil record. Science 215, 1501–1503.
Ravichandran, M., 2004. Interactions between mercury and dissolved organic matter – a review. Chemosphere 55, 319–331.
Ray, J.S., Pande, K., 1999. Carbonatite alkaline magmatism associated with continental flood basalts at stratigraphic boundaries: cause for mass extinctions. Geophys. Res. Lett. 26, 1917–1920.
Retallack, G.J., Huang, C.M., 2011. Ecology and evolution of Devonian trees in New York. USA. Palaeogeogr. Palaeoclimatol. Palaeoecol. 299, 110–128.
Ricci, J., Quidelleur, X., Pavlov, V., Orlov, S., Shatsillo, A., Courtillot, V., 2013. New 40Ar/39Ar and K–Ar ages of the Viluy traps (Eastern Siberia): further evidence for a relationship with the Frasnian–Famennian mass extinction. Palaeogeogr. Palaeoclimatol. Palaeoecol. 386, 531–540.
Riquier, L., Tribovillard, N., Averbuch, O., Devleeschouwer, X., Riboulleau, A., 2006. The Late Frasnian Kellwasser horizons of the Harz Mountains (Germany): two oxygen-deficient periods resulting from different mechanisms. Chem. Geol. 233, 137–155.
Roberts, G.G., Mannion, P.D., 2019. Timing and periodicity of Phanerozoic marine biodiversity and environmental change. Sci. Rep. 9 (6116), 1–11.
Sageman, B.B., Lyons, T.W., 2003. Geochemistry of fine-grained sediments and sedimentary rocks. Treatise on Geochemistry 7, 115–158.
Sames, B., Wagreich, M., Conrad, C.P., Iqbal, S., 2020. Aquifer-eustasy as the main driver of short-term sea-level fluctuations during Cretaceous hothouse climate phases. Geological Society, London, Special Publications 498https://doi.org/10.1144/SP498-2019-105. in press.
Sandberg, C.A., Ziegler, W., 1996. Devonian conodont biochronology in geologic time calibration. Senckenberg. Lethaea 76, 259–265.
Sandberg, C.A., Morrow, J.R., Ziegler, W., 2000. Late Devonian events and mass extinctions. In: Catastrophic Events and Mass Extinctions: Impacts and Beyond. 1053. Lunar and Planetary Institute Contribution, Houston, Texas, pp. 188–189.
Sandberg, C.A., Morrow, J.R., Ziegler, W., 2002. Late Devonian sea-level changes, catastrophic events, and mass extinctions. Geol. Soc. Am. Spec. Pap. 356, 473–487.
Sanei, H., Grasby, S.E., Beauchamp, B., 2012. Latest Permian mercury anomalies. Geology 40, 63–66.
Scaife, J.D., Ruhl, M., Dickson, A.J., Mather, T.A., Jenkyns, H.C., Percival, L.M.E., Hesselbo, S.P., Cartwright, J., Eldrett, J.S., Bergman, S.C., Minisini, D., 2017. Sedimentary mercury enrichments as a marker for submarine large igneous province volcanism? Evidence from the Mid-Cenomanian Event and Oceanic Anoxic Event 2 (Late Cretaceous). Geochem. Geophys. Geosyst. 18, 4253–4275.
Schindler, E., 1993. Event-stratigraphic markers within the Kellwasser Crisis near the Frasnian/Famennian boundary (Upper Devonian) in Germany. Palaeogeogr. Palaeoclimatol. Palaeoecol. 104, 115–125.
Schobben, M., van de Schootbrugge, B., Wignall, P.B., 2019. Interpreting the carbon isotope record of mass extinctions. Elements 15, 331–337.
Shen, J., Chen, J.B., Algeo, T.J., Yuan, S.G., Feng, Q.L., Yu, J.X., Zhou, L.A., O'Connell, B., Planavsky, N.J., 2019a. Evidence for a prolonged Permian–Triassic extinction interval from global marine mercury records. Nature Comm. 10 (1563), 1–9.
Shen, J., Algeo, T.J., Chen, J.B., Planavsky, N.J., Feng, Q.L., Yu, J.X., Liu, J.L., 2019b. Mercury in marine Ordovician/Silurian boundary sections of South China is sulfide-hosted and non-volcanic in origin. Earth Planet. Sci. Lett. 511, 130–140.
Sheremet, E.M., 2014. On the genesis of kimberlites of the Ukrainian Shield. In: In: 30th International Conference on "Ore Potential of Alkaline, Kimberlite and Carbonatite Magmatism", Antalya – Turkey, pp. 174–175.
Sial, A.N., Chen, J., Lacerda, L.D., Korte, C., Spangenberg, J.E., Silva-Tamayo, J.C., Gaucher, C., Ferreira, V.P., Barbosa, J.A., Pereira, N.S., Benigno, A.P., 2020. Globally enhanced Hg deposition and Hg isotopes in sections straddling the Permian–Triassic boundary: link to volcanism. Palaeogeogr. Palaeoclimatol. Palaeoecol. 540 (109537), 1–20.
Sinninghe Damsté, J.S., Köster, J., 1998. A euxinic southern North Atlantic Ocean during the Cenomanian-Turonian oceanic anoxic event. Earth Planet. Sci. Lett. 158, 165–173.
Smit, J., Koeberl, C., Claeys, P., Montanari, A., 2016. Mercury anomaly, Deccan volcanism, and the end-Cretaceous mass extinction: Comment. Geology 44, e381.
Sobolev, D.N., 1928. Earth and Life. III. On the Causes of Extinction of Organisms. Kiev, Science-Popular Library of the Ukrainian Department of the Geological Committee 74 p. (In Russian).
Spalletta, C., Perri, M.C., Over, D.J., Corradini, C., 2017. Famennian (Upper Devonian) conodont zonation: revised global standard. Bull. Geosci. 92, 31–57.
Stachacz, M., Uchman, A., Rodríguez-Tovar, F.J., 2017. Ichnological record of the Frasnian–Famennian boundary interval: two examples from the Holy Cross Mts (Central Poland). Int. J. Earth Sci. 10, 157–170.
Stanley, S.M., 2016. Estimates of the magnitudes of major marine mass extinctions in Earth history. Proc. Natl. Acad. Sci. U. S. A. 113, 6325–6334.
Stein, W.E., Berry, C.M., Morris, J.L., VanAller Hernick, L., Mannolini, F., Ver Straeten, C., Landing, E., Marshall, J.E.A., Wellman, C.H., Beerling, D.J., Leake, J.R., 2020. Mid-Devonian *Archaeopteris* roots signal revolutionary change in earliest fossil forests. Curr. Biol. 30, 1–11.
Stepanenko, V.I., 2016. The Kanin–Timan–Pechora Province of Late Devonian intraplate magmatism (position and size). Dokl. Earth Sci. 467, 337–340.
Stigall, A.L., 2012. Speciation collapse and invasive species dynamics during the Late Devonian "Mass Extinction" GSA Today 22, 4–9.
Strelchenko, T.V., Kruchek, S.A., 2013. Lower Famennian conodont based stratigraphy of the Pripyat Trough. Stratigr. Geol. Correl. 21 (2), 22–42.
Swanson-Hysell, N.L., Macdonald, F.A., 2017. Tropical weathering of the Taconic orogeny as a driver for Ordovician cooling. Geology 45, 719–722.
Szrek, P., Salwa, S., 2020. High-energy events in the Frasnian–Famennian boundary interval of the Płucki section in the Holy Cross Mountains, Poland. Facies 66 (9), 1–16.
Szulczewski, M., Belka, Z., Skompski, S., 1996. The drowning of a carbonate platform: an example from the Devonian–Carboniferous of the southwestern Holy Cross

Mountains. Poland. Sediment. Geol. 106, 21–49.
Tabor, C.R., Bardeen, C.G., Otto-Bliesner, B.L., Garcia, R.R., Toon, O.B., 2020. Causes and climatic consequences of the impact winter at the Cretaceous-Paleogene boundary. Geoph. Res. Lett. 47 (e60121), 1–10.
Tankersley, T.B., Dunning, N.P., Owen, L.A., Huff, W.D., Park, J.H., Kim, C., Lentz, D.L., Sparks-Stokes, D., 2018. Positive platinum anomalies at three late Holocene high magnitude volcanic events in Western Hemisphere sediments. Sci. Rep. 8 (11298), 1–6.
Them, T.R., Jagoe, C.H., Caruthers, A.H., Gill, B.C., Grasby, S.E., Gröcke, D.R., Yin, R., Owens, J.D., 2019. Terrestrial sources as the primary delivery mechanism of mercury to the oceans across the Toarcian Oceanic Anoxic Event (Early Jurassic). Earth Planet. Sci. Lett. 507, 62–72.
Thornton, U.B., Junium, C., Boyer, D.L., Cohen, P.A., Day, J.E., 2019. Biogeochemical controls on black shale deposition during the Frasnian-Famennian biotic crisis in the Illinois and Appalachian Basins, USA, inferred from stable isotopes of nitrogen and carbon. Palaeogeogr. Palaeoclimatol. Palaeoecol. 531, 1–14 A, 1; 108787.
Timmerman, M.J., 2008. Palaeozoic magmatism. In: McCann, T. (Ed.), The Geology of Central Europe. Precambrian and Palaeozoic 1. Geological Society, London, pp. 665–748.
Tomshin, M.D., Kopylova, A.G., Konstantinov, K.M., Gogoleva, S.S., 2018. Basites of the Vilyui paleorift: geochemistry and sequence of intrusive events. Russ. Geol. Geophys. 59, 1204–1216.
Torsvik, T.H., Cocks, R.M., 2017. Earth History and Palaeogeography. Cambridge Univ, Press, Cambridge 317 p.
Trabucho-Alexandre, J., 2015. More gaps than shale: erosion of mud and its effect on preserved geochemical and palaeobiological signals. Geological Society, London, Special Publications 404, 251–270.
Tribovillard, N., Algeo, T.J., Lyons, T.W., Riboulleau, A., 2006. Trace metals as paleoredox and paleoproductivity proxies: an update. Chem. Geol. 232, 12–32.
Tyson, R.V., 2005. The “productivity versus preservation” controversy: cause, flaws, and resolution. SEPM Special Publication 82, 17–33.
Uddin, M.K., 2017. A review on the adsorption of heavy metals by clay minerals, with special focus on the last decade. Chem. Eng. J. 308, 438–462.
van de Schootbrugge, B., Gollner, S., 2013. Altered primary production during mass-extinction events. Paleontological Society Papers 19, 1–27.
Veimarn, A.B., Korneeva, G.A., 2007. Global geological events at Frasnian/Famennian boundary. Biul. Mosk. Obsch. Ispyt. Prirody, Otd. Geol. 82 (1), 48–68 (In Russian).
Veimarn, A.B., Kuzmin, A.V., Kononova, L.I., Baryshev, V.N., Vorontzova, T.N., 1997. Geological events at the Frasnian/Famennian boundary on the territory of Kazakhstan, Urals and adjacent regions of the Russian plate. Cour. Forschungsinst. Senckenberg 199, 37–50.
Veimarn, A.B., Milanovsky, E.E., 1990. Famennian riftogenesis in Kazakhstan and other regiones of Eurasia. Biul. Mosk. Obsch. Ispyt. Prirody, Otd. Geol. 65 (4), 9–23 34–47; (6). (In Russian).
Ver Straeten, C.A., Over, D.J., Baird, G.C., 2020. Arc-to-craton: Devonian airfall tephras in the Eastern United States. In: Geological Society of America Special Paper, in revision.
Veron, J.E.N., 2008. Mass extinctions and ocean acidification: biological constraints on geological dilemmas. Coral Reefs 27, 459–472.
von Raumer, J.F., Nesbor, H.D., Stampfli, G.M., 2017. The north-subducting Rheic Ocean during the Devonian: Consequences for the Rhenohercynian ore sites. Int. J. Earth Sci. 106, 2279–2296.
Wall, F., Zaitsev, A.N. (Eds.), 2004. Phoscorites and Carbonatites from Mantle to Mine: the Key Example of the Kola Alkaline Province. The Mineralogical Society of Great Britain and Ireland, London 503 p.
Walliser, O.H. (Ed.), 1996. Global Events and Event Stratigraphy in the Phanerozoic. Springer Verlag, Berlin, pp. 1–333.
Wang, Y.I., Luo, H., Aitchison, J.C., 2007. Influence of the Frasnian-Famennian event on radiolarian faunas. Eclogae geol. Helv. 99 (Suppl. 1), S127–S132.
Wang, X., Liu, S.A., Wang, Z.R., Chen, D.Z., Zhang, L.Y., 2018. Zinc and strontium isotope evidence for climate cooling and constraints on the Frasnian-Famennian (~372 Ma) mass extinction. Palaeogeogr. Palaeoclimatol. Palaeoecol. 498, 68–82.
Wedepohl, K.H., 1991. The composition of the upper earth's crust and the natural cycles of selected metals. Metals in natural raw materials. Natural Resources. In: Merian, E. (Ed.), Metals and Their Compounds in the Environment. Weinheim, Verlag Chemie (VCH), pp. 3–17.
Weiner, T., Kalvoda, J., Kumpan, T., Schindler, E., Šimíček, D., 2017. An integrated stratigraphy of the Frasnian-Famennian boundary interval (Late Devonian) in the Moravian Karst (Czech Republic) and Kellerwald (Germany). Bull. Geosci. 92, 257–281.
Weissert, H., 2019. Mesozoic C-cycle perturbations and climate: evidence for increased resilience of the Cretaceous biosphere to greenhouse pulses. Can. J. Earth Sci. 56, 1366–1374.
Wendt, J., Kaufmann, B., Belka, Z., Farsan, N., Bavandpur, A.K., 2005. Devonian/Lower Carboniferous stratigraphy, facies patterns and palaeogeography of Iran. Part II. Northern and central Iran. Acta Geol. Pol. 55, 31–97.
Whalen, M.T., Śliwiński, M.G., Payne, J.H., Day, J.E., Chen, D.Z., Da Silva, A.C., 2015. Chemostratigraphy and magnetic susceptibility of the Late Devonian Frasnian–Famennian transition in western Canada and southern China: implications for carbon and nutrient cycling and mass extinction. Geological Society, London, Special Publications 414, pp. 37–72.
White, D.A., Elrick, M., Romaniello, S., Zhang, F.F., 2018. Global seawater redox trends during the Late Devonian mass extinction detected using U isotopes of marine limestones. Earth Planet. Sci. Lett. 503, 68–77.
Wignall, P.B., 2016. The Worst of Times. How Life on Earth Survived Eighty Million Years of Extinctions. Princeton University Press, Princeton, pp. 224.
Wilder, H., 1994. Death of Devonian reefs – implications and further investigations. Cour. Forsch. Inst. Senck. 172, 241–247.
Wilson, M., Lyashkevich, Z.M., 1996. Magmatism and the geodynamics of rifting of the Pripyat-Dnieper-Donets Rift, East European Platform. Tectonophysics 268, 65–81.
Winter, J., 2015. Vulkanismus und Kellwasser-Krise – Zirkon-Tephrostratigrafie, Identifizierung und Herkunft distaler Fallout-Aschenlagen (Oberdevon, Synklinorium von Dinant, Rheinisches Schiefergebirge, Harz). Z. Dt. Ges. Geowiss. 166, 227–251.
Yang, S.C., Hu, W.X., Wang, X.L., Jiang, Y.B., Yao, S.P., Sun, F.N., Huang, Z.C., Zhu, F., 2019. Duration, evolution, and implications of volcanic activity across the Ordovician–Silurian transition in the Lower Yangtze region, South China. Earth Planet. Sci. Lett. 518, 13–25.
Yazikov, A.Y., Izokh, N.G., Saraev, S.V., Bakharev, N.K., Gonta, T.V., Sobolev, E.S., 2013. New data on the Upper Devonian biostratigraphy and sedimentology of Stolb Island (Lena River delta). Russ. Geol. Geophys. 54, 780–791.
Yudina, A.B., Racki, G., Savage, N.S., Racka, M., Malkowski, K., 2002. The Frasnian–Famennian events in deep-shelf succession, Subpolar Urals: biotic, depositional and geochemical records. Acta Palaeontol. Pol. 47, 355–372.
Yudovich, J.E., Ketris, M.P., Fridlender, N.G., Aldanazarov, R.A., 1986. Geochemistry of mercury in black-shale formations of Pai-Khoi and the North of the Urals. Geokhimiya 1986, 810–818 (In Russian).
Yutkina, E.V., Nosova, A.A., Sazonova, L.V., Larionova, Y.U., Kondrashov, I.A., Shumlyanskyy, I.V., Albekov, A.Y., Savko, K.A., 2017. Devonian volcanics of the Voronezh crystalline massif, East European Platform: evolution of melts and peculiarities of crustal contamination. Petrology 25, 233–264.
Zapalski, M.K., Nowicki, J., Jakubowicz, M., Berkowski, B., 2017. Tabulate corals across the Frasnian/Famennian boundary: architectural turnover and its possible relation to ancient photosymbiosis. Palaeogeogr. Palaeoclimatol. Palaeoecol. 487, 416–429.
Zeng, J.W., Xu, R., Gong, Y.M., 2011. Hydrothermal activities and seawater acidification in the Late Devonian F-F transition: evidence from geochemistry of rare earth elements. Sci. China Ser. D Earth Sci. 54, 540–549.
Zhang, L., Chen, D., Huang, T., Yu, H., Zhou, X., Wang, J., 2020. An abrupt oceanic change and frequent climate fluctuations across the Frasnian–Famennian transition of Late Devonian: constraints from conodont Sr isotope. Geol. J. https://doi.org/10.1002/gj.3657. in press.
Zimmerle, W., 1985. New aspects on the formation of hydrocarbon source rocks. Geol. Rdsch. 74, 385–416.